

CROSS-LAYER ENERGY EFFICIENCY OF PLC SYSTEMS FOR SMART GRID APPLICATIONS

A THESIS SUBMITTED IN PARTIAL FULFILMENT OF THE REQUIREMENTS OF THE
MANCHESTER METROPOLITAN UNIVERSITY
FOR THE DEGREE OF DOCTOR OF PHILOSOPHY

2017

By
Augustine Ikpehai
School of Computer Science

Contents

Abstract	10
Acknowledgement	12
List of Abbreviations	14
List of Mathematical Notations	19
List of Variables	20
1 Introduction	23
1.1 Motivation	24
1.2 Research Objectives	25
1.3 Key Contributions	25
1.4 Thesis Organisation	26
1.5 List of Publications	28
2 Background Theory	31
2.1 Smart Grid and Communication Technologies	31
2.1.1 Smart Grid and its Motivation	31
2.1.2 Communication Challenges in Smart Grid	34
2.1.2.1 Integration and Interoperability	35
2.1.2.2 Scale and Complexity	35
2.1.2.3 Distributed Intelligence	36
2.1.2.4 Security and Privacy	36
2.1.3 Reference Design and Communication Architecture	36
2.1.4 Smart Grid Applications and Traffic Characteristics	40
2.1.5 Smart Metering	40
2.1.6 Demand Response	40

2.1.7	Plug-in Electric Vehicle	42
2.1.8	Substation Automation	42
2.1.9	Distributed Energy Resources (DERs) and Microgrids .	43
2.1.10	Wide Area Measurement System (WAMS)	44
2.1.11	Distributed Supervision	44
2.2	Wireline and Wireless Technologies	46
2.3	Power Line Communication	48
2.3.1	PLC Overview	48
2.3.2	Standards and Regulations	51
2.3.3	PLC Channel Characterisation and Measurements . . .	53
2.3.3.1	Top-down Approach	53
2.3.3.2	Bottom-up Approach	54
2.3.3.3	Numerical Examples	60
2.3.4	Signal Propagation and Challenges in PLC	64
2.3.4.1	Noise	64
2.3.4.2	Multipath Propagation and Frequency- Selectivity	70
2.3.4.3	Cable Losses (Attenuation)	71
2.3.4.4	EMC and Regulatory Constraints on Transmit Power	71
2.3.4.5	Topology Variation	76
2.4	Energy-Efficient Communication System in Smart Grid	76
2.5	Methodology	77
2.6	Chapter Summary	78
3	Efficient BPLC Topology for Clustered AMI	79
3.1	Advanced Metering Infrastructure and Clustering	80
3.1.1	Clustered Advanced Metering Infrastructure	80
3.1.2	Broadband PLC for Clustered AMI: System Model . . .	81
3.1.3	Smart Metering	82
3.1.4	Demand Response	83
3.2	Model Evaluation	84
3.2.1	Methodology	84
3.2.2	Simulation Setup	84
3.3	Results and Performance Analysis	88
3.3.1	Network Reliability	88

3.3.1.1	Communication Latency	92
3.3.1.2	Effect of Packet Size on Latency	94
3.3.1.3	Probability of Packet Delivery	96
3.3.2	Network Energy Efficiency	100
3.4	Chapter Summary	102
4	Low-Power PLC for Energy Management Systems	103
4.1	Home Energy Management System	104
4.1.1	IPv6-enabled Low-Power PLC (6LoPLC)	106
4.1.2	Hanadu PLC Transceivers	106
4.2	6LoPLC System Evaluation	108
4.2.1	Methodology	108
4.2.2	Experimental Set-up and Measurement	108
4.2.3	System Parameterisation and Traffic Analysis	113
4.2.4	NS-3 Model for HEMS Network	116
4.3	Results and Performance Analysis	117
4.3.1	Communications Delay	118
4.3.2	Network Capacity	123
4.3.3	Network Reliability	124
4.3.4	Effects of Impulsive Noise	127
4.3.5	Power Line Channel Performance	128
4.4	Chapter Summary	130
5	Energy-Efficient Vector-OFDM In PLC Systems	132
5.1	Effects of Communication Network on Smart Grid Applications	133
5.2	V-OFDM in PLC Systems	135
5.3	V-OFDM Model	136
5.4	PAPR and Transmit Power in V-OFDM	139
5.5	Output SNR of V-OFDM With Conventional Blanking and Clipping	142
5.6	Energy Efficiency in V-OFDM with DPTE	144
5.6.1	Dynamic Peak-Based Threshold Estimation Technique	144
5.6.2	Signal Peak Estimation	146
5.6.3	Output SNR of V-OFDM with DPTE	148
5.6.4	Comparative SNR Performance for Various Impulsive Noise Cases	149

5.6.5	DPTE Gain Relative to Coventional Blanking	152
5.7	Chapter Summary	154
6	Conclusions and Future Work	155
6.1	Conclusions	155
6.2	Future Work	158
	Bibliography	160
	Production Notes	178

List of Tables

2.1	Traffic characteristics and communication requirements	45
2.2	Wireline and wireless communication technologies	47
2.3	Global regulation of BPLC and NPLC frequency bands	52
3.1	PLC parameters	85
3.2	Wi-Fi parameters	85
3.3	AMI applications parameters	86
4.1	System information comprising of communication and applica- tion parameters	115

List of Figures

1.1	Thematic organisation	28
2.1	A schematic of smart grid showing energy and communication networks using wireless and wireline technologies [1]	34
2.2	End-to-end smart grid communication model based on IEEE 2030-2011 reference model [2]	38
2.3	European distribution network showing the power line last mile [3]	50
2.4	Equivalent circuit of 2-port transmission line	55
2.5	Two-port network showing the source and receiver	57
2.6	Transmission line with one branch [4,5]	58
2.7	Equivalent circuit of Figure 2.6 [4,5]	58
2.8	Topology of PLC network in main lab	61
2.9	CTF experimental power line network	62
2.10	CTF of TL with different branch lengths	63
2.11	Types of noise in power lines	64
2.12	Amplitude (in mV) of noise pulses generated by a laptop charger	66
2.13	Impulsive noise in time and frequency domain from a drilling machine	67
2.14	Radiated emission measurement	72
2.15	Conducted emission	73
2.16	Conducted emissions measurements with current clamp	74
2.17	Conducted emissions	75
3.1	Logical topology of smart metering network over the LV power line network	82
3.2	Transmission of peak price signal over PLC network.	82

3.3	Variation of meter reading upload with cluster size	89
3.4	Packet delivery ratio as a function of network load in smart metering	90
3.5	Comparing lost packets in Wi-Fi, BPLC and PLC NPLC in smart metering	90
3.6	Successful peak price downloads versus number of smart meters	91
3.7	Smart metering round-trip latency versus number of smart meters	93
3.8	Peak price one-way delay versus number of smart meters . . .	93
3.9	Variation of metering round-trip delay with application size . .	95
3.10	Probability of packet delivery of flat and clustered AMI	97
3.11	Variation of PPD performance with DC (relay) position	98
3.12	DC position on PPD (with NPLC last mile)	99
4.1	HEMS model showing various types of in-home loads.	105
4.2	Protocol stack showing 6LoPLC.	107
4.3	Experimental PLC network in the main lab	109
4.4	Evaluation testbed for 6LoPLC	110
4.5	Constrained Application Protocol (CoAP) interface showing the monitoring (sensor) and control (lamp) windows.	112
4.6	Samples of two-way delay	113
4.7	HEMS traffic analysis with Wireshark	114
4.8	A schematic showing the end-to-end delay.	118
4.9	Model validation by comparing RTT from simulation with measurement.	119
4.10	One-way delay for the sensor and lamp	120
4.11	Statistical distribution of one-way latency for various HEMS .	122
4.12	System throughput as a function of application data size. . . .	123
4.13	Packet delivery ratio vs number of nodes.	124
4.14	Distribution of lost packets for various HEMS	126
4.15	Effect of impulsive noise on one-way delay.	127
4.16	System BER performance as a function of SNR.	128
4.17	BER performance with various impulsive noise probabilities (p) using DBPSK.	129
5.1	Variation of communication delay with throughput and data size using uncoded OFDM with DBPSK	134

5.2	V-OFDM block diagram showing nonlinear preprocessors at the receiver	136
5.3	PAPR performance of V-OFDM system as a function of the number of VBs for different values of α , ($M = 1$ is equivalent to conventional OFDM), $n = 10^5$, $N = 256$, 16QAM	141
5.4	Output SNR performance of the V-OFDM system versus the threshold with blanking and clipping using input SNR = 25 dB, SINR = -10 dB and $p = 0.01$, 16QAM	143
5.5	V-OFDM with DPTE system showing the peak extractor at the receiver	145
5.6	CCDF as a function of V-OFDM symbol peak values for various N and VB ($M = \{16, 32, 64, 128\}$) using 10^5 symbols. Analytical and simulated CCDF of the conventional OFDM are also included.	147
5.7	SNR performance of DPTE and COB in V-OFDM system with input SNR = 25dB, $p = 0.001$, $n = 5 \times 10^4$ and $N = 256$	148
5.8	Blanker output SNR as a function of SINR using DPTE with parameters $N = 256$, $n = 10^4$ symbols in 16QAM, $p = 0.001$ input SNR = 25dB.	150
5.9	Comparative SNR performance of DPTE and COB in various impulsive noise conditions using $p = \{0.001, 0.01\}$ SNR=25, $N = 256$, 16QAM, $n = 10^4$	151
5.10	Relative SNR gain of V-OFDM with DPTE over COB for different impulsive noise probabilities for $N = 256$ and $M = 64$ at input SNR = 30 dB, $p = 0.05$, $n = 10^4$, 16QAM	153

Abstract

Though opinions are still divided over the specific choices of technology for smart grid, there is a consensus that heterogeneous communications network is most appropriate. Power line communication (PLC) is promising because it is readily available and it aligns with the natural topology of power distribution network. One of the emerging realities is that the communication system enabling smart grid must be energy-efficient. This thesis employs a cross-layer approach to address energy efficiency of PLC networks in different smart grid scenarios.

At network layer, this work exploits the topology of a PLC-enabled advanced metering infrastructure (AMI) to improve the probability of successful packet delivery across the network. The technique, termed AMI clustering, leverages the traditional structure of the low voltage (LV) network by organising the smart meters into clusters and locally aggregating their readings. Improvement in packet delivery inherently reduces energy wastage.

Next, the adaptation layer exploits the low data rate transmission techniques to reduce the energy requirements of PLC nodes. To achieve that, this work developed a network model in NS-3 (an open-source network simulator) that considers PLC transceivers as resource-constrained devices and interconnects them to emulate home energy management system (HEMS). The model was validated with experimental results which showed that in the home area network (HAN), low-rate applications such as energy management can be supported over low-power PLC networks.

Furthermore, at physical layer, this thesis proposes a more energy-efficient multi-carrier modulation scheme than the orthogonal frequency division multiplexing (OFDM) used in most of the current PLC systems. OFDM is widely

known for its high peak-to-average-power ratio (PAPR) which degrades energy efficiency of the systems. This thesis found that by employing vector-OFDM (V-OFDM), power requirements of PLC transmitter can be reduced. The results also showed the energy efficiency can be further improved by using a dynamic noise cancellation technique such as dynamic peak-based threshold estimation (DPTE) at the receiver.

By applying the proposed methods, packet delivery can be improved by 3% at network layer (which conserves energy) and reduced data rate can save about 2.6014 dB in transmit power. Finally, at physical layer, V-OFDM and DPTE can respectively provide 5.8 dB and 2.1 dB reduction in power requirements of the PLC transceivers. These signify that if V-OFDM is combined with DPTE, future PLC modems could benefit from energy-efficient power amplifiers at reduced cost.

Acknowledgement

Praise to the Almighty God for the gift of life and the strength throughout the PhD journey. The last few years have been impactful, insightful and challenging but overall a rewarding experience. It has also provided an opportunity to flip a new page in my life. There were times I needed help, motivation and encouragement. Some special people were readily handy to offer the needed support.

In that regard, I will also like to thank my supervisory team; Prof. Nicholas Bowring and Dr. Bamidele Adebisi for overseeing the research leading to this thesis. Immense gratitude to my DoS; Dr. Bamidele Adebisi for the various perspectives, insights and guidance from the beginning of my PhD research. Those pieces of advice were immeasurably helpful.

Special gratitude to Dr. Khaled Rabie, you were never wearied by my endless questions and queries. Thanks to my colleague in the Smart Microgrid Lab, Matjaz Rozman for always offering to help during the bench work and measurements. I will also thank Dr. Kelvin Anoh for the pieces of advice.

*To My Family; Tegah, Aimalohi, Imagheohi and
Ohiomokhai.*

*Thank you for the encouragement, understanding and endless support.
We went through this journey together, you are simply the best I could
wish or have.*

List of Abbreviations

6LoWPAN	IPv6 over LoWPAN
ACSI	Abstract Communication Service Interface
AMI	Advanced Metering Infrastructure
AMR	Automated Meter Reading
ARIB	Association of Radio Industries and Businesses
ARQ	Automatic Repeat Request
AWGN	Additive White Gaussian Noise
BAN	Building Area Network
BER	Bit Error Rate
BPSK	Binary Phase Shift Keying
BPLC	Broadband Power Line Communication
CA	Collision Avoidance
CCDF	Complimentary Cumulative Distribution Function
CENELEC	European Committee for Electrotechnical Standardisation
CoAP	Constrained Application Protocol
COB	Conventional Optimal Blanking
CPN	Customer Premises Network
CPP	Critical Peak Pricing
CSMA	Carrier Sense Multiple Access
CTF	Channel Transfer Function

D8PSK	Differential 8 Phase Shift Keying
DBPSK	Differential Binary Phase Shift Keying
DER	Distributed Energy Resources
DF	Decode-and-Forward
DG	Distributed Generation
DNO	Distribution Network Operator
DoD	Department of Defence
DPSK	Distributed Phase Shift Keying
DQPSK	Distributed Quadrature Phase Shift Keying
DPTE	Dynamic Peak-Based Threshold Estimation
DR	Demand Response
DS	Distributed Storage
DSL	Digital Subscriber Line
EMC	Electromagnetic Compacibility
EMS	Energy Management System
ESI	Energy Service Interface
EUT	Equipment Under Test
FAN	Field Area Network
FCC	Federal Communications Commission
FFT	Fast Fourier Transform
FIFO	First-in First-out
FM	Frequency Modulation
FPGA	Field-Programmable Gate Array
FTP	File Transfer Protocol
G2V	Grid-to-Vehicle
GPS	Global Positioning System

HAN	Home Area Network
HEMS	Home EMS
HPA	Highly-Linear Power Amplifier
HTTP	Hypertext Transfer Protocol
HV	High Voltage
HVAC	Heating, Ventilation and Air-Conditioning
IAN	Industrial Area Network
IAP	Interoperability Architectural Perspective
ICMP	Internet Control Message Protocol
ICT	Information and Communication Technology
IED	Intelligent Electronic Device
IETF	Internet Engineering Task Force
IFFT	Inverse Fast Fourier Transform
IP	Internet Protocol
IPv6	Internet Protocol Version 6
ISI	Inter-Symbol Interference
LAN	Local Area Network
LED	Light-Emitting Diode
LoWPAN	Low-Power Wireless Personal Area Network
LV	Low Voltage
M2M	Machine-to-Machine
MAC	Media Access Control
MDMS	Meter Data Management Server
MIMO	Multiple-Input, Multiple-Output
MTU	Maximum Transmission Unit
MV	Medium Voltage

NAN	Neighbourhood Area Network
NPLC	Narrowband Power Line Communication
OFC	Optical Fibre Cable
OFDM	Orthogonal Frequency-Division Multiplexing
OSI	Open Systems Interconnect
PA	Power Amplifier
PAPR	Peak-to-Average Power Ratio
PDF	Probability Density Function
PDR	Packet Delivery Ratio
PEV	Plug-in Electric Vehicle
PDU	Protocol Data Unit
PHY	Physical Layer
PLC	Power Line Communication
PMU	Phasor Measurement Unit
PPD	Probability of Packet Delivery
PRIME	Power Line Intelligent Meter Evolution
PSD	Power Spectral Density
PTR	Peak Time Rebate
PV	Photovoltaic
QAM	Quadrature Amplitude Modulation
QoE	Quality-of-Experience
QoS	Quality-of-Service
RFC	Request For Comments
RLC	Remote Load Control
RMS	Root Mean Square
RTP	Real Time Pricing

RTT	Return-Trip Time
SCR	Silicon Controlled Rectifier
SEP	Smart Energy Profile
SINR	Signal-to-Impulsive Noise Ratio
SNR	Signal-to-Noise Ratio
TCP	Transmission Control Protocol
TDMA	Time Division Multiple Access
TL	Transmission Line
TOU	Time-of-Use
UART	Universal Asynchronous Receiver/Transmitter
UDP	User Datagram Protocol
V2G	Vehicle-to-Grid
VB	Vector Block
V-OFDM	Vector Orthogonal Frequency-Division Multiplexing
WAMS	Wide Area Measurement System
WAN	Wide Area Network
Wi-Fi	Wireless-Fidelity
WiMAX	Worldwide Interoperability for Microwave Access
WLAN	Wireless LAN

List of Mathematical Notations

\prod	product symbol
$\sinh(\cdot)$	hyperbolic sine function
$\cosh(\cdot)$	hyperbolic cosine function
$\tanh(\cdot)$	hyperbolic tangent function
$\exp(x)$	exponential function e^x
\sum	summation symbol
j	imaginary unit $j = \sqrt{-1}$
$f(\cdot)$	probability density function
$!$	factorial operator
$\Pr(x)$	Probability of x
$\log_x(\cdot)$	logarithmic function to base x
$ \cdot $	magnitude of a complex number
$(\cdot)^*$	conjugate
\max	maximum of the argument
$(\cdot)^T$	transpose
$*$	convolution operation
$\mathbb{E}[\cdot]$	expectation value of a random variable
$Q(\cdot)$	Gaussian Q-function
$\mathcal{G}(\cdot)$	Gaussian PDF

List of Variables

τ	Time Delay
k	Attenuation exponent factor
a_o/a_1	Attenuation parameters
g_i	Weighting factor
v_p	Velocity of propagation
f	Frequency
A	Impulsive index
H	Channel transfer function
ϵ_r	Dielectric constant
d	Distance
c	Speed of light
R	Distributed resistance
L	Distributed inductance
C	Distributed capacitance
G	Distributed conductance
μ	Permeability

ε	Permittivity
σ	Conductivity
γ	Propagation constant
Z_c	Characteristic impedance
ω	Angular frequency
α	Attenuation constant
β	Phase constant
Z_{eq}	Equivalent impedance
l	Length
Z_S	Source impedance
Z_L	Load impedance
p	Probability of impulsive noise occurrence
Γ	Gaussian-to-impulsive-noise ratio
σ_g^2	Variance of background noise power
σ_i^2	Variance of impulsive noise power
σ_t^2	Variance of total noise power
σ_m^2	Variance of the power of the mth pulse
g_k	White Gaussian noise with zero mean
N	Number of sub-carriers
b_k	Bernouli process parameter
σ_s^2	Variance of transmitted signal power

T_b	Blanking threshold
T_c	Clipping threshold
V_S	Source voltage
V_L	Load voltage
E	Total signal power at the output of nonlinear preprocessor
$G_{Relative}$	Relative gain
$r^{(k)}$	k-th received symbol
y_k	Output of nonlinear preprocessor
\bar{s}_q	Time-domain signal after IFFT
K_0/K	Scaling factor
$Peak_0$	Threshold peak value used by nonlinear preprocessor
\bar{r}_k	Input of nonlinear preprocessor
$Peak(k)$	Peak value associated with the k-th received symbol

Chapter 1

Introduction

The energy industry is in the centre of an unprecedented transformation. Although the challenges are enormous, so are the opportunities. Development of smart grid represents a giant leap towards an intelligent, secure and sustainable energy future. However, it requires intellectual horsepower, new initiatives from stakeholders and cross-sectoral integration between energy and ICT. The last few decades witnessed proliferation of communication technologies, a fundamental design choice in smart grid is whether the enabling communication system will be based on wireless or wireline technology.

PLC has made remarkable strides to emerge as a candidate technology for smart grid and other cyberphysical systems [6]. Although smart grid will be supported by heterogeneous set of communications systems [7,8], one of the main advantages of PLC is that the electric cables are readily available which reduces the cost of communication and further simplifies the network management. A shared requirement among smart grid applications is that the enabling communication network must consistently provide error-free transmissions. However, given that power cables were not custom-made for communication, they pose severe challenges to data signals [9–11]. In particular, impedance, noise and attenuation vary with time, location and frequency, hence they are highly unpredictable [10, 12]. Other challenges include frequency selectivity and multi-pathing. These factors degrade system performance in terms of achievable throughput, bit-error rate (BER), latency, signal-to-noise ratio (SNR) at the receiver and can also impact the power requirements of the PLC system.

1.1 Motivation

To address the multitude of challenges confronting the power grid, integration of two-way communication systems has been identified as a critical element. Although PLC has evolved in terms of standardisation and use-cases including smart grid applications over the last two decades, there are new indications that energy efficiency is crucial for the underlying communication systems. Unlike other aspects of PLC such as channel characterisation and noise modelling, energy efficiency of PLC system has not received much attention so far. This issue can be investigated with practical and information theoretic approaches [13]. To manage power requirements of PLC systems, a variety of techniques has been proposed, such as distributed space-time block coding [14], opportunistic decode-and-forward (DF) relaying [15], resource allocation optimisation [13] and incremental DF relaying [16]. Recently, [17] and [18] considered energy harvesting at the relay nodes in a cooperative PLC network. Both studies concluded that energy efficiency of the system can be remarkably improved if PLC nodes are capable of harvesting the unwanted high energy of the non-Gaussian noise present in the power line channel.

In terms of experimental studies, [19] reported that in a DF relay-assisted PLC network, energy efficiency can be improved by optimal time allocation in the relaying scheme. A recent measurement campaign across six European countries [20], concluded that static power consumption in PLC networks can be reduced by deploying DF multiple-input, multiple-output (MIMO) relays. Further experiments with the MIMO PLC devices [21] revealed that although energy consumption is mostly dominated by static power, dynamic power can be up to 50% in some modems, with the average being 40%. Within the dynamic power, it was also observed that data reception consumes less energy than transmission by 20-25%.

It can be inferred from those studies that energy optimisation in PLC can be addressed in a variety of ways including optimised transceiver design and advanced signal processing. The key motivation for this work is therefore the possibility to explore these areas and develop new energy-efficient techniques for PLC systems.

1.2 Research Objectives

This thesis investigates and proposes techniques that can aid energy efficiency in PLC systems. In designing the system components, a combination of modelling, measurements, experimentation and numerical analysis is required. To fulfill this mandate, it is necessary to test the proposed systems components on a layer-by-layer basis. In view of that, the optimisation of energy discussed in this thesis is carried out at three layers of the transmission control protocol (TCP)/Internet protocol (IP) stack; namely network, adaptation¹ and physical (PHY).

- At the network layer, part of this work investigates the topology of LV distribution network and considers clustering of smart meters in the neighbourhood area network (NAN) into smaller sub-networks to improve efficiency of data transmission.
- At the adaptation layer, the second part of this thesis investigates energy optimisation by considering a HAN where devices are constrained to transmit at low data rate in order to save energy. This approach is based on the premise that power consumption in PLC modems is a function of traffic load [21, 22], hence reduction in data rate invariably reduces power consumption.
- The third piece of work exploits advanced signal processing techniques for modulation and dynamic noise cancellation method at PHY layer to reduce the energy requirements of PLC transceivers.

1.3 Key Contributions

The main contributions of this thesis are outlined below.

- By intelligently altering the communication network configuration over the LV power lines, it is shown that communication between smart meters and utility network can be enhanced in terms of coverage and reliability which impact on energy requirements.

¹The adaptation layer sits between data-link and network layer to provide the fragmentation and reassembly required between constrained PLC and convention IPv6-capable networks (RFC 4944)

- Demonstration of low-power PLC network for energy management networks suitable for customer premises such as homes, offices and small industrial facilities. A part of this thesis provides strong evidence that in-building monitoring and control application can be suitably supported by the proposed low-power PLC network model since they typically require low data rates. This outcome can potentially open up new opportunities in building management services for home and industrial users.
- Symbol vectorisation in multi-carrier modulation system. This approach allows a smart trade-off between complexity and energy-efficiency in PLC transceivers by taking advantage of the vector blocks in vector OFDM to support variable inverse fast Fourier transform (IFFT) size. This brings new flexibility to the design of future PLC systems for smart grid applications without losing the fundamental benefits of OFDM as a multi-carrier scheme.
- Proposal of a more efficient impulsive noise cancellation technique. The proposed method determines signal peaks based on the values received from the transmitter-side and does not require detailed measurement of noise characteristics at the receiver. Unlike the typical blanking methods, shifting peak measurement to the transmitter-side can reduce the effects of transmitter-receiver unbalanced complexity in systems design.

It is believed that the next few years will witness rapid actualisation of many smart grid applications over power lines. These results can lead to improved packet routing and more efficient PLC transceivers at reduced cost.

1.4 Thesis Organisation

The remaining part of this thesis is organised as follows. Chapter 2 provides a general background to this thesis. It covers a brief literature review on smart grid and its applications, power line channel and noise. Numerical analyses of widely-used channel characterisation and noise modelling techniques are also provided and the chapter ends with a brief review of energy efficiency in PLC systems. In chapter 3, efficient PLC network topology for clustered AMI is discussed. In this chapter, rather than direct transmission from smart

meters to the concentrator, the meters are reorganised into clusters and a local aggregator is introduced within each cluster. With this approach, network coverage and packet delivery can be enhanced, both of which positively impact energy consumption.

Chapter 4 demonstrates low-power PLC networks for monitoring and control applications in HEMS. This chapter describes the network model developed in NS-3 and the experimental testbed used for validating simulation results and includes all system parameters used in the study. In chapter 5, energy efficiency is addressed with two complimentary approaches; use of V-OFDM for multi-carrier modulation and application of a dynamic noise mitigation technique at the receiver. In the chapter, performance of the proposed V-OFDM is compared with conventional OFDM on one hand while DPTE is compared with typical noise cancellation techniques such as conventional optimal blanking (COB) on the other, highlighting the performance gain in both cases. In chapter 6, the main conclusions of the various pieces of work in this thesis are discussed. The thematic organisation of this thesis is presented in Figure 1.1. It should be noted that Chapters 3, 4 and 5 address the energy optimisation at network, adaptation and physical layers respectively. These represent three methods which can be implemented independently and that is the approach adopted in this thesis. In practical systems, it may be possible to combine them in various ways depending on specific application requirements but they are generally complimentary techniques.

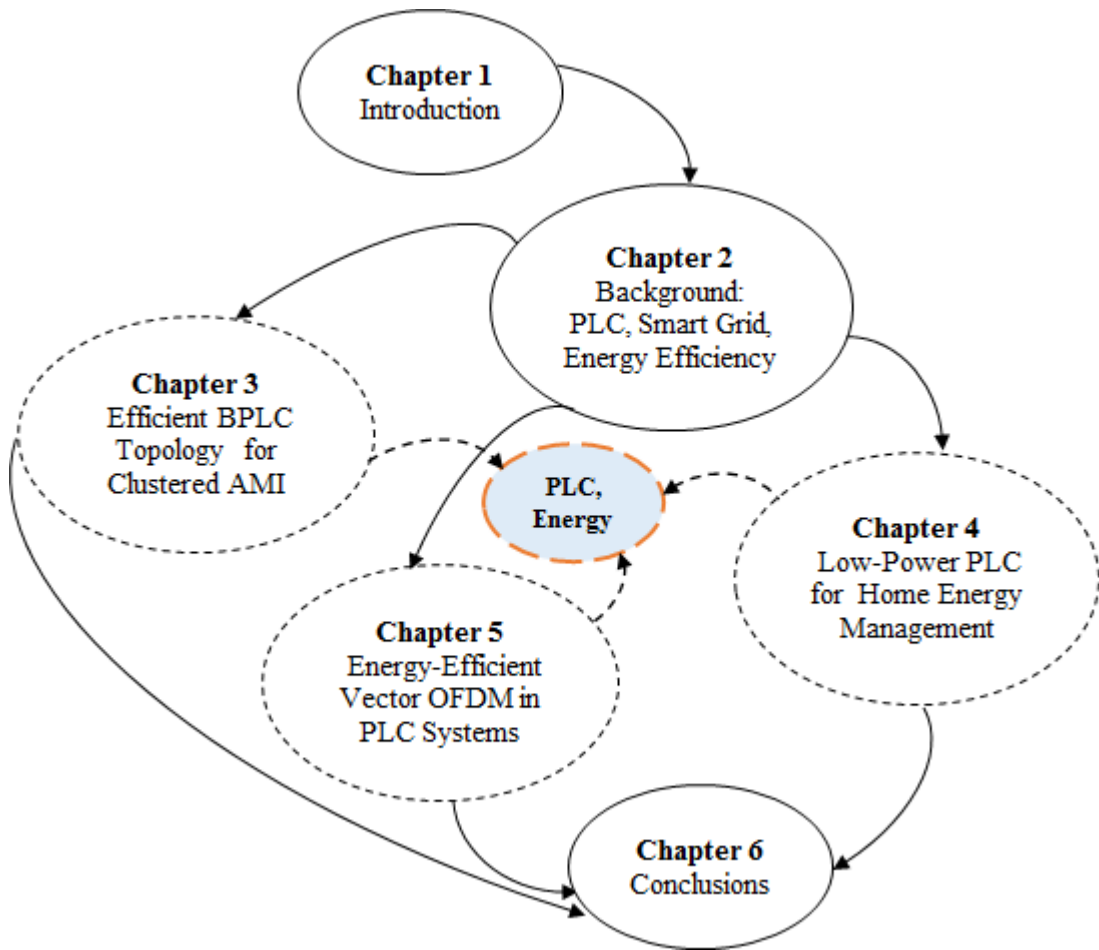


Figure 1.1: Thematic organisation

1.5 List of Publications

Journal Papers

1. **Augustine Ikpehai**, Bamidele Adebisi and Khaled M. Rabie, "Energy-Efficient Vector OFDM PLC With Dynamic Peak-Based Threshold Estimation", IEEE Access, May 2017.
2. Khaled M. Rabie, Bamidele Adebisi, Haris Gacanin, Galymzhan Naurzybayev and **Augustine Ikpehai**, "On the Energy Efficiency of Multi-hop Relaying Power Line Communication Systems", Journal of Communications and Networks, 2017 (Accepted 23rd March 2017, to appear).

3. Matjaz Rozman, Michael Fernando, Bamidele Adebisi, Khaled M. Rabie, Rupak Kharel, **Augustine Ikpehai** and Haris Gacanin, "Combined Conformal Strongly-Coupled Magnetic Resonance for Efficient Wireless Power Transfer", *Energies*, vol. 10, no. 4, pp. 498, April 2017.
4. Bamidele Adebisi, Khaled M. Rabie, **Augustine Ikpehai**, Cinna Soltanpur and Andrew Wells, "Vector OFDM Transmission Over Non-Gaussian Power Line Communication Channels", *IEEE Systems Journal*, no. 99, pp. 1-9, March 2017.
5. Yakubu Tsado, Kelum A.A. Gamage, Bamidele Adebisi, David Lund, Khaled M. Rabie and **Augustine Ikpehai**, "Improving the Reliability of Optimised Link State Routing in a Smart Grid Neighbour Area Network based Wireless Mesh Network Using Multiple Metrics", *Energies*, vol. 10, no. 3, pp. 287, Feb. 2017.
6. **Augustine Ikpehai**, Bamidele Adebisi, Khaled M. Rabie, Russell Hagggar and Mike Baker, "Experimental Study of 6LoPLC for Home Energy Management Systems", *Energies*, vol. 9, no. 12, pp. 1046, Dec. 2016.
7. **Augustine Ikpehai**, Bamidele Adebisi, and Khaled M. Rabie, "Broadband PLC for Clustered Advanced Metering Infrastructure (AMI) Architecture", *Energies*, vol. 9, no. 7, pp. 569, Jul. 2016.
8. Arshad Ali , **Augustine Ikpehai**, Bamidele Adebisi, and Lyudmila Mihaylova, "Location Prediction Optimisation in WSNs using Kriging Interpolation", *IET Wireless Sensor Systems*, vol. 6, no. 3, pp. 74-81, Jun. 2016.
9. Peter O. Aiyelabowo, Nor Kamariah Noordin, **Augustine Ikpehai** and Bamidele Adebisi, "Cooperative Relaying in Power Line Environment: A Survey and Tutorial", *International Journal of Innovative Research in Computer and Communication Engineering* vol. 3, no. 5, May 2015.
10. Yusuf Sha'aaban, Augustine Ikpehai, Khaled M. Rabie, Bamidele Adebisi, "Optimal Coordination of Electric Vehicles in Virtual Power Plants Using Model Predictive Control", (Submitted to *Computer Networks* 2nd June 2017, under review).

Conference Papers

1. **Augustine Ikpehai**, Bamidele Adebisi, and Rupak Kharel, "Smart Street Lighting over Narrowband PLC in a Smart City: The Triangulum Case Study", in Proc. IEEE 21st International Workshop on Computer Aided Modelling and Design of Communication Links and Networks (CA-MAD), Toronto, Ontario, Canada, pp. 242-247, Oct. 2016.
2. **Augustine Ikpehai** and Bamidele Adebisi, "Home Energy Management System over Low-Power Narrowband PLC", in Proc. IEEE 10th International Symposium on Communication Systems, Networks and Digital Signal Processing (CSNDSP), Prague, Czech Republic, pp. 1-6, Jul. 2016.
3. Matjaz Rozman, **Augustine Ikpehai**, Bamidele Adebisi, and Khaled M. Rabie, "Channel Characterisation of Cooperative Relaying Power Line Communication Systems", in Proc. IEEE 10th International Symposium on Communication Systems, Networks and Digital Signal Processing (CSNDSP), Prague, Czech Republic, pp. 1-6, Jul. 2016.
4. **Augustine Ikpehai** and Bamidele Adebisi, "6LoPLC for smart grid applications", in Proc. IEEE International Symposium on Power Line Communications and its Applications (ISPLC), Austin, Texas, USA , pp. 211-215, Mar. 2015.
5. Arshad Ali, Xydeas Costas, Lyudmila Mihaylova, Bamidele Adebisi and **Augustine Ikpehai**, "Kriging Interpolation Based Sensor Node Position Management in Dynamic Environment", in Proc. IEEE 9th International Symposium on Communication Systems, Networks & Digital Signal Processing (CSNDSP), Manchester, UK, pp. 293-297, Jul. 2014.

Chapter 2

Background Theory

This chapter provides a review of smart grid, its applications, potential communication technologies the requirements of various traffic types. Section 2.1 provides a brief overview of smart grid and its communication challenges. This is followed by a review of the IEEE 2030 reference design with its architectural perspectives mapped into a logical network to produce a representative model of the smart grid. Description of the various smart grid applications and their traffic characteristics are also included. In Section 2.2, a comparative analysis of different communication technologies is carried out, highlighting their capabilities, strengths and weaknesses with respect to smart grid while Section 2.3 focuses on PLC as a promising communication technology for smart grid applications. Various aspects of PLC such as channel characteristics, attenuation, noise and spectrum regulations are discussed. Section 2.4 identifies energy-efficient communication as a gap in smart grid development and proposes a cross-layer approach. In doing that, the Section also analyses the current trend in energy optimisation in PLC systems and adopts a cross-layer approach. Section 2.5 concludes this chapter.

2.1 Smart Grid and Communication Technologies

2.1.1 Smart Grid and its Motivation

Electrification is viewed as the most significant achievement of the 19th century, as it is one service that affects everyone. However, the power grid has

been recently described as a product of rapid urbanisation [7]. That declaration may have originated from the fact that the current power infrastructure is not significantly different from when it started over 100 years ago. Depleting natural reserves, rising concerns on green-house emissions and global warming, call for sustainable generation as well as the need to guarantee energy security have all indicated that the traditional grid can no longer meet the challenges faced by modern society. While local circumstances may vary across jurisdictions, the key issues are summarised below [23], [24]

1. Ageing infrastructure that has mostly reached the end of its useful life, which results in suboptimal performance.
2. Steady rise in electricity demand which has resulted in grid imbalance, overloading or unplanned brownouts and blackouts.
3. Increased distance between generation sites and point of consumption, which aggravate losses.
4. Environmental concerns on the primary energy sources
5. Variable energy mix that includes distributed generation which are not readily supported by the traditional grid.
6. Adoption of more renewable sources for sustainable generation, however, given their intermittent nature, sophisticated monitoring and control are needed to consistently maintain a balanced grid.
7. Need to develop new consumption and pricing models to support flexible consumption such as plug-in electric vehicle (PEV) charging at off-peak periods.
8. Increasing cost of maintenance.
9. Consumer protection and regulatory pressure for more competitive and lower energy prices
10. Capacity margin to secure supply in case of abrupt increase in demand.

While the above list is by no means exhaustive, it reasonably justifies the call for modernisation of the grid. Advent of PEVs is revolutionary and has further exposed the limitations of the legacy power grid. However, if properly

harnessed, PEVs will help to uncover new opportunities in terms of operating them as energy islands to provide power to homes during peak demands, thereby avoiding the huge costs associated with running of high-capacity generators. Stakeholders in the energy sector (utilities, vendors, equipment manufacturers, regulators, consumers, the research community) have realized the enormous challenges plaguing the traditional grid and in response, the idea of next generation power grid, also known as *smart grid* was developed as part of the new energy management strategy. To avoid the same pitfalls as the traditional infrastructure, the smart grid integrates the cyber and physical elements of the grid to uncover new possibilities such as integrating renewables into the energy mix, employing smart demand management methods and reducing the energy losses over the power lines [25].

The smart grid will not only fulfil its traditional role of delivering electricity but will also support evolution of end-use applications on sustainable basis. In describing the smart grid, there is no single universally-accepted definition, it can be defined in simple terms and ways that are more complex [26]. However, the definitions include some common themes such as ICT, integration, automation and control all of which ensure sustainable, economic and secure end-to-end processes within the energy value chain. Therefore, a smart grid integrates advanced monitoring and control functionalities into the electricity grid using the power of ICT. This improves efficiency, reliability and reduces environmental pollution. Although the legacy grid contains limited intelligence, it is mostly concentrated in central locations such as generation and large transmission stations, while remote components such as customer domains are totally passive [27]. By including these themes, the power grid transforms to a more responsive and self-healing infrastructure that not only empowers consumers to become active stakeholders but also provide them with more information to make informed choices regarding their participation either as producers or consumers of energy.

The promises of smart grid include lower transmission/congestion cost, improved reliability, power quality, flexible peak shaving, sustainability, energy security, higher efficiency and reduced cost of maintenance (due to lower wear-and-tear in large generators). At the end, the smart grid is beneficial to both utilities and consumers. Following these realisations, it is widely agreed that development of a smarter grid is rather a necessity than choice. In view

of this, system-wide monitoring and control have been identified as major design components to be included in the smart grid. The role of the communication technologies is to facilitate timely exchange of information for sensing and control operations that will ensure efficient generation, transmission, delivery and storage of electricity [25].

2.1.2 Communication Challenges in Smart Grid

The traditional power grid is viewed in terms of some central stations generating electricity and supplying it to end users with limited communication. In contrast, the underpinning technology that interconnects smart grid system components is communication. Smart grid deployment can be approached in many ways.

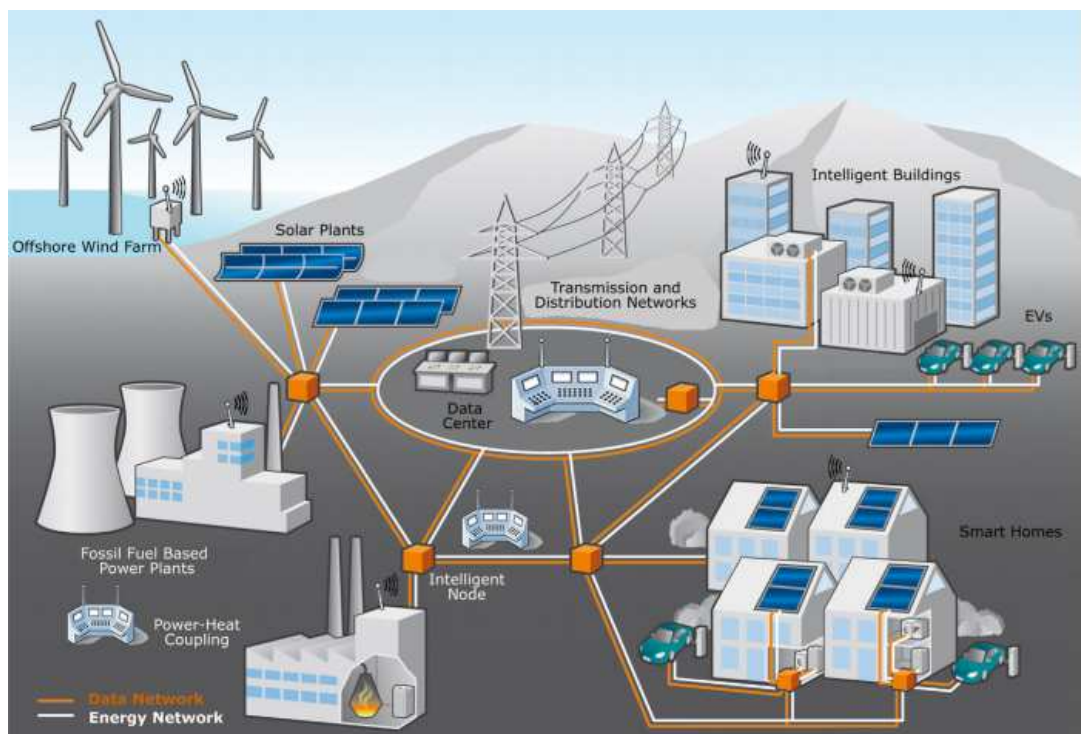


Figure 2.1: A schematic of smart grid showing energy and communication networks using wireless and wireline technologies [1]

Figure 2.1 illustrates the smart grid concept showing the communication and power components, the communication system can be wireless, wired or hybrid. While it is possible to simply design the functional components and integrate them, inclusion of large scale ICT solutions also necessitates a

rethink of the power system as an autonomic, self-organised platform whose operations can be deterministically guaranteed within acceptable limits [28] -the hallmark of a truly smart grid. Therefore, the grid is as reliable as the enabling communication system. The implication is that grid performance will depend heavily on the communication network. This impose new burdens on the communication systems as outlined below [28], [29].

2.1.2.1 Integration and Interoperability

The smart grid should allow utilities and consumers to procure hardware or software and deploy them into different areas of the grid in a plug-and-play manner. As smart grid integrates technologies from different vertical domains which are at different levels of maturity and investment, it is expected that development of various aspects of smart grid from conception to implementation will naturally happen at different speeds – application layer services (fastest), ICT (fast), power (relatively slower). It is therefore possible to encounter application-layer services without due regard for how they perform in different system operating conditions and their impacts on other system components in terms of co-existence and interoperability. Considering the scope of smart grid, a large variable set needs to be tested. However, given the critical nature of power grid and the huge investment it requires, it is practically challenging to conduct such tests on a large scale. To address this issue, the communication systems must be based on standard design paradigms and protocols such as TCP/IP in order to drastically reduce interoperability and integration challenges in real implementations.

2.1.2.2 Scale and Complexity

The power grid is evolving toward an automated infrastructure that uses smart technologies to monitor and manage power availability and quality, the immediate and predicted load demands as well as the status of supporting systems. As communication and information technology (IT) industries converge to create larger and more complex system-of-systems, the explosive amount of data arising from end-use applications and their dependencies may rise to a scale unprecedented. To manage, store and use this data,

power system and ICT need proper handshake and coordination. It is therefore necessary to understand the demands for communication resources in such distributed interactions.

2.1.2.3 Distributed Intelligence

One of the key drivers of smart grid concept is that as more consumers become self-reliant at different times due to local energy management systems or renewable generation, demand on the grid will vary accordingly. While this is a reasonable expectation, the variation may occur almost unpredictably. This requires that a significant amount of intelligence be devolved from the core of the power network, towards the edges to allow end devices respond to network stimuli whenever they occur.

2.1.2.4 Security and Privacy

Expanded capabilities for power grid systems and networks such as distributed intelligence and broadband capabilities can greatly enhance efficiency and reliability, but they may also introduce new security concerns that are more complex than imagined. The concerns cover a wide spectrum ranging from physical security of ICT and electrical equipment to cyber security including the vulnerabilities in hardware and software that will run in the power network. Similar to conventional data networks, providing remote access to power network assets through communication links increases accessibility, security risks and vulnerabilities as the entire network can be compromised through a single node. For example smart meters are the most common components on the demand-side acting as gateway in many cases. Unauthorised access to the smart meters can help an attacker steal valuable information or disrupt normal operation of the facility.

2.1.3 Reference Design and Communication Architecture

In order to discuss the smart grid network, it is necessary to first describe its architecture. The smart grid is a convergence of technologies and services from multiple industries such as power, communications, and information technologies. That combined with the scale, complexity and cross-functional

nature of the system makes it difficult to agree on a precise architecture. However, the IEEE 2030 is widely accepted as a reference model. The IEEE 2030 reference architecture [29], which eventually evolved into the smart grid interoperability reference model (SGIRM), consists of two broad components: (i) the smart grid interoperability architectural perspectives (IAPs) and (ii) the characteristics of the data that flows between entities within the perspectives. From implementation point of view, the IAP components provide insights from power systems and information and communications technology domains. In order to address the uniqueness of each area and promote interoperability among the system components, three IAPs were subsequently defined as power system IAP (PS-IAP), information technology IAP (IT-IAP) and communications technology IAP (CT-IAP). While the (PS-IAP) focuses on generation, delivery and consumption of power, the (IT-IAP) is mainly concerned with data management and process control. Lastly, the CT-IAP focuses on the connectivity, providing guidelines for communication networks, protocols, media and performance. It is such interoperability that laid the foundation for supporting critical systems/services such as AMI and PEV. The CT-IAP is of most interest in this thesis. For design purposes, the CT-IAP specifies three types of networks summarized as follows [30], [31].

- The customer premises network (CPN)/energy service interfaces (ESIs), the CPN comprises customer-side networks such as HANs, building area networks (BANs) and industrial area networks (IANs) for connecting intelligent electronic devices (IEDs) in the consumer domains to allow energy status to be monitored and remotely controlled.
- The NANs, to interconnect energy service interface (ESI) and smart meters to utility operations and control centre.
- The backhaul, for interconnecting utility network to other networks in the distribution and consumer domains.

These CT-IAP specifications are mapped into the logical networks presented in Figure 2.2.

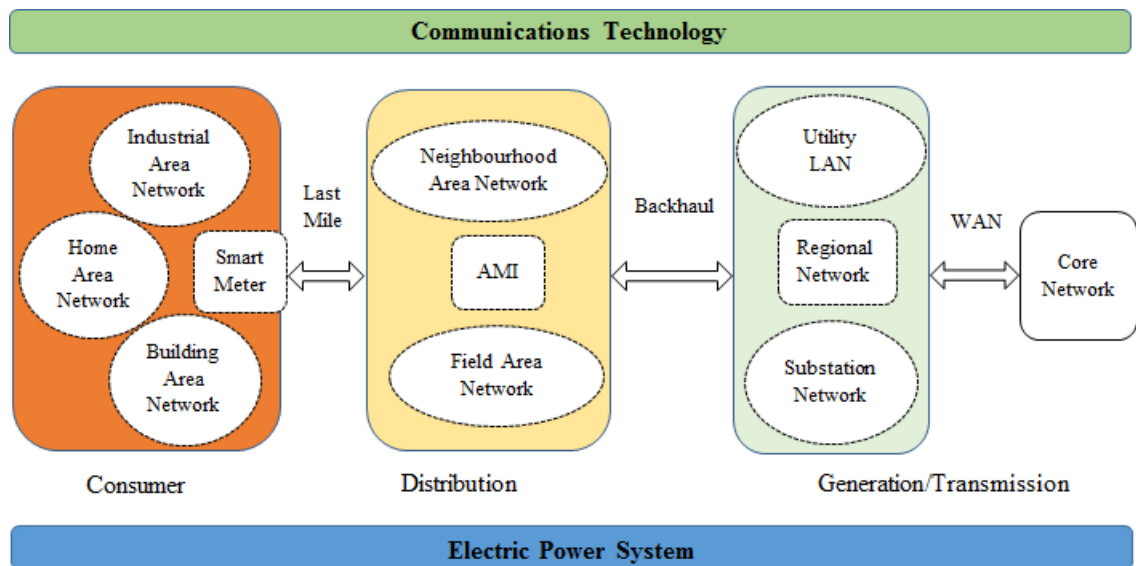


Figure 2.2: End-to-end smart grid communication model based on IEEE 2030-2011 reference model [2]

- ESIs/customer premises network: ESIs are special class of device in that they are used as gateway in customer premises networks such as HAN, building area network (BAN) and industrial area network (IAN). The ESIs allow services such as remote load control (RLC), reading of non-energy meters and integration with building management systems. They are also capable of logging transactions between utility and HAN.
- Field area network: FANs connects the distributed substations, distributed energy resources (DERs)/microgrids to the utility operations and control centre.
- Utility local area network (LAN) (operations and control center): monitors, controls, supervises and manages processes and data flow. The control/operations centre can be a single integrated entity that manages transmission and distribution or one control entity for each transmission and distribution segment.
- NAN: connects smart meters, DERs/microgrids to the utility operations and control center.
- Wide area network (WAN): a communication network that connects other network segments (substations, backhaul, last mile) to the utility control centre. WAN typically covers large geographic area, may be

wired or wireless.

- **Backhaul:** this communication link connects the utility control/operations centre and major subsystems such as the AMI to the downstream network segment through the WAN. It is usually owned or managed by the utility/third party and can be wireless or wired. A typical NAN or FAN usually has more than one backhaul to the WAN.
- **Workforce mobile network:** used by utility's workforce to provide dispatch, maintenance and normal day-to-day operations.
- **Last mile:** connects the energy consumer to other parts of the network.
- **Regional network:** interconnects a utility network to other utilities through private or public networks, usually with optical fibre cable (OFC).
- **Substation network:** interconnects devices within a distribution substation. It is controlled and supervised remotely via backhaul, also connected to DER/microgrid, NAN/FAN.

The power generation and transmission domains consist of plants and large substations connected via communication system provided by third party network providers. Interconnection between these domains is mostly provided through wireline technologies such as OFC and digital subscriber line (DSL). The distribution domain covers a vast geographical spread containing feeders and end-user loads. From communications perspective, the distribution domain also includes the last mile to customer premises as it extends services to buildings through the meters and enables applications such as smart metering and demand response (DR). The WAN can also connect distribution domain to utility's backbone network. The consumer domain is the most visible part of the grid to the end-user. It consists mainly of user loads such as home appliances, machineries (in factory environment), PEV and other loads whose operation and control are consumer's responsibility. In the case of PEV, while it can be used to store excess energy from the grid during a grid-to-vehicle (G2V) event, it can also feed electricity back to the grid in vehicle-to-grid (V2G) operation when it is most needed at peak demand. The former process is called valley-filling while the latter is known as peak-shaving. Apart

from losses due to dissipation and other wastages, most energy consumption take place in customer domain. Hence, achieving energy efficiency there, can significantly impact the other power domains.

2.1.4 Smart Grid Applications and Traffic Characteristics

A plethora of commercial applications has emerged in smart grid, the notable application shall be discussed in this Section [2], [32].

2.1.5 Smart Metering

Smart metering automatically obtains consumption, status and diagnostic information from a power metering device and send them to the utility through a communication network. Such information can be used for billing, forecast, planning and troubleshooting. It is the most basic smart grid application. With smart metering, routine meter reading by personnel of utility companies is no longer required. Several standards have been published to regulate its implementation, most notable ones are ANSI C12.1-2008, IEEE 1377 and IEC 61968-9. Specific services associated with smart metering include:

- **Meter reading:** the smart meter uploads its reading to a meter data management server (MDMS) via available communication link according to a predefined schedule. Upload may also be on-demand to enable utility attend billing inquiries or verification of outage and service restoration.
- **Events and alarms:** based on embedded intelligence, a smart meter may report system log or alarm to indicate current or impending service failures. Such messages include tamper alarm, disconnection, hardware failure, under voltage, over voltage, abnormal power condition or any unusual event in the meter. These messages are sent to MDMS for further analysis and resolution.

2.1.6 Demand Response

Demand response (DR) enables utility to optimally balance generation with demand by either offering incentives in form of flexible pricing or employing

some load scheduling programs. By dynamically changing energy tariff, customers are encouraged to reduce power consumption at peak periods or shift their loads to less critical periods in order to take advantage of lower off-peak tariffs. Here, the communication link helps to convey the price signal from utility server to the home display unit via the smart meter. Upon receiving the price information, the customer decides to either reduce consumption or shift some (or all) loads. Some dynamic pricing programs are already available, they include

- Time of use (TOU): a DR program in which each day of the week is subdivided into contiguous blocks of hours and energy price varies from one block to another. The highest tariff is allocated to the block containing peak-period hours.
- Real time pricing (RTP): a practice in which electricity tariff varies on hourly basis as a reflection of actual cost of delivering energy at that moment.
- Critical peak pricing (CPP): it is similar to TOU but applies to relatively smaller number of days.
- Peak time rebates (PTR): here, the customer receives a rebate for not consuming energy at all during peak hours. A more innovative way of implementing this is to use remote load control (RLC) program in which response of domestic devices to such rebates is automated via machine-to-machine (M2M) communication [2]. For instance, the energy management system (EMS) could dynamically program the thermostat to change the threshold temperature in response to price signal. To achieve the desired level of efficiency, the RLC needs to be aware of nature of the loads under its control. The controllable loads can be classified as below.
 - Interruptible loads: the normal operations of these loads can be interrupted at peak hours and suspended till less critical hours of the day. Examples include washing machine, water sprinkler, dryer and dish washer. These loads are expected to become active after the peak period when demand or overall consumption should have

averaged out. These types of load require simple control signal to interrupt and reschedule their operations.

- Reducible loads: these are the types of loads that can be reduced for certain duration of time. For instance, at peak period, the thermostat of an air-conditioner or a refrigerator can be set to a higher threshold temperature in order to reduce total load in the house.
- Partially interruptible loads: for this type of loads, their operations can be staggered in response to price information by adjusting their duty cycle. For example, a 50% duty cycle of a washing machine will result in 30 minutes run-time per hour. For such loads, two control signals are required; one to start the reduced duty cycle and the other to restore normal operations.

2.1.7 Plug-in Electric Vehicle

A PEV is a motor vehicle propelled by one or more electric motors. The electric motors derive their energy from on-board rechargeable batteries. Therefore, every PEV contains a battery bank that can be recharged from the electricity grid. Though most PEVs are expected to be recharged at home, public charging stations are already available and are becoming popular. According to [33], when PEVs connect back to the grid for after-work charging, if not properly managed, they could result in daily charging peak in the evening. This scenario can also cause overloading of the distribution circuit of traditional power grid [2] the effect of which include higher loss on transmission line and damage of utility equipment [34–36]. Smart charging [37–39] has been proposed to leverage the 2-way communication of smart grid to mitigate these problems. Additionally, PEVs was suggested in [40][12] to store energy from renewable sources and convey it back to the grid as a way to mitigate the effects of intermittent generation from renewable sources, this is the essence of V2G [41].

2.1.8 Substation Automation

This refers to the use of information from IEDs and control subsystems to monitor, protect and control substation and feeder equipment. IEC 61850 and

distributed network protocol, version 3 (DNP3) are the most widely accepted standards for such implementation. While the DNP3 covers communication for low-bandwidth monitoring and control operations only, the IEC 61850 specifies requirements for real-time, bandwidth-intensive protection and control applications and most aspects of substation automation system [2]. The IEC 61850 supports communication between IEDs either within substation (e.g. protection signal to circuit breaker) or on feeders (e.g. automated switches along a feeder responding to isolate a fault). Many types of IEDs are defined in IEC 61850. IEC 61850 also defines abstract communication service interface (ACSI) that includes querying devices, setting parameters, reporting and logging [40]. Message exchange in ACSI is similar to file transfer protocol (FTP) session in which communication starts with handshaking (negotiation of connection parameters), followed by data exchange and session termination.

2.1.9 Distributed Energy Resources (DERs) and Microgrids

They are smaller sources of power or storage connected to the power grid to meet demands. DERs can be renewable or non-renewable. They can also be distributed generation (DG) or distributed storage (DS). Examples include photovoltaic (PV) cells, battery banks, fuel cells and wind turbine. They are essentially smaller energy sources that can be combined to meet regular demands. As the electricity grid continues to transform, DERs such as DS and advanced renewable technologies are facilitating the transition to a “smarter” grid. A microgrid is a localised power setup consisting of one or more DERs and load. In the event of fault or maintenance on main grid, a microgrid can operate autonomously; providing power to the local load [42,43][29][30]. A microgrid can be utility microgrid; operating as part of the utility or industrial/commercial microgrid serving specific customer’s facilities only. While the DER/microgrid systems are located in the distribution domain, energy transfer between them must be coordinated, IEEE 1547.3-2007 standard was specifically drafted for this purpose.

2.1.10 Wide Area Measurement System (WAMS)

Wide area measurement system (WAMS) is a sophisticated sensing and measurement technology for monitoring the electricity grid; it is necessary for situational awareness of grid condition. Measurements include system state and power quality. The main sensors in WAMS are the phasor measurement units (PMUs). A PMU at a substation measures voltage and current phasors and measurements can be reported at the rate of 20-60 times per second [2]. With such a high resolution, PMU measurements have strict delay bounds such that a measurement must be transmitted before the next one becomes available. In a WAMS, each measurement is time-stamped by global positioning system (GPS) units integrated in PMU. Traditionally, PMUs were installed in the high voltage regions (generation and transmission domains) due to the top-down flow of electricity. To achieve real-time monitoring of entire energy infrastructure, PMU needs to be extended to the distribution segment of power grid [44,45].

2.1.11 Distributed Supervision

The role of distributed supervision is to provide additional layer of monitoring for the electricity distribution domain and help to proactively identify impending failures before they jeopardize public safety or lead to service outages or obstructions. Unlike the sensing and measurement applications at specific locations in the power grid, the scope of distributed supervision is extensive and covers even passive elements such as transmission lines and branching points [46]. It is therefore expected that in smart grid, overhead lines will be fitted with sensing devices and actuators for continuous and preventive monitoring. Similarly, the underground transmission lines will have sensors to measure the ambient conditions around the buried conductor. Sensors can also be used to monitor weather conditions since they affect renewable sources. For instance, solar energy is usually unavailable at night when it is dark and energy from wind farm depends on wind direction and speed. In addition, PV cells require temperature and radiation sensor to forecast energy output. These are all required to optimize power generation [47]. The IEEE 1451 defines a family of open standards that are network-agnostic for communication between sensors and actuators in this area.

Having presented the various smart grid applications, it is now necessary to discuss their traffic characteristics and communication requirements. Based on the reference architecture outlined in Section 2.1.3, various services can be rendered using the applications. The communication requirements of the various services are summarised in Table 2.1 [2, 27, 48, 49].

Table 2.1: Traffic characteristics and communication requirements

Application	Data (bytes)	Latency	Reliability(%)
Meter reading(on-demand)	100	<15 s	>98
Meter reading(scheduled)	0.4-2.4k	<4 hr	>98
Bulk meter reading	MB	<2 hr	>99.5
Pricing-signalling	≤ 100	<1 min	>98
Electric service prepayment	50-150	<30 s	>98
DR (RLC, peak price signal)	60-100	<1 min	>99.5
DA (CBC, VR)	0.1-1k	<5 s	>99.5
DA (open/close switch)	150-250	<5 s	>99.5
Outage management	25	<20 s	>98
V2G, G2V	100-255	2s -5 mins	>98
Firmware update	0.4-2k	<2 min-7 days	>98
Configuration update	25-50k	<5 min-3 days	>98
TL monitoring (cable tilt, strain)	8	15-200 ms	>98
TL monitoring (power quality)	16	15-200 ms	>98
Home energy management	≤ 100	0.3-2 s	>98
Asset management	≤ 100	2 s	99

CBC: capacitor bank controller, VR: voltage regulator, TL: transmission line,
DA: distribution automation

2.2 Wireline and Wireless Technologies

Bi-directional communication is an indispensable part of smart grid but the specific technologies will be chosen from existing array and adapted to support the diverse needs of the grid. This Section provides a comparative analysis of wireline and wireless technologies as well as their suitability in the various network segments of the power grid. It is observed that the architecture in Figure 2.2 follows a hierarchical design. As each of the network segment carries out different functions, the hierarchy suggests that their requirements will also differ. For example, while the WAN covers a reasonably large geographical space (generating plants to transmission stations) and requires long range technologies such as worldwide interoperability for microwave access (WiMAX) or optical fibre, Ethernet, wireless fidelity (Wi-Fi) and ZigBee are suitable in HANs. In reality, the end-to-end connectivity will be deployed on the basis of mix-and-match to cater for each network segment from consumer-side to the utility. The list of communication technologies and their features is summarised in Table 2.2 [1, 49, 50].

Table 2.2: Wireline and wireless communication technologies

Technology	Standard	Data rate (bps)	Range	Network
Fibre optic	PON	155 M-40 G	≤ 100 km	WAN
DSL	ADSL, HDSL, VDSL	1- 100 M	≤ 5 km	NAN,FAN
Coaxial	DOCSIS	172 M	≤ 28 km	NAN,FAN
PLC	Broadband	14-1000 M	≤ 200 m	CPN
	Narrowband	10-500 k	≤ 150 km	NAN,FAN,WAN
Ethernet	IEEE 802.3	10 Mbps-10 G	≤ 100 m	CPN
Wi-Fi	802.11	2-1000 M	≤ 100 m	CPN, NAN,FAN
Z-Wave	Z-Wave	40 k	≤ 30 m	CPN
Bluetooth	IEEE 802.15.1	721 k	≤ 100 m	CPN
ZigBee	ZigBee	250 k	≤ 100 m	CPN
WiMAX	IEEE 802.16	75 M	1 – 100 km	NAN,FAN,WAN
Cellular	2G,2.5G,3G,3.5G,4G	14.4k- 100 M	1 – 100 km	NAN,FAN
Satelite	LEO, MEO, GEO	1 M	100-6000 km	WAN

Asymmetric/high-bit-rate/very-high-bit-rate DSL: digital subscriber line, Wi-Fi: wireless fidelity, WiMAX: worldwide interoperability for microwave access, PON: passive optical network, DOCSIS: data over cable service interface specification, LEO: low earth orbit, MEO: medium earth orbit, GEO: geostationary earth orbit

It is observed in Table 2.2 that PLC can support the CPN, FAN and the WAN. In other words, end-to-end communication can be provided over the same power lines that convey electricity. Following these realisations, PLC has attracted intense research interest in the last two decades. The result is that today, there are application-specific PLC standards for smart grid. For

example the narrowband PLC (NPLC) solutions are PLC-G3, power line intelligent metering evolution (PRIME) and IEEE 1901.2. In addition, there are proprietary solutions localized in different regions of the world as evidenced by recent field trials and experiments in different countries [49, 51–55]. This is not surprising, given the scale of the electricity network, a pervasive communication network is required to ensure connectivity throughout the infrastructure. Of all the communication technologies, only PLC aligns with the natural topology of power distribution network, no wonder it is sometimes referred to as *through-grid technology* [56]. However, given that the cables were primarily designed to conduct electricity, they typically provide harsh and noisy communication channels for communication signals, hence advance modulation and signal processing are required to make the environment more communication-friendly. The next Section is dedicated to PLC.

2.3 Power Line Communication

2.3.1 PLC Overview

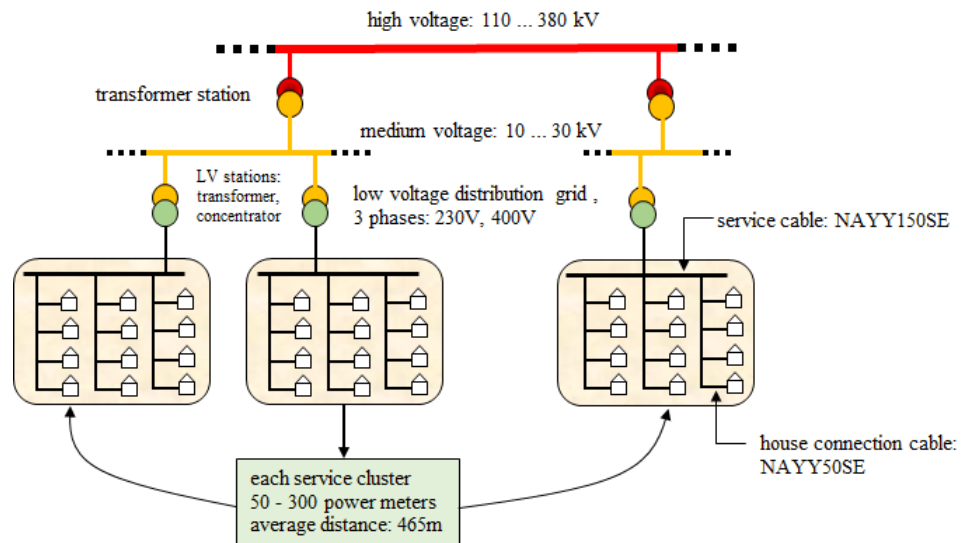
The development of PLC began in the early 1900's when it was used for automation within the medium voltage (MV), high voltage (HV) regions and other non-commercial operations by utilities [54]. By the middle of that century, Landis & Gyr, Brown Boveri and some other companies developed ripple control systems for central load management in the electric power distribution grid based on one-way PLC [24, 57]. However, it was later found that the important applications such as automated meter reading (AMR) required two-way communication with higher data rates. This motivated the development of second generation PLC. Again, time-sensitive applications such as distribution automation and advanced metering solutions required higher data rate than second generation PLC could provide which necessitated the use of larger bandwidth.

At such larger bandwidths, the frequency-selectivity of power line channel becomes more noticeable. To overcome that, the single carrier system was replaced with OFDM to combat the frequency-selectivity and improve the data rate, this is the foundation of the third generation upon which most current

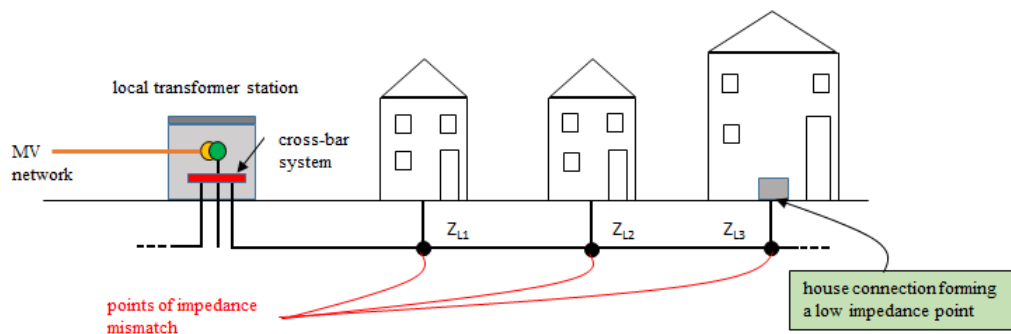
PLC systems are implemented. The result is that today, PLC is not only a commercial reality, PLC modems can be purchased off-the-shelf to serve various purposes such as home networking and general LAN requirements of small-offices. The ongoing revolution in the power sector has once again attracted attention to PLC, considered by many [58, 59] as the natural communication technology for smart grid.

PLC is a technique for conveying data through the wiring traditionally designed and installed for electricity distribution. In principle, it is superposition of high frequency modulation signal on 50/60 Hz (electricity signal). PLC systems can be grouped in terms of frequency of operation into narrowband (125 Hz – 500 KHz) and broadband (1.8 – 100MHz) [50, 60]. Most PLC systems use OFDM technique at PHY layer while carrier sense multiple access with collision avoidance (CSMA/CA) is combined with time division multiple access (TDMA) at the medium access control (MAC) sublayer of data link. Except for some adaptations such as combination with TDMA, the CSMA/CA in PLC is similar to that found in wireless systems. For achievable data rate, NBPLC can deliver few a hundreds of kbps at PHY layer and some tens of kbps at application layer. On the other hand, BPLC can achieve about 1Gbps at PHY layer and some hundreds Mbps at application layer [60]. Since the power line infrastructure was traditionally built to deliver electricity, data signals suffer various forms of distortion and impairments as they transit it. Some of these are caused by the sudden turning “off” and “on” of electrical systems by in-house users or neighbours. Such actions change the electrical configurations or background noise in the channel. In terms of physical properties, topology and structure, the power lines considerably differ from other wireline media such as twisted pair, coaxial or fibre optics, therefore special signal processing techniques are required to improve the reliability of PLC [61, 62].

The European power network is divided into three in terms of voltage levels, namely the HV, MV and LV domains. The LV domain is of special interest because it is the closest to the consumers and offers the opportunity to exploits the transmission lines between the substation and consumers’ premises for last mile communication. This can effectively support smart metering, demand response and other consumer-side applications. The European LV network and power line last mile are illustrated in Figure 2.3.



(a) European power supply network showing the LV domain



(b) LV distribution network showing last mile in residential area

Figure 2.3: European distribution network showing the power line last mile [3]

Generally, the use of PLC would be partly determined by the local or regional grid topology. For example, unlike the US where there are typically less than ten households per transformer, in Europe, the number of power meters per the MV/LV transformer is within 50–300 range, with average distance of 465 m from MV/LV transformer to consumer meters [63]. Although, this implies that PLC is more economically viable in Europe, however, deployments is also subject to regulatory constraints in terms of spectrum and emission limits. Hence, the ultimate choice of PLC for smart grid in a particular region will be based on numerous factors including technical considerations, economic viability and regulatory constraints.

2.3.2 Standards and Regulations

Due to the diversity of the environment in which PLC may be applied, a lot of regulatory framework and standardisation effort have been made at promoting co-existence and ensuring that PLC does not adversely affect other communication systems, especially wireless transmission in similar or close spectrum. Today, PLC systems are implemented in 9kHz - 100MHz band. In terms of spectrum regulation, Europe is a large market for PLC systems and European Committee for Electrotechnical Standardisation (CENELEC) is charged with regulating the strength of signal coupled to the power lines and the frequency band of operation. Given that the electric cable were made to carry 50Hz/60Hz, when PLC signals are coupled to power lines, EM emissions occur. Since the wavelength of BPLC signals are significantly short relative to the length of the transmission lines, the regulation of BPLC differ from that of NPLC. NPLC generally operate below 500 kHz, in Europe, the European Norm (EN) 50065 allows four frequency bands defined as CENELEC band A (3-95 kHz), CENELEC band B (95-125 kHz), CENELEC band C (125-140 kHz) and CENELEC band D (140-148.5 kHz). The complete spectrum band is presented in Table 2.3 [50].

Table 2.3: Global regulation of BPLC and NPLC frequency bands

Region	Regulation	Remark
Narrowband PLC		
Europe	EN 50065	CENELEC band A for utility, bands B-D for consumer use band C for CSMA/CA
	IEEE 1901.2 148.5-500 kHz	Not yet harmonised in Europe
USA	FCC part 15 9kHz - 490 kHz	Rules for carrier current devices
Japan	ARIB STD-T84	CSMA/CA required
Broadband PLC		
Europe	EN 50561-1 1.6065-30 MHz	Dynamic power control static and dynamic notching
	EN 50561-3 30-87.5 MHz	Dynamic power control static and dynamic notching
USA	FCC part 15 1.705-80 MHz	Subpart G for access BPLC, interference mitigation,

FCC: Federal Communications Commission, CENELEC: European Committee for Electrotechnical Standardisation, ARIB: Association of Radio Industries and Businesses

It is clear from Table 2.3 that Europe is more restrictive in terms of spectrum usage.

2.3.3 PLC Channel Characterisation and Measurements

One of the advantages of PLC is its use of existing power cables as communication channels. However, the powerline channel is severely challenging for communication signals due to the factors later described in Section 2.3.4. There are two acclaimed methods to determine the characteristics of a power line channel namely; top-down and bottom-up. They are described below.

2.3.3.1 Top-down Approach

In this approach, the power line channel is considered a black box in which measurements are carried out to determine the model parameters, a common example is the multipath model. In multipath model, channel behaviour is determined by the number of signal paths present from which the physical propagation behaviour is analysed in terms of echoes arising from multiple reflections from points of impedance mismatch or discontinuity [12,62,64–66]. However, such measurements are subject to equipment calibration and errors caused by fine-grain details that might have been over looked. The channel transfer function (CTF) can be expressed as [62]

$$H(f) = \sum_{i=1}^n g_i \cdot A(f, d_i) \cdot e^{-j2\pi f \tau_i} \quad (2.1)$$

where i is the number of paths (path with the shortest delay has index $i = 1$), g_i is the weighting factor for path i , d_i is length of path i and τ_i the delay of path i . Furthermore, g_i is a product of transmission and reflection factors such that $|g_i| \leq 1$, paths with more transmissions and reflection have small value of g_i . Also, longer paths contribute less to the signal arriving at the destination. The delay τ_i of a path is defined as

$$\tau_i = \frac{d_i \sqrt{\epsilon_r}}{c} = \frac{d_i}{\nu_p} \quad (2.2)$$

where ϵ_r is the dielectric constant of the insulating material and c , the speed of light. In (2.1), the losses of the cable cause attenuation $A(f, d_i)$ which increases with frequency and distance and can be expressed as

$$A(f, d_i) = e^{-\alpha(f) \cdot d} = e^{-(a_0 + a_1 \cdot f^k) \cdot d} \quad (2.3)$$

where a_0 and a_1 are attenuation parameters and k is the exponent of attenuation factor. We can see that although (2.3) captures the physical properties, they must be measured for each network to derive the channel model. By combining (2.1) - (2.3), we obtain

$$\begin{aligned} H(f) &= \sum_{i=1}^n g_i(f) \cdot e^{-(a_0+a_1 \cdot f^k) \cdot d_i} \cdot e^{-j2\pi f(\tau_i)} \\ &= \sum_{i=1}^n |g_i(f)| \cdot e^{-(\gamma) \cdot d_i} \cdot e^{-j2\pi f(\tau_i)} \end{aligned} \quad (2.4)$$

Equations (2.1)-(2.4) imply that the CTF can be modelled using the weighting factor g , cable attenuation $A(f, d)$, and propagation delay $e^{-j2\pi f(\tau_i)}$. When the system is matched, signal does not reflect back and there is no multi-path. The frequency response $H(f)$ of a matched transmission line of length l simplifies to

$$H(f) = e^{-(\gamma l)}. \quad (2.5)$$

In the event of unmatched network, the signal undergoes three types of attenuation as it propagates toward the receiver [12].

- Attenuation caused by the heat loss and radiations along the power line. This line attenuation is always present and increases with length and frequency (derived from (2.3)).
- Attenuation caused by reflections at unmatched joints. The interference of reflected signal with incident signal will increase or decrease attenuation depending on whether such reflection gives rise to destructive or constructive interference.
- The delayed version of the forward-propagating signal falling out of phase with the main incident forward signal results in destructive interference, hence adding to the overall signal attenuation.

2.3.3.2 Bottom-up Approach

The transmission line (TL) theory is regarded as a bottom-up approach. Unlike the multipath technique, it allows a-priori derivation of model parameters. At high frequencies, signal wavelength is much smaller than the length of

the TL. This causes phase difference at different points in the circuits. Therefore power cables ordinarily used for 50/60 Hz electrical signal may not be suitable for carrying signals whose oscillation rate is in the order of millions or billion times per second because energy tends to reflect from discontinuities along the cable such as connectors and joints and travel back toward the source. These reflections prevent full signal power from reaching the destination. Given that wavelength is inversely related to frequency of electromagnetic wave carried on the line, TL analysis is required when the cable is longer than the transmitted signal's wavelength. Therefore, unlike circuit theory, the cable length is important in TL analysis.

In PLC, the live (L) and neutral (N) cables are used to form a 2-conductor TL. The conductors are positioned within the insulator parallel to each other and are assumed to have uniform separation between them. On that basis, the 2-port transmission channel can be analyzed as an electric circuit in which each subsequent section acts as a small lumped circuit element to form an infinite series of two-port elementary components, each representing a short segment of the TL.

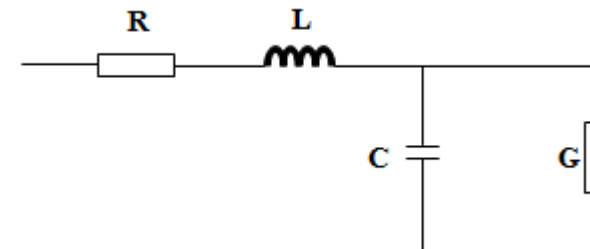


Figure 2.4: Equivalent circuit of 2-port transmission line

The equivalent circuit of one segment is illustrated in Figure 2.4 where the resistor R , in series with the inductor L represents the distributed resistance and inductance of the line respectively. The capacitor created by the two lines is represented by capacitance C of the circuit and G represents conductance of the material that separates the cables. R , L , G and C are distributed values measured per unit length (m) and sometimes denoted as R' , L' , G' and C' . The parameters L , G and C are related to the physical properties of the material filling the space between the two cables such that [67]

$$LC = \mu\varepsilon \quad (2.6)$$

and

$$\frac{G}{C} = \frac{\sigma}{\varepsilon} \quad (2.7)$$

where μ , ε , σ are the permeability, permittivity and conductivity of the medium around the conductors. R is the distributed resistance (in Ω/m), L the distributed inductance due to magnetic field around the conductors (in H/m), C is the capacitor created by the conductors represented by a shunt capacitor (in F/m) and G is the conductance of the dielectric material that separates the conductors measured in siemens per metre (S/m). R , L , G and C are called the primary line constants from which secondary line constants (attenuation constant, propagation constant and phase constant) can be derived. The two most important parameters in TL analysis are the propagation constant γ and the characteristic impedance Z_c which are defined as [4,5]

$$\gamma = \sqrt{(R + j\omega L)(G + j\omega C)} \quad (2.8)$$

where angular frequency (in rad/s) $\omega = 2\pi f$. The propagation constant γ (which determines speed and attenuation of the electromagnetic wave) is a complex variable of the form $\alpha + j\beta$ whose real part, α is the attenuation constant and imaginary part β is the phase constant. Similarly, characteristic impedance of the line is given as

$$Z_c = \sqrt{\frac{(R + j\omega L)}{(G + j\omega C)}} \quad (2.9)$$

With the 2-port representation of the circuit, the transmission can be represented by its ABCD matrix; a 2x2 matrix showing relationship between input/output line voltage and current as illustrated in Figure 2.5.

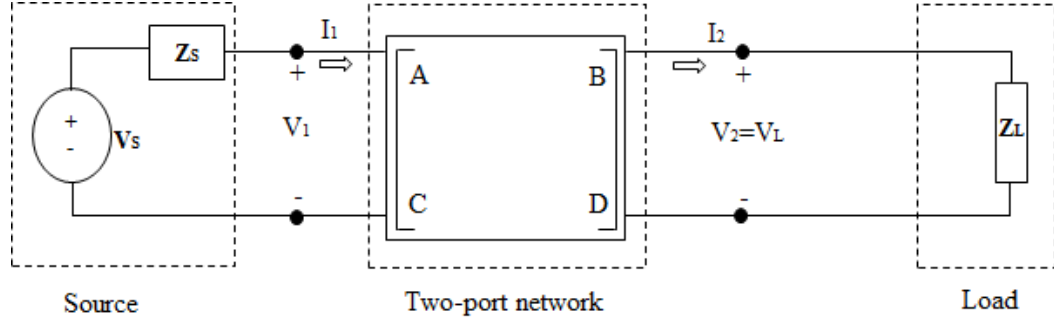


Figure 2.5: Two-port network showing the source and receiver

Elements of the matrix are complex numbers that depend on frequency. The ABCD matrix provides a mathematically convenient way to generate the CTF. For a two-port network, the ABCD matrix is defined as

$$\begin{bmatrix} V_1 \\ I_1 \end{bmatrix} = \begin{bmatrix} A & B \\ C & D \end{bmatrix} \begin{bmatrix} V_2 \\ I_2 \end{bmatrix} \quad (2.10)$$

The CTF (H) of the network in Figure 2.5 can be computed as

$$H(f) = \frac{V_L}{V_S} = \frac{Z_L}{AZ_L + B + CZ_L Z_S + DZ_S} \quad (2.11)$$

where Z_S and Z_L are source and load impedance respectively. The input impedance (Z_1) of the two-port circuit can also be calculated as

$$Z_1 = \frac{V_1}{I_1} = \frac{AZ_L + B}{CZ_L + D} \quad (2.12)$$

The transmission matrix of a TL with characteristic impedance Z_c , propagation constant γ and length l is given by

$$T = \begin{bmatrix} A & B \\ C & D \end{bmatrix} = \begin{bmatrix} \cosh(\gamma l) & Z_c \sinh(\gamma l) \\ \frac{1}{Z_c} \sinh(\gamma l) & \cosh(\gamma l) \end{bmatrix} \quad (2.13)$$

Equation (2.13) has been extensively used in literature [4, 5, 68], it is popularly known as the *ABDC matrix* and it shows that for a single segment 2-port transmission line of cable length l with primary line constants R , L , C , G , characteristic impedance Z_c and propagation constant γ , the ABCD matrix can be mathematically derived, from which the CTF is computed without

actual measurements. Hence, with the TL technique, transfer characteristics is topology-dependent, making it flexible and more predictable [68,69], however, it is more computationally complex. Using the TL theory, complex networks can be approximated into series of cascaded two-port networks for easy analysis and modelling. Once the equivalent two-port sub-circuits are obtained, it is possible to represent the entire power line channel with their transmission (ABCD) matrices [4,5,69]. For example, consider a network with a branch¹ in Figure 2.6.

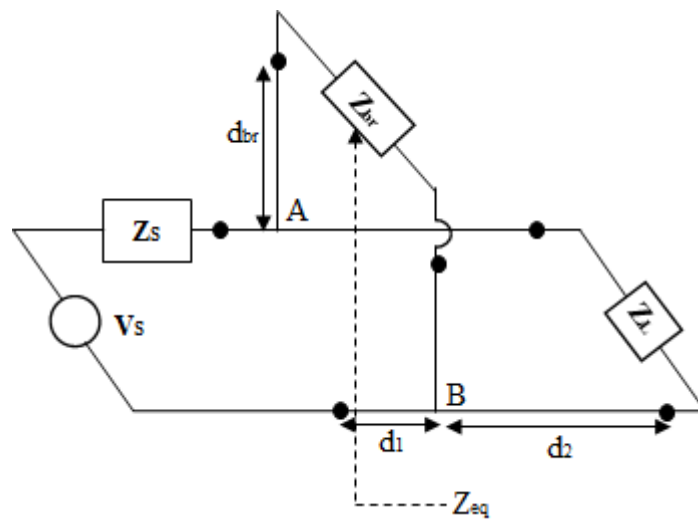


Figure 2.6: Transmission line with one branch [4,5]

By replacing the branch with the equivalent impedance Z_{eq} , which can be seen by terminals A and B, the network in Figure 2.6 can be represented by the equivalent circuit in Figure 2.7.

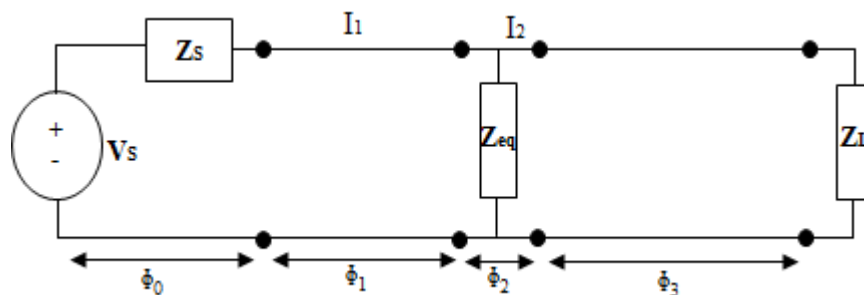


Figure 2.7: Equivalent circuit of Figure 2.6 [4,5]

¹some numerical examples are published in [70]

It can be seen that Figure 2.7 is a cascade of four two-port sub-circuits, denoted as $\Phi_0 - \Phi_3$. For each sub-circuit, the transmission matrix can be derived such that the ABCD matrix for the complete circuits is given by

$$\Phi = \prod_{i=0}^3 \Phi_i. \quad (2.14)$$

From previous studies in this area, the ABCD matrices of the respective sub-circuits are reported as [4, 5],

$$\Phi_0 = \begin{bmatrix} 1 & Z_c \\ 0 & 1 \end{bmatrix}, \quad (2.15)$$

$$\Phi_1 = \begin{bmatrix} \cosh(\gamma_1 l_1) & Z_1 \sinh(\gamma_1 l_1) \\ \frac{1}{Z_1} \sinh(\gamma_1 l_1) & \cosh(\gamma_1 l_1) \end{bmatrix} \quad (2.16)$$

$$\Phi_2 = \begin{bmatrix} 1 & 0 \\ \frac{1}{Z_{eq}} & 1 \end{bmatrix}, \quad (2.17)$$

where Z_{eq} is the equivalent impedance due to the branch circuit as shown in Figure 2.6 and is defined as

$$Z_{eq} = Z_c \frac{Z_{br} + Z_c \tanh(\gamma_{br} l_{br})}{Z_c + Z_{br} \tanh(\gamma_{br} l_{br})} \quad (2.18)$$

Z_{eq} is the equivalent impedance of the branch connected to the node i . Z_{br} is the impedance of the load that it is connected to the branch. Z_c is the characteristic impedance of the cable of the branch and γ_{br} is the propagation constant for that cable. The length of the branch is l_{br} .

Lastly,

$$\Phi_3 = \begin{bmatrix} \cosh(\gamma_2 l_2) & Z_2 \sinh(\gamma_2 l_2) \\ \frac{1}{Z_2} \sinh(\gamma_2 l_2) & \cosh(\gamma_2 l_2) \end{bmatrix}. \quad (2.19)$$

In (2.16) and (2.19), Z_1 , γ_1 , Z_2 and γ_2 are respectively the characteristic impedances and propagation constants of the second and fourth sub-circuits in Figure 2.7. By substituting (2.15) - (2.17) and (2.19) into (2.14), the ABCD

of the entire network can be expressed as

$$T = \begin{bmatrix} T_{11} & T_{12} \\ T_{21} & T_{22} \end{bmatrix} \quad (2.20)$$

The overall CTF can thus be expressed as

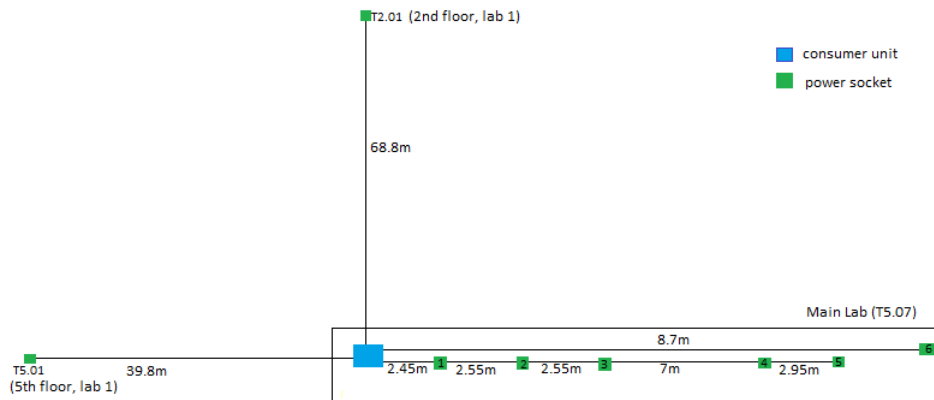
$$H(f) = \frac{Z_L}{T_{11}Z_L + T_{12} + T_{21}Z_S Z_L + T_{22}Z_S}. \quad (2.21)$$

This is the model adopted in this work, hence the power line channel used in the analysis and simulations in subsequent chapters are based on the TL theory.

2.3.3.3 Numerical Examples

The CTF basically measures the attenuation on the TL. It can be seen in (2.11) and (2.21) that H is dependent on frequency and length. Some numerical examples are provided in this Section to illustrate CTF in the BPLC frequency range 0 - 30 MHz. Using the electrical properties of LV 2.5mm indoor cable, the primary line constants R , L , C , G were derived as $0.3674\Omega/m$, $3.54882e-06H/m$, $9.4539e-12F/m$ and $7.63149e-05S/m$ respectively. The model also considered that $Z_S = Z_L = 50\Omega$.

The experimental power line channel consist of 68.8 m indoor electric cable spanning four floors (floor 2 to floor 5) of a building on one hand, another 39.8 m branch connected across two laboratories on the same floor and 8.7 m line within the main lab. In each case, the power lines comprises of three-conductor (2.5mm live and neutral, 1.5mm earth) electric cables interconnected at the consumer unit. Various lengths of off-grid power lines and sockets are also available with which power line network can be extended when necessary. The power line network is presented in Figure 2.8.



(a) Physical layout of the power line network



(b) The consumer unit for enabling variable power line configurations

Figure 2.8: Topology of PLC network in main lab

With this configuration, it is possible to isolate individual circuits and study various scenarios in terms of length and topology. Measurement of the CTF was carried out between main lab (T5.07) and lab T2.01 by connecting a power line coupler at each end. Using digimess SG200 signal generator, a signal was then fed into the power line channel at lab T2.01 and the received power was measured with the spectrum analyser connected to socket 1 in the main lab. As power line channel is time-variant, the measurements were averaged over four days. Using the topology information in Figure 2.8, an equivalent model was consequently developed in MATLAB and compared with measured values. The result is presented in Figure 2.9.

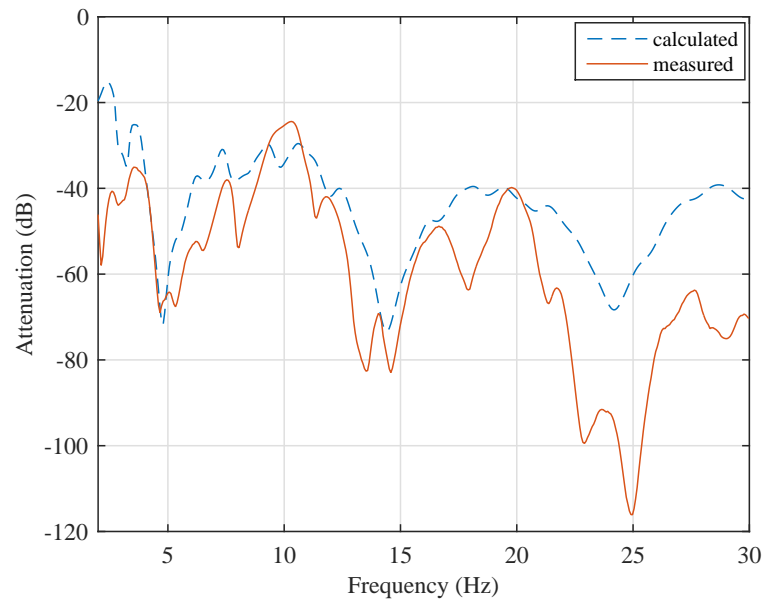
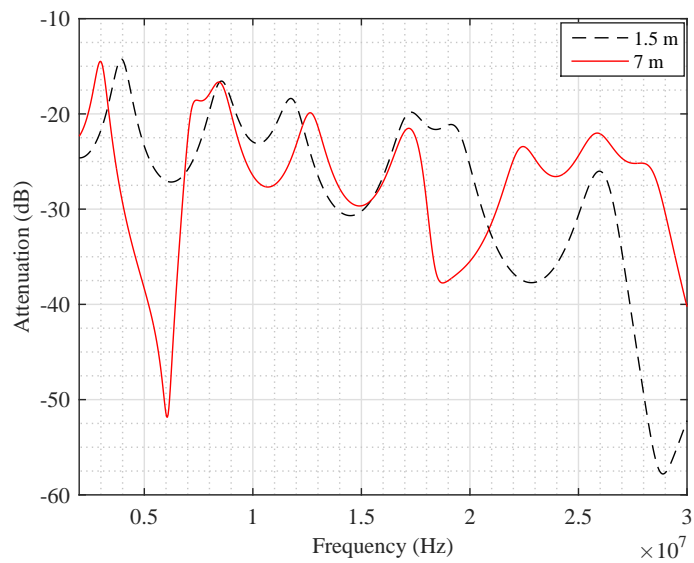
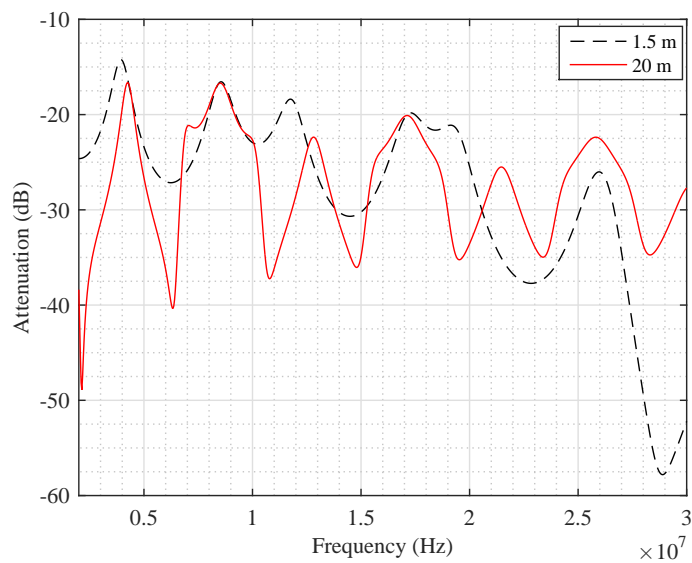


Figure 2.9: CTF experimental power line network

It can be seen in Figure 2.9 that attenuation on the TL increases with frequency. Using the same cable specifications, here we created another model with a single branch connected at 10 m from the source and vary its length from 1.5 m to 20 m to establish its impacts on signal propagation.



(a) Attenuation of TL with 1.5 m and 7 m branches



(b) Attenuation of TL with 1.5 m and 20 m branches

Figure 2.10: CTF of TL with different branch lengths

It can be seen in Figure 2.10 that as the branch length increases from 1.5 m to 20 m, the number of notches also rises. Such repeated occurrence of notches in CTF will intensify attenuation in real life networks which will degrade PLC performance.

2.3.4 Signal Propagation and Challenges in PLC

Communication signals are typically affected by various factors as they propagate through the power line channel. This section examines the challenges experienced during signal propagation in power lines and illustrates them with some examples.

2.3.4.1 Noise

Like all other communication systems, PLC is affected by noise. However, the noise in power lines is complicated as it consists of Gaussian and non-Gaussian components which can be worse if multiple sources are concurrently emitting non-Gaussian noise on the network. For instance, the noise pattern in the substations is highly non-Gaussian; it is generally impulsive or bursty [71,72]. Therefore, noise in power lines differs from the usual additive white Gaussian noise (AWGN) found in most other communication systems and overcoming the non-Gaussian components such as impulsive noise is one of the biggest challenges in PLC [73]. Noise in power lines can be categorised into five groups as shown in Figure 2.11.

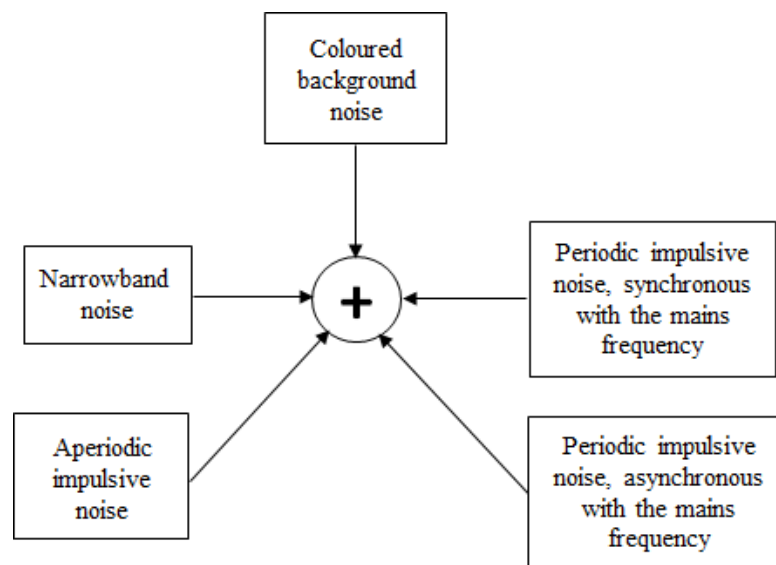


Figure 2.11: Types of noise in power lines

They are described as follows [15,72,74,75]:

1. Coloured background noise: it occurs with relatively low power spectral density (PSD), varying with frequency. It is caused by summation of

numerous low power noise samples generated by in-home electronic devices.

2. Narrowband noise: unlike coloured background, narrowband noise originates from broadcast stations such as amplitude modulation (AM), frequency modulation (FM) stations, citizens' radios and other external sources transmitting within the 1-22MHz [76-78].
3. Periodic impulsive noise, asynchronous with the mains frequency: it is usually emitted by switched power supplies such that it occurs at a repetition rate between 50 and 200 kHz, with a discrete line spectrum spaced according to the impulse repetition rate [75].
4. Periodic impulsive noise, synchronous with the mains frequency: this occurs with a repetition rate of 50 or 100 Hz (in Europe). The impulses are of short duration (some microseconds) and have a PSD decreasing with frequency. This type of noise is caused mainly due to operations of silicon-controlled rectifiers (SCRs) which switch a certain number of times in every 50Hz (synchronously with the mains). For example, switching mode power supplies (in light dimmers) and direct current (DC)-DC converters are known sources of this type of impulse noise [72,74].
5. Aperiodic impulsive: this type of noise is sporadic in nature, with rapidly varying amplitude. This is caused by switching transients arising from connection and disconnection of electrical devices in the network. The impulses have duration of some microseconds up to a few milliseconds with random occurrence [79].

In the noise types 1 and 2, the root mean square (rms) of their amplitudes vary slowly and remain stationary for a long period ranging from minutes, hours to days, they are collectively classified as background noise while the last three are categorised as impulsive noise. Impulsive noise is characterised by short duration (microseconds to milliseconds) and high PSD which results in bit or burst errors in data communications. Other known sources of impulsive noise include drilling machine, vacuum cleaner, television set, liquid crystal display (LCD) monitor, CRT monitor, washing machines and other household

appliances. For instance, Figure 2.12 presents the noise pulses generated by a laptop charger in a PLC network.

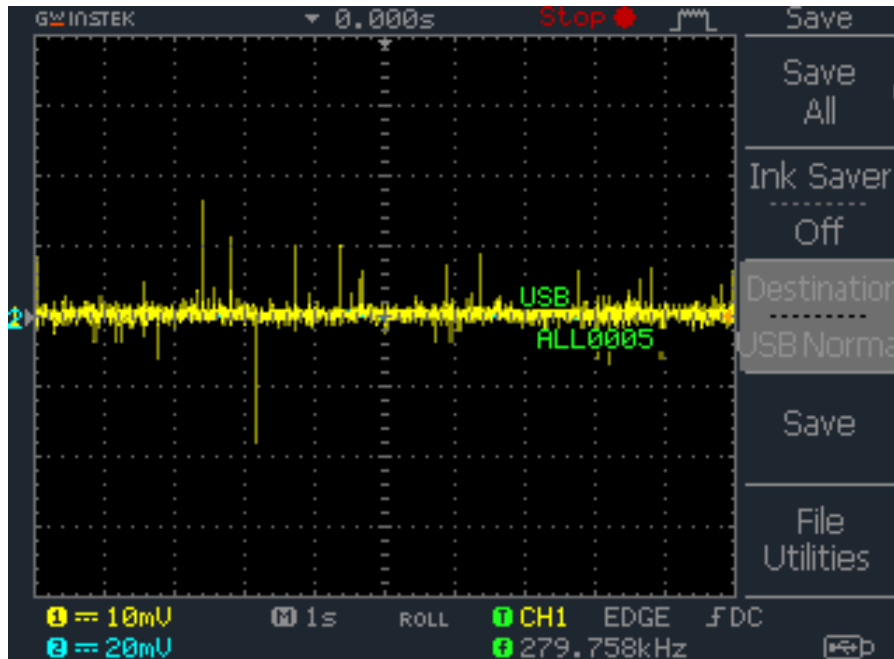
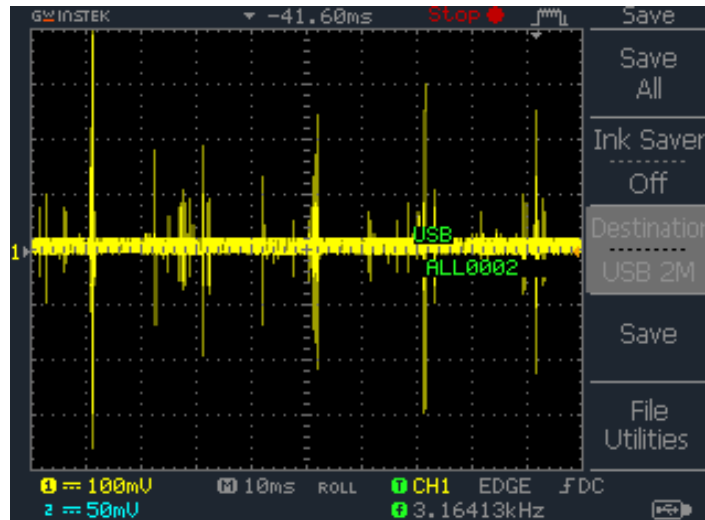
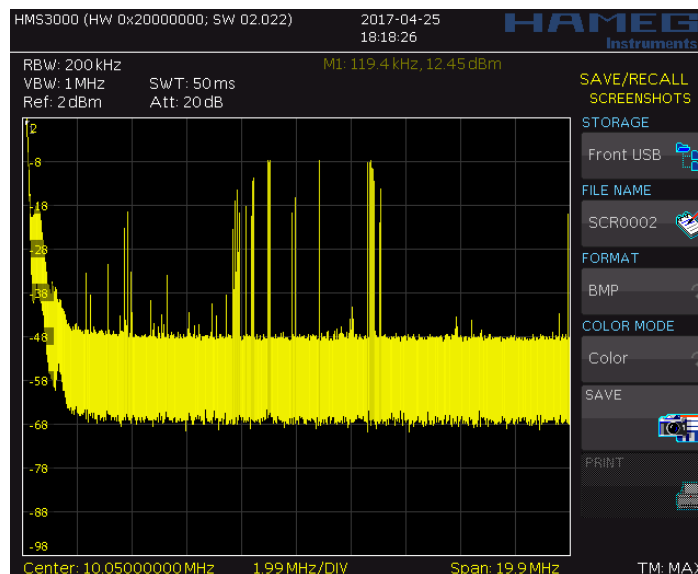


Figure 2.12: Amplitude (in mV) of noise pulses generated by a laptop charger

Figure 2.12 is an example of aperiodic impulsive noise. It was generated by a 90 W laptop charger. Impulsive noise can be studied in frequency and time domains, for example, Figure 2.13 illustrates the impulsive noise events from a drilling machine rated 50 Hz 240 V 400 W 1.75 A .



(a) Amplitude (mV) and interval (ms) of impulsive noise in time domain



(b) Impulsive noise in frequency domain

Figure 2.13: Impulsive noise in time and frequency domain from a drilling machine

The first pulse in the time domain (Figure 2.13a) was generated when the AC motor in the drilling machine started while the subsequent ones were injected into the power line channel during the drilling process. As seen in the figure, the pulses occurred at regular interval and therefore signify periodic impulsive noise. Similarly, Figure 2.13b shows the same noise events in the frequency domain. The essence of frequency domain analysis is to identify

the frequency at which the pulses occur and their peak power. Whereas the time domain provides the inter-arrival time of the pulses and their durations, the frequency domain shows the peak power within the observation window. Therefore, in order to investigate the impact of impulsive noise on communication performance, the fundamental questions are:

- when do the pulses occur (in time and frequency domains),
- how strong are the pulses (the amplitude or peak power) and
- how long do they last.

Previous experimental studies [72,79] showed that impulsive noise is usually higher than background noise by at least 10 dB and may be as much as 50dB. In general, impulsive noise is more dominant in PLC network and evidence from some recent studies show that it is one of the most significant factors that can degrade PLC system performance in terms of BER, SNR, latency, and general reliability [80,81]. These explain why investigation of mitigation techniques in PLC continues to attract attention in the research community.

Substantial amount of work has been done on noise modelling in PLC [61, 71, 79] following which various noise modelling techniques were proposed. However, the Middleton class-A [73,82,83] and two-component Gaussian [84–86] are the two widely-used noise modelling techniques. For the sake of completeness, these techniques are briefly described as follows.

- **Middleton Class-A Model**

This model considers noise in power lines as a superposition of background noise with random pulses, hence, it is affected by the number of impulsive components. The probability density function (PDF) of Middleton class-A noise sample n_k , where k is the discrete-time index is expressed as [71,73]

$$f(n_k) = \sum_{m=0}^{\infty} \frac{\exp(-A)A^m}{m!} \frac{1}{\sqrt{2\pi\sigma_m^2}} \exp\left(-\frac{n_k^2}{2\sigma_m^2}\right), \quad (2.22)$$

where

$$\sigma_m^2 = \sigma_t^2 \left(\frac{m + \Gamma}{1 + \Gamma} \right), \quad (2.23)$$

$$\sigma_t^2 = \sigma_g^2 + \sigma_i^2, \quad (2.24)$$

$$\Gamma = \frac{\sigma_g^2}{\sigma_i^2}, \quad (2.25)$$

while σ_g^2 , σ_i^2 and σ_t^2 denote the powers of Gaussian, impulsive and the total noise respectively, A is the impulsive index which represents the average number of concurrent impulses, σ_m^2 is the variance of the m^{th} pulse and Γ is the Gaussian-to-impulsive-noise ratio. It can be seen that the noise n_k includes the typical AWGN (which can be obtained apart from the impulsive component). Equations (2.22) - (2.25) clearly show that in Middleton class-A model, noise can be fully characterised by three parameters, namely A , Γ and σ_t^2 . The practical significance of A is as follows, A can be considered as the product of impulse rate λ (average number of impulse per unit time) and impulse mean duration \bar{T} , that is

$$A = \lambda * \bar{T} \quad (2.26)$$

In (2.26), a reduction in the value of A signifies a lower number of impulsive events and/or shorter duration of the pulses, which corresponds to impulsive noise. Conversely, as the value of A is increased, the noise becomes continuous and the Middleton class-A gets closer to Gaussian noise [71]. These observations agree with the other results in the literature such as [56].

• Two-Component Gaussian Model

The two-term component model is a special case of the multi-component mixture-Gaussian model [87]. The most common two-component Gaussian formulation widely used is the Bernoulli-Gaussian model. In time-domain, the total noise is represented as [88]

$$n_k = w_k + i_k \quad (2.27)$$

where

$$i_k = b_k g_k, \quad k = 0, 1, 2, \dots, N - 1, \quad (2.28)$$

n_k is the total noise, w_k is the AWGN with zero mean and variance σ_w^2 , i_k is the impulsive noise and is Gaussian distributed with zero mean and large

variance σ_i^2 ($\sigma_i^2 > \sigma_w^2$). The g_k is complex white Gaussian noise with zero mean and b_k is the Bernoulli process with probability mass function

$$Pr(b_k) = \begin{cases} p & b_k = 1 \\ 0, & b_k = 0 \end{cases} \quad k = 0, 1, 2, \dots, N - 1, \quad (2.29)$$

p is the probability of impulsive noise occurrence. Therefore, the PDF of the noise sample n_k for the special case of multi-component mixture with $m = 2$, is given by

$$P_{n_k}(n_k) = \sum_{m=0}^1 p_m \mathcal{G}(n_k, 0, \sigma_m^2) \quad (2.30)$$

$$P_{n_k}(n_k) = p_0 \mathcal{G}(n_k, 0, \sigma_0^2) + p_1 \mathcal{G}(n_k, 0, \sigma_1^2) \quad (2.31)$$

where $\mathcal{G}(\cdot)$ is the Gaussian PDF defined as $\mathcal{G}(x, \mu, \sigma_x^2) = \frac{1}{\sqrt{2\pi\sigma_x^2}} \exp\left(-\frac{(x-\mu)^2}{2\sigma_x^2}\right)$, $p_0 = (1 - p)$, $p_1 = p$, $\sigma_0^2 = \sigma_w^2$ and $\sigma_1^2 = \sigma_w^2 + \sigma_i^2$. The variances σ_w^2 and σ_i^2 denote the background and impulsive noise powers from which the input SNR and signal-to-impulsive noise ratio (SINR) can be respectively derived as

$$\text{SNR} = 10 \log_{10} \left(\frac{\sigma_s^2}{\sigma_w^2} \right) \quad (2.32)$$

and

$$\text{SINR} = 10 \log_{10} \left(\frac{\sigma_s^2}{\sigma_i^2} \right) \quad (2.33)$$

where σ_s^2 is the transmitted signal variance.

2.3.4.2 Multipath Propagation and Frequency-Selectivity

In Figure 2.3b, due to the structure of the LV network, cables are typically joined at different points along the transmission line (e.g between service cable, home connection cable, house distribution boxes). This phenomenon leads to discontinuity and impedance mismatch due to difference in the characteristic impedance of connected lines. In effect, between the substation and the consumers' premises, signals do not propagate along the direct paths alone; at junctions (points of mismatch) they are scattered along multiple

paths (echoes) and such scattering is more pronounced at high frequencies. This results in multi-path propagation with frequency-selective fading [61] which is typically mitigated using multi-carrier modulation schemes.

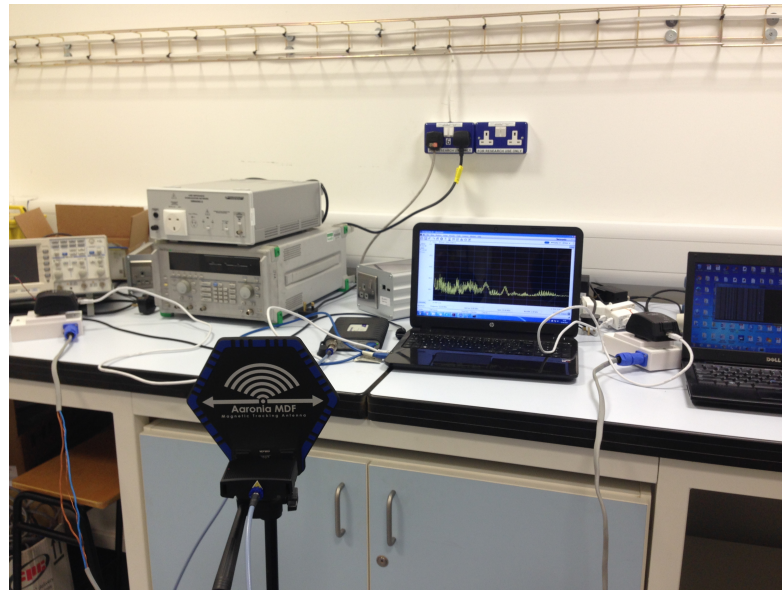
2.3.4.3 Cable Losses (Attenuation)

Unlike twisted pair data cable such as CAT5 and CAT6 Ethernet cables, electrical cables used in power distribution are not suitably screened and terminated, hence are not perfect for data signal propagation. Therefore data signals over power lines are prone to various degrees of losses which increase with distance and operating frequency as discussed in Section 2.3.3.

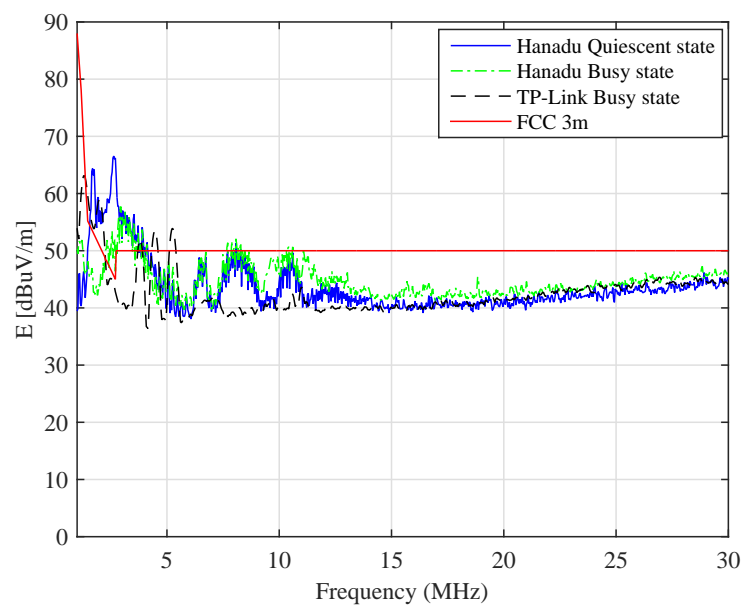
2.3.4.4 EMC and Regulatory Constraints on Transmit Power

Electric cables generally are designed to transport electricity at 50Hz/60Hz, hence the conductors are not electromagnetically shielded. The result is that at high frequencies, power lines behave like antenna emitting electromagnetic energy which can cause interference with nearby AM transmissions, amateur radio and other radio operations [76,77]. To avoid this unwanted effects, transmit power in PLC is regulated by regional bodies such as FCC and CENELEC and the conformance requirement is termed electromagnetic compatibility (EMC). Generally, the EMC standards specify the maximum electric field strength that an electromagnetic radiator such as power line network is allowed to emit. The field strength is usually measured at a specific distance (typically 3 m) from the equipment under test (EUT) [76,77]. Emissions in PLC can be measured in two parts; radiated and conducted emissions [76,77]. While the radiated emissions account for the unintentional magnetic field that propagates away from the TL, conducted emissions are internal and they propagate along the conductors. In addition, high transmit power is a potential source of inefficiency, hence it is generally desirable to keep the transmit power low. A measurement bench was set up to examine these components as follows.

- Radiated emission: The measurement set-up consists of PLC modems and active magnetic direction antenna (MDF 960X) positioned at 3m distance from the PLC channel as shown in Figure 2.14 and in accordance with FCC standard.



(a) Measurement of radiated emission



(b) Comparison of radiated emission with FCC limit

Figure 2.14: Radiated emission measurement

Using two brands of PLC modem, radiated emissions in quiescent and busy states are compared with FCC limit for BPLC (1.8-30MHz), the results are shown in Figure 2.14b. Although the Hanadu modem radiated less emissions in quiescent state than busy state, it can be seen that both modems mostly comply with FCC limits, except for a few spikes in the low frequency (<

6MHz for TP-Link and < 11 MHz for Hanadu). The TP-Link is generally more compliant than Hanadu, indeed that is expected since Hanadu is an evaluation unit whereas TP-Link is a commercial product already.

- **Conducted emission:** Conducted emissions are the currents that are passed out through an equipment's AC power cord and propagated on the common power network. This was measured using a current clamp as shown in Figure 2.15.

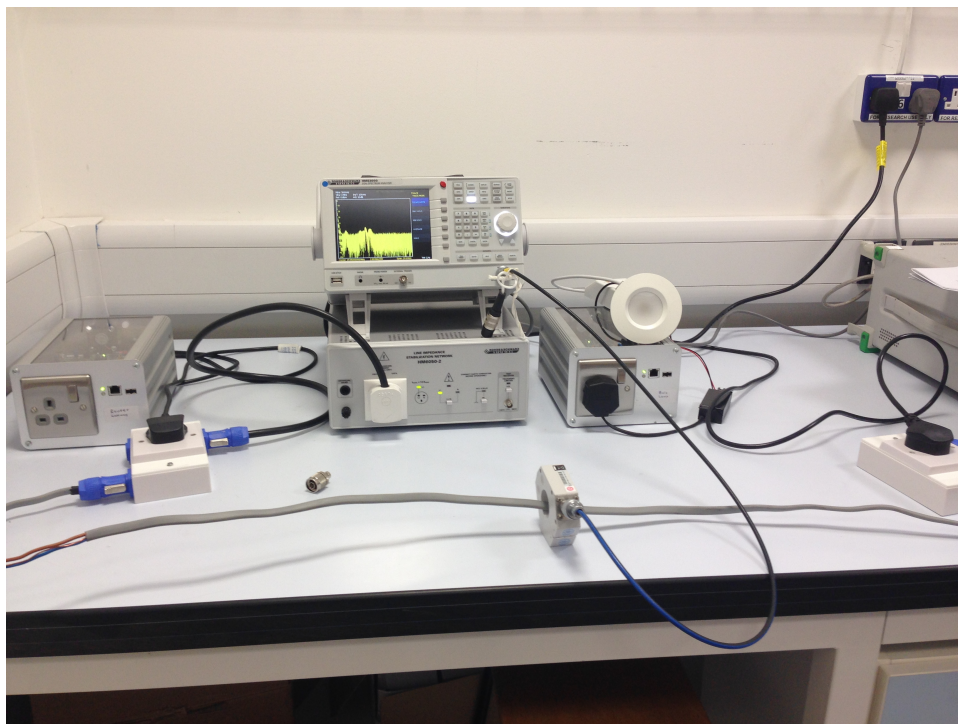
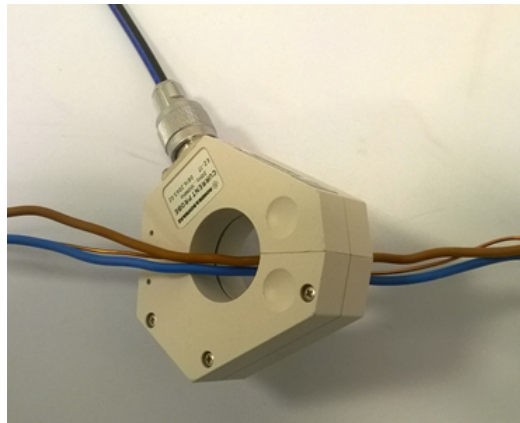
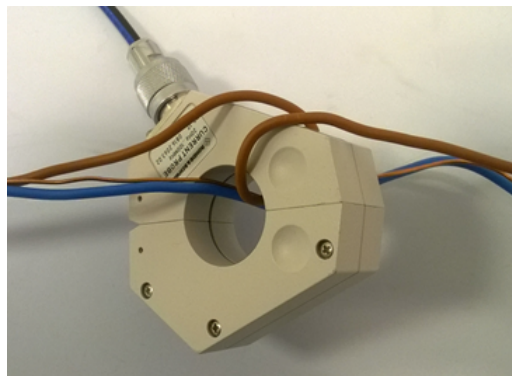


Figure 2.15: Conducted emission

A piece of house wiring cable typically contains three conductors; the L, N and earth (E) cables. The conducted emissions are usually measured in common and differential modes. To measure common mode current, the three conductors were enclosed in the current clamp connected to spectrum analyser, whereas for differential mode current, the L cable was wound round the clamp and turned at 360 degree to emulate current flow in opposite direction as shown in Figure 2.16. It should be noted this method of investigating differential mode current is in line with similar works in literature [89].

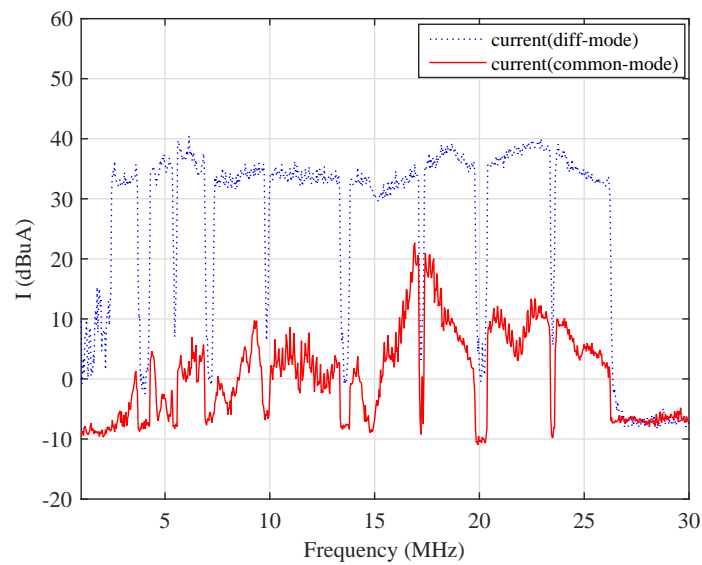


(a) Common mode current

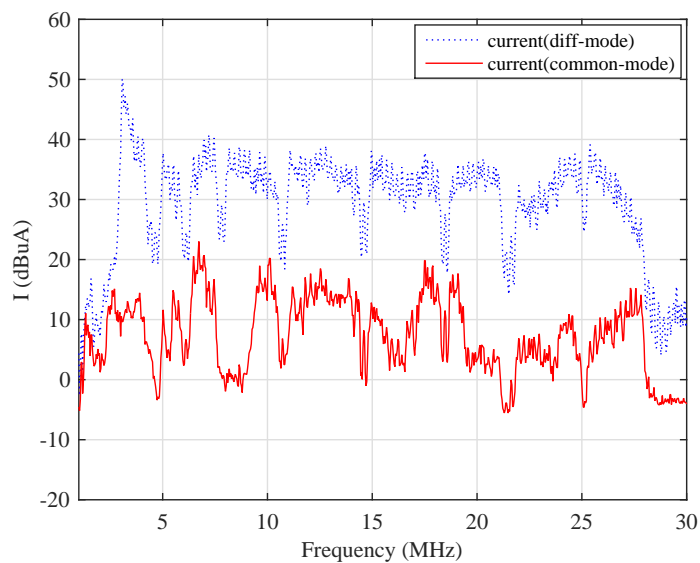


(b) Differential mode current

Figure 2.16: Conducted emissions measurements with current clamp



(a) TP-Link conducted emissions



(b) Hanadu conducted emissions

Figure 2.17: Conducted emissions

It can be seen in Figure 2.17 that in both modems, conducted emission is higher in differential mode than in common mode and emissions from the Hanadu modems are much higher than those of TP-Link. While the peak reached 40dBuA at 6.7MHz in TP-Link, the peak emission of 50dBuA was observed in Hanadu at 3.6MHz.

2.3.4.5 Topology Variation

Power line generally exhibits time-varying channel response. For example, the sudden switching "off"/ "on" or connection/disconnection of electrical loads by users in neighbourhoods such as NANs can change the electrical configurations of the network. The effects of such variations can range from a few ohms to several kilo-ohms which can worsen the unpredictability of the power line channel [90].

2.4 Energy-Efficient Communication System in Smart Grid

There is a rising awareness of the high energy consumption by communication infrastructure across different domains and the need to curb the trend. For example, combined electricity demand of telecommunication networks and data centres is reported to be equivalent to the demand of the fifth largest country [25]. In particular, the telecommunication industry consumes 3% of global energy while the entire ICT sector accounts for 2-4% of global CO_2 emissions [91, 92]. This is equivalent to 25% of all car emissions and approximately equals all airplane emissions in the world [92]. In view of this, various sub-sectors within the ICT and research community have approached the issue of energy efficiency with renewed vigour. These have resulted in different energy-optimisation techniques for wireless technologies. For example, considering that base transceiver stations consume 50-80% of the power in cellular networks [93], the lesson for other communication systems such as PLC is that optimising the power associated with transmit and receipt of data can drastically reduce the energy budget.

The power amplifier (PA) is one of the main energy-consuming components of the transmitters [93] and its function is to boost the transmit power to enable the signal to overcome channel impairments such as attenuation and interference. To achieve maximum power efficiency, the PAs typically operate in the dynamic range [94]. Energy efficiency and spectral efficiency are two important characteristics of the PA. While spectral efficiency provides the data rate needed by smart grid applications, energy efficiency ensures that optimum number of bits per unit energy are transmitted. Therefore,

optimised design of PA is crucial to the energy efficiency of PLC systems. Furthermore, PLC transceivers consume power in two forms; static and dynamic power [19, 20]. While the static power is fixed, the dynamic power (transmit power) is load-dependent. Thus, energy efficiency challenge can be approached from different perspectives including circuit design and signal processing [13].

A holistic framework for energy efficiency is a subject of future research, however, in a bid to reduce the power requirements, low-power wireless systems such as ZigBee are commonly deployed in applications with low data rate requirements such as home monitoring and control. For this class of devices, although the IEEE802.15.4 standard specifies up to 75 m range, coverage can be as low as 10-20 m in some indoor environments [95–97]. In order to monitor and control the in-home appliances, several repeaters may be employed which increases the management complexity and cost. Given the pervasive nature of power cables, it provides the unique opportunity to extend communication coverage to the areas that are challenging for wireless technologies generally.

In doing this, it is also important to minimise the power consumption in each smart grid scenario. This work adopts a cross-layer approach by exploiting various attributes such as network topology (network layer), reduced data rate (adaptation layer) and multi-carrier modulation (physical layer) to optimise energy requirements of PLC systems for various smart grid applications and scenarios.

2.5 Methodology

The central argument in this thesis is that PLC provides some unique opportunities to improve energy efficiency of smart grid communication. In view of the above, this thesis investigates methods of improving energy efficiency of PLC systems at three open systems interconnect (OSI) layers, namely the physical, adaptation and network. At the physical layer, investigations are carried out through simulation in MATLAB and the proposed techniques are studied in various channel conditions in terms of impulsive noise events. At the adaptation layer, a model of HEMS is developed in NS-3 and validated

with experimental results following which two exemplar applications- temperature sensing and light control are studied. In the study, simulation results are used to determine the system performance limits such as the maximum size of application data required to guarantee acceptable latency and system reliability. The communication network and application parameters used are extracted from a tested bed. In order to ensure that results are reproducible in NS-3, a fixed seed value is used in each simulation. Finally, at the network layer, the main theme is that AMI application performance could be improved by organizing the smart meters into clusters such that consumption data are locally aggregated. In that case, the aggregator transmits only the composite data to the concentrator instead of transmissions from individual smart meter to the concentrator found in flat AMI. The smart grid application parameters used in that section are derived from field trial reported in [53] and smart metering guideline published in [98]. Throughout this thesis, the power line channel model employed is based on transmission line theory since it is topology-dependent and more practical [68,69].

2.6 Chapter Summary

This chapter provided a background to the various aspects of this thesis. It began with the introduction of smart grid, its motivations, applications, traffic characteristics and communication requirements. It went further to highlight key communication challenges in smart grid. Various communication technologies were compared and PLC was identified as a promising communication technology while its challenges were analysed. Also, this chapter provided comprehensive analyses of noise modelling and channel characterisation techniques. Lastly, energy efficiency in PLC was identified as an area that has not received sufficient research attention.

Chapter 3

Efficient BPLC Topology for Clustered AMI

The expectation that smart grid must be self-healing, with system-wide monitoring and control capabilities among other features raises vital questions about the types of communication systems to consider. In contrast with other technological concepts such as Internet-of-things (IoT) which has been considered a key driver of 5G wireless technology [99, 100], smart grid does not enjoy clean-slate development of purpose-made communication technologies. The evolution of power systems have not kept pace with rapid advancements in ICT, for example, for over a century, the basic structure of the power grid remained unchanged [101]. The result is that current communication technologies were developed without consideration for smart grid applications requirements and one of the current challenges is how to cost-effectively retrofit these communication technologies in smart grid [102]. In doing that, two fundamental questions are i) what extent of changes and retrofitting are required in order to deliver acceptable quality-of-service (QoS) to the multitude of applications and ii) considering the crucial role of back-haul in the end-to-end connectivity, what are cost-effective options feasible to achieve the service objectives?

While there are no easy guesses, the solution lies in considering a wide range of factors including availability, cost and ubiquity. BPLC can provide a viable answer. In this chapter, it is shown that BPLC can adequately support AMI application in terms of key network performance measures such as latency, throughput and reliability. We further show that, when metering data

is locally aggregated and the data collector (DC) is located at the middle of the NAN, probability of packet delivery increased by 3% relative to the flat AMI. This chapter is organised as follows. In section 3.1, clustered AMI and some of its services are introduced. The section also presents the model studied in this work which maps the LV network into two AMI topologies for investigating smart metering and DR applications. Section 3.2 presents the methodology and simulation set up used in evaluating the proposed model, including the system parameters used. In section 3.3, the simulation results are presented and discussed in various network configurations while the main conclusions are summarised in section 3.4.

3.1 Advanced Metering Infrastructure and Clustering

According to [103], the AMI is not a single technology but an integration of multiple technologies that provides intelligent connection between consumers and system operators. AMI is viewed as the first major step toward the power grid modernisation as observed in various studies and field trials [53, 103]. In terms of service composition, they are mostly standard customer-focused services such as meter reading, price notification, outage notification, remote connection/disconnection, power quality, firmware upgrade etc [48]. Within the AMI, NANs consist of several HANs connected to a utility's network through communication links. In terms of ubiquity, only wireless LANs (WLANs) rival power line networks, given that they are both prevalent in most homes. However, employing PLC in AMI could help to overcome blind spots and other deployment challenges where wireless technologies are either cost-ineffective or impracticable.

3.1.1 Clustered Advanced Metering Infrastructure

Clustering methods are increasingly being applied to residential smart meters, which provides a number of important opportunities for distribution network operators (DNOs) to manage and plan LV networks. Clustering has a

number of potential advantages for DNOs, including the identification of suitable candidates for DR, grouping of consumption behaviours and improvement of energy profile modelling [104–106]. The communication network can also benefit from the technique by organising the smart meters within the NAN into clusters. In each cluster, a DC exists such that all the smart meters communicate with the concentrator using the DC as a relay (gateway).

By this clustering approach, the last hop connectivity from the utility is subdivided into backhaul and last mile. While BPLC is used in the backhaul, each of NPLC, BPLC and Wi-Fi is used in the last mile for comparison. To assess the performance of the AMI network over BPLC, two important types of smart grid application traffic; smart metering and DR are simulated. It will be shown at the end of this chapter that with some modifications in existing network topology, using power line can result in savings in terms of space and energy requirements. The system model employed is shown and discussed in the next section.

3.1.2 Broadband PLC for Clustered AMI: System Model

This work is based on the European LV network discussed in section 2.3 in which smart meters are fitted with advanced solid-state components that collect and dispatch time-based measured data. The role of communication is to facilitate the transmission of the data to the utility's data centre for further processing, hence, bidirectional communication is vital. Unlike other media such as Wi-Fi, Ethernet or fibre optic cables which requires dedicated infrastructure, PLC naturally aligns with existing electrical network and provides connectivity directly to devices without separate wirings. However, data signals experience various forms of distortions and losses as they propagate through it. These factors affect performance of AMI and its application. For instance, the sudden switching "off" and "on" of electrical loads by users in the neighbourhood can change the electrical configuration, characteristics and noise level in the NAN as described in Section 2.3.4.5.

IEEE 2030 broadly provides architectural perspectives for integrating ICT with power systems. The HAN, NAN, WAN and longhaul are covered within the communication technology perspectives. In this work, these specifications are mapped into AMI and the resulting networks are illustrated in Figures 3.1 and 3.2.

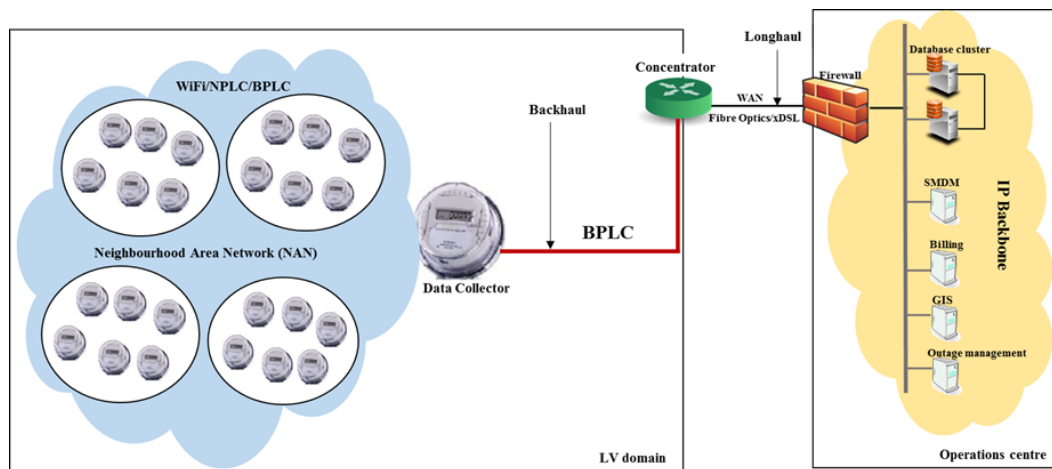


Figure 3.1: Logical topology of smart metering network over the LV power line network

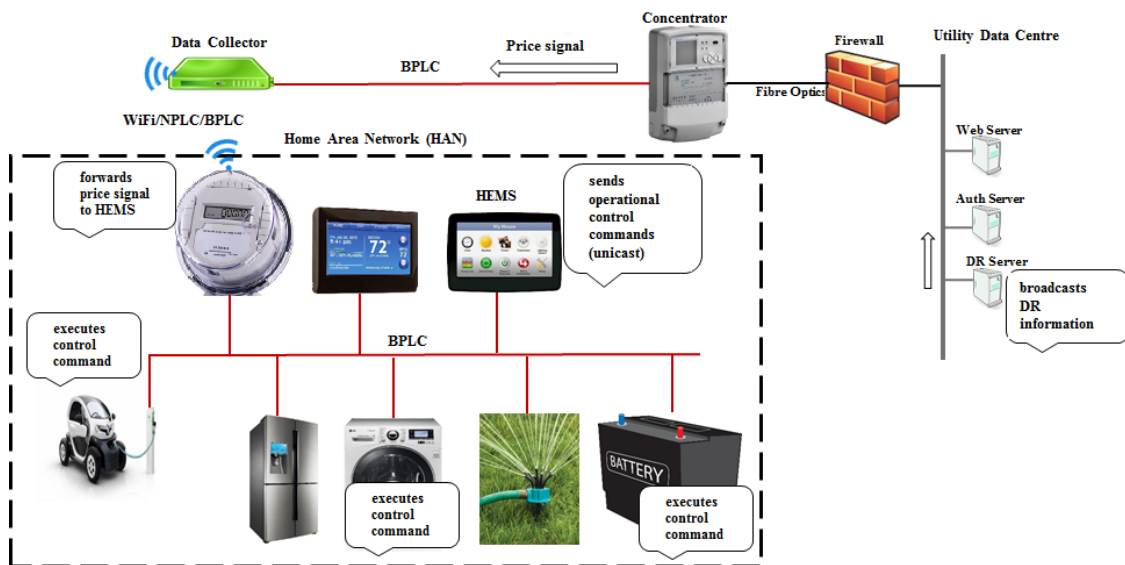


Figure 3.2: Transmission of peak price signal over PLC network.

3.1.3 Smart Metering

Typically, each meter may send its reading periodically according to predefined schedule or on-demand. Figure 3.1 illustrates smart meters in a NAN connected to the concentrator through a BPLC backhaul. In the proposed

model, a DC has been introduced to locally aggregate consumption information from other smart meters, validate and transmit them to the meter data management server (MDMS) using concentrator as the gateway. It should be noted that, in this model, DC is also a smart meter. The concentrator is assumed to be co-located with the transformer at the local or secondary substation where it collates and tracks measurements from one or more DCs, while ensuring that the data is uploaded to utility network in a timely fashion over the WAN. The DC, acting as a network relay, backhauls the traffic via BPLC to the utility. This logically reduces the distance-related losses, especially for meters located at the far end of the service region. At the end of this chapter, the performance of BPLC backhaul is discussed when each of Wi-Fi, BPLC and NPLC is used as the last mile between the DC and smart meters.

3.1.4 Demand Response

Similar to smart metering, transmission of peak price signals is also considered. DR can be implemented in many ways. Apart from peak shaving and load relief in emergencies, DR programs can also be used to provide ancillary services. The description and delay requirements of various load-driven ancillary services are outlined in [107]. The DR studied in this chapter emulates the implementation in [53]. By inducing consumption patterns in response to reserve level or unforeseen changes in the grid, this type of price-driven DR program can also be used for load shedding or shifting, thus providing an additional degree of freedom in terms of grid reliability. While it is possible for each customer to administer the EMS in the home, it is also possible for a provider to control customer's loads directly through the local EMS. A typical HAN consists of everyday smart domestic loads connected to the energy distribution network through the smart meter. The loads register with the EMS which monitors, controls and coordinates their operations. Figure 3.2 illustrates a simple DR model over the power line network showing exchange of price and control signals between utility and home EMS.

3.2 Model Evaluation

3.2.1 Methodology

In order to evaluate the proposed model, a field geometry is created such that smart meters are separated by (10m, 10m) in the x-y Cartesian plane, yielding an Euclidean distance of 14.142 m between any two adjacent meters. Then the performance of two basic applications namely, meter reading and price notification are examined using BPLC in the AMI network. To identify the performance gain, the proposed clustered network is compared with flat [31] AMI network¹.

3.2.2 Simulation Setup

This section presents the simulation setup used in this study. As the investigation of AMI network requires cross-layer approach, the multicarrier modulation and media access specifications in IEEE 1901 are adopted for the PHY and MAC layers respectively. At network layer, the AMI is modelled as an IP network in which valid network addresses are assigned to the smart meters, DC and concentrator. Although other network simulators such as OMNeT++ or OPNET are feasible, NS-3 has been chosen for two reasons: (i) cable models that take into account their electrical properties are available (new ones can be created) in the power line channel model provided in [108] which can be integrated into mainstream NS-3, a free network simulator. This power line channel model is based on TL theory, (ii) within NS-3 environment, upper layer protocols (IP, transport, application) can run on top of the PHY/MAC provided in the PLC module to investigate complete PLC systems and smart grid applications. The provided PLC module supports BPLC and NPLC which can be modified to meet IEEE 1901 (Homeplug) and 1901.2 specifications.

Power line is a time-, frequency- and location-variant channel. Accordingly, impedance can be fixed, time-variant and/or frequency-dependent [70]. For simplicity, a fixed line impedance is applied for the duration of meter reading and DR activities. The AMI is simulated using some libraries provided in [108]. Integrating some of the C++ libraries, the respective networks

¹In this thesis, a flat AMI is regarded as one in which the smart meters communicate directly with the concentrator.

are consequently designed to emulate topologies shown in Figures 3.1 and 3.2 using Wi-Fi and NPLC and BPLC (with reduced data rate) in the last mile. In each of these networks, BPLC is employed at the backhaul. The complete AMI simulation parameters is given in Tables 3.1-3.3.

Table 3.1: PLC parameters

	BPLC	NPLC
Frequency	1.8-30 MHz	1-500 KHz
Line impedance	50 Ω (fixed)	50 Ω (fixed)
Number of OFDM subcarriers	1155 (917 active)	511 (384 active)
Subcarrier spacing	24.41 KHz	976.6 Hz
Symbol length	41 μs	1024 μs
Modulation	BPSK	BPSK
Bits per symbol	1	1
Background noise PSD	-80 dBm/Hz	-80 dBm/Hz
MAC (NAN only)	CSMA/CA	CSMA/CA

Table 3.2: Wi-Fi parameters

Specification	802.11b
Propagation loss model	Log distance
MTU	2200 bytes
Receiver gain	Constant position

Maximum transmission unit (MTU)

Table 3.3: AMI applications parameters

Meter reading	480 bytes
Peak price signal	60 bytes
Number of smart meters	150
Distance between smart meters	14.142 m
Upload window	30 minutes

In Table 3.3, the 30 minutes window has been selected to reflect the half hourly reading upload defined in the smart metering implementation guideline for UK [98]. The IEEE 1901 prescribes carrier sense multiple access with collision avoidance (CSMA/CA) and TDMA at MAC layer. While the smart meters use CSMA/CA to access the power line channel, TDMA provides contention-free data transmission, [109, 110]. As TDMA is deterministic, in this work, only CSMA/CA has been used to observe the network performance in a contention-based NAN which represents a near-extreme situations where all meters attempt to upload or download data at the same time. In addition, the range of measured background noise varies widely in literature [111], [112] and -80 dBm/Hz applies in this chapter. Also, impulsive noise is considered in the simulation as random pulses with peak power, inter-arrival time and duration of -40 dBm, 0-2 ms and 0-1 ms, respectively. The metering application traffic is modelled as client-server communication, utilising user datagram protocol (UDP) at transport layer. The sever application is installed on the SMDM server while the client is installed on the smart meters. That way, the smart meters send their readings, and as a response the SMDM server returns per flow acknowledgement to each smart meter, indicating the number of packets received in the flow.

Generally, the choice of TCP or UDP is a matter of trade-off between efficiency (throughput and delay) on one hand, and delivery guarantees with flow control on the other. However, given that transmission of metering information is typically characterised by short transactions that do not require persistent connection between SMDM servers and the smart meters, it may be more beneficial to employ UDP, nevertheless both protocols applicable. In the

case of DR, since peak price advertisement is multicast traffic which does not elicit acknowledgement, it is simply modelled as a UDP-based application in which the client (installed on DR server) sends price signals to the UDP server (installed on smart meters). UDP is generally beneficial for services in which per-packet in-band acknowledgement and error-correction are unnecessary or can be done at the application layer. This relieves the application of the extra overhead associated with error-correction and flow control at transport layer. In other words, by encoding error-control into the metering software, using UDP, the smart metering application can communicate reliably without incurring the retransmission delay and other performance constraints imposed by TCP congestion control mechanisms. Using basic performance indices, the AMI is assessed in terms of latency, successful upload/downloads and reliability. In principle, communication latency comprises mainly of queuing delay and wireline delay. The connection between the concentrator and the utility data centre (Figures 3.1 and 3.2) is modelled as a high capacity link (fibre optic) with 2 ms latency. The queuing delay is directly proportional to the buffer size of the intervening DC and concentrator, and the wireline delay is determined by data rate of the power line channel. In general, communication delay can be expressed as

$$D = \frac{Load}{Capacity}. \quad (3.1)$$

Given application size S (in bits) with P number of packets and total protocol overhead A (in bits), the wireline delay for each packet can be calculated as

$$D_{wireline} = \frac{A + \frac{S}{P}}{C} \quad (3.2)$$

where C is the link capacity in bps. The latency per switch is given by

$$Delay = D_{queueing} + D_{wireline} \quad (3.3)$$

$D_{queueing}$ is the time interval between when a packet arrive a switch (DC or concentrator) and when it is transmitted. Without traffic prioritisation, (3.3) applies to all switching devices on the communication path. Therefore the total latency experienced by the AMI applications is given by

$$Latency_{end-to-end} = \sum_i^n Delay \quad (3.4)$$

where n is the number of switches such that $0 < i \leq n$. Equations (3.1) - (3.4) hold true for all first-in, first-out (FIFO) schedulers where packets are scheduled for transmission in the order they arrive. As a measure of performance, the packet delivery ratio in this work is defined as the percentage of the packets successfully acknowledged during the meter reading upload window.

3.3 Results and Performance Analysis

In this section, the simulation results are presented and analysed². As seen in Figure 3.1, this work employs a clustered architecture in which data from smart meters are locally aggregated by the DC. Rather than individual transmission to the concentrator, this simplified approach empowers the DC to upload reading for many or all households in a single flow in the case of periodic reading. This is considered more efficient and beneficial for smart meters at the far end of the service area. While maintaining BPLC at the backhaul, each of Wi-Fi, NPLC and BPLC is employed in the last mile and the performance of the application in each case is evaluated.

3.3.1 Network Reliability

In reality, applications respond differently to network characteristics. For instance, to download a 500 MB firmware unto a smart meter, a relatively slower but reliable link is preferable to ensure completeness rather than a fast but intermittent link. Conversely, near real-time applications such as outage notification, peak price or other alarm signals would generally favour fast links given that their sizes are smaller and the probability of packet loss is small too. Therefore, completeness is a key performance indicator for smart metering. To demonstrate this, we investigate reliability of the network by computing PDRs and successful transmission for various packet sizes.

²Note that the results contained in this chapter are mostly published in [31]

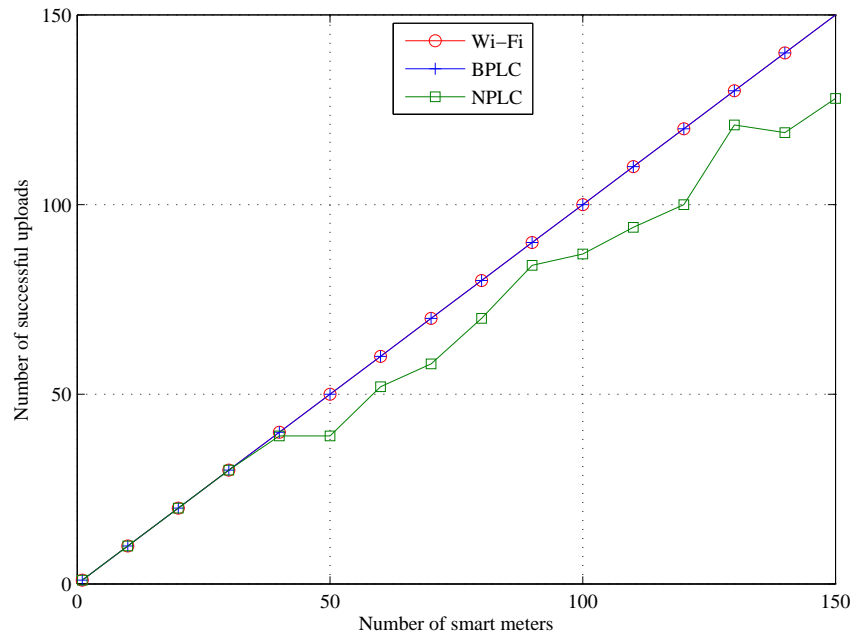


Figure 3.3: Variation of meter reading upload with cluster size

A successful upload is considered as one in which 100% of transmitted packets are received and acknowledged by the SMDM within a window of 30 minutes. Figure 3.3 illustrates the number of successful uploads of meter reading as the cluster size is varied from 1 to 150. It is worthy to note that the specification of BPLC deployed at the last mile is same as the backhaul. This result implicitly means that BPLC can also support a flat architecture where each smart meter connects directly with the concentrator. The figure also reveals that when used in the last mile, BPLC adequately meets traffic requirements of smart metering. Figures 3.4 and 3.5 show the relationship between the number of smart meters and packet delivery.

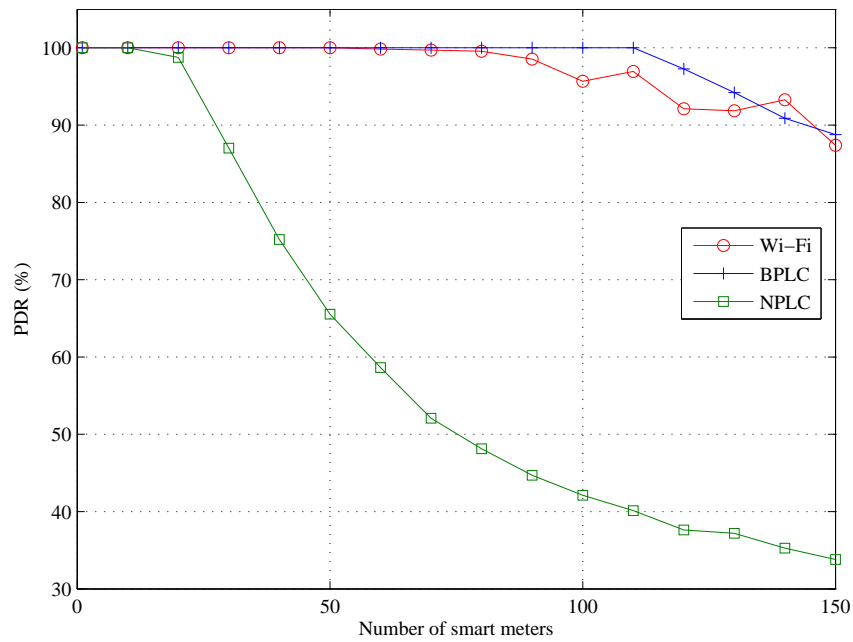


Figure 3.4: Packet delivery ratio as a function of network load in smart metering

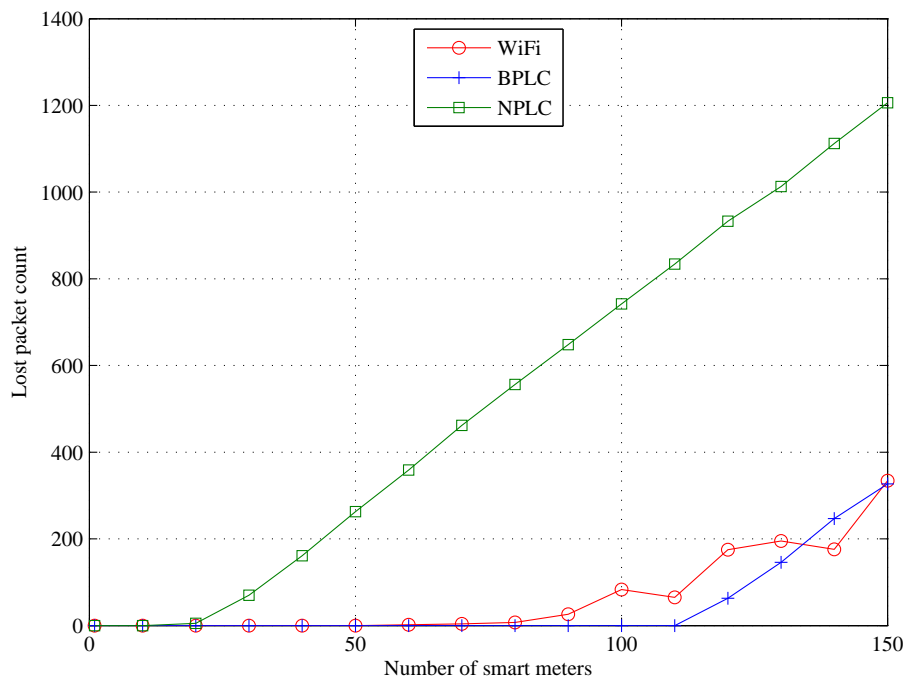


Figure 3.5: Comparing lost packets in Wi-Fi, BPLC and PLC NPLC in smart metering

The 802.11 specification supports maximum payload of 2304 bytes (before encryption). Basic encryption such as Wi-Fi protected access with advanced

encryption standard WPA AES adds an extra 16 bytes of header. Hence, MTU of 2320 bytes is configurable on 802.11, 2200 bytes was applied in this study. Whereas BPLC supports 1500 bytes, 1280 bytes was applied to enable it transmit complete IPv6 packets without fragmentation. The higher MTU of Wi-Fi should ordinarily enable larger amount of data in each flow, Figures 3.3 - 3.5 show that apart from MTU, data rate affects packet delivery. This is further affirmed by the wide disparity between Wi-Fi and NPLC. Theoretically, NPLC delivers maximum of 500 kbps at PHY layer, and the model used in this work provided 363.233 kbps, whereas Wi-Fi used 2 Mbps. In terms of performance, it can also be inferred from the results that the reliability degrades as the cluster size increases. This is reasonable as a higher number of smart meters implies more network load and contention within the NAN.

Nevertheless, based on the network configuration employed, it is evident that Wi-Fi, BPLC and NPLC can effectively support smart metering in cluster sizes up to 30. It is therefore natural to assume that with appropriate cluster sizing, BPLC can potentially provide the backhaul connectivity for smart metering, irrespective of the last mile. The AMI is generally a low data environment (except firmware upgrade), with advanced error correction, more flexibility, robust modulation and coding schemes, real networks can achieve better performance than the basic one discussed here.

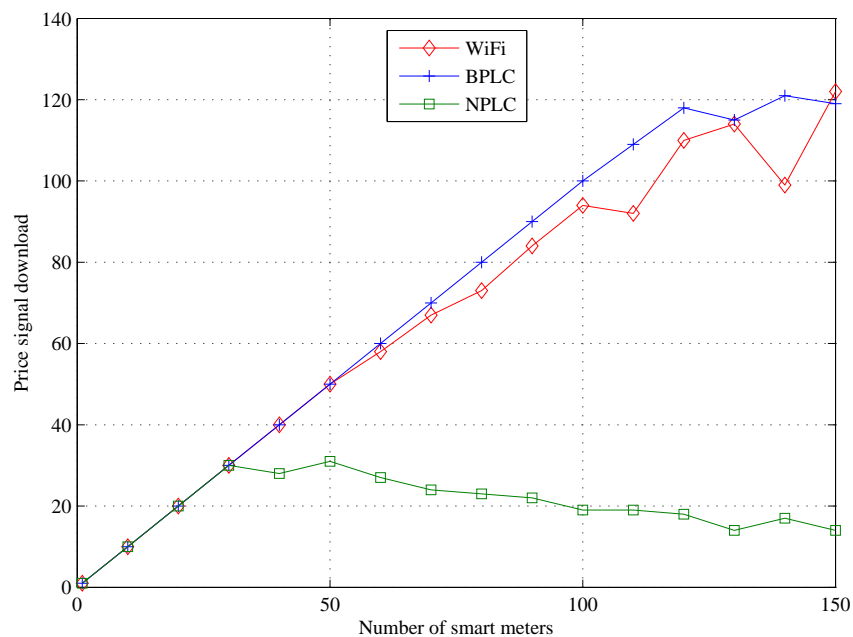


Figure 3.6: Successful peak price downloads versus number of smart meters

Peak price signalling is also investigated, and the result is presented in Figure 3.6. Since price information is time-bounded, price signals are usually less than 100 bytes [48, 53] to facilitate timely delivery. DR application size of 60 bytes is applied in this study. The concentrator receives peak price messages and forwards them to the DC. Since the DC shares a network with other smart meters, it simply forwards the price signal as multicast. From the results presented in Figure 3.6, it follows that if all other conditions are unchanged, BPLC backhaul is adequate to support peak price broadcast from DR server to smart meters. Though the degree of success differs among the three communication systems in the lastmile, what is clear is that given a clustered AMI, BPLC is not a bottleneck and can reliably support smart metering at potentially lower cost than traditional backhaul solutions such as fibre optics.

3.3.1.1 Communication Latency

Using the same network of 150 smart meters, here we evaluate the average latency performance of packets as they traverse from the smart meters to the SMDM server and vice versa. The BPLC in the backhaul and last mile employed 1.8-30 MHz with 19.7204 Mbps PHY rate. A modest binary phase shift keying (BPSK) has been employed in this study, in real implementation, the backhaul may employ a higher order modulation scheme to deliver higher data rate. To simulate completeness of metering information, we model meter readings as UDP echo traffic and consequently investigate various forms of delays associated with smart metering and DR applications. The results are presented in Figures 3.7 and 3.8.

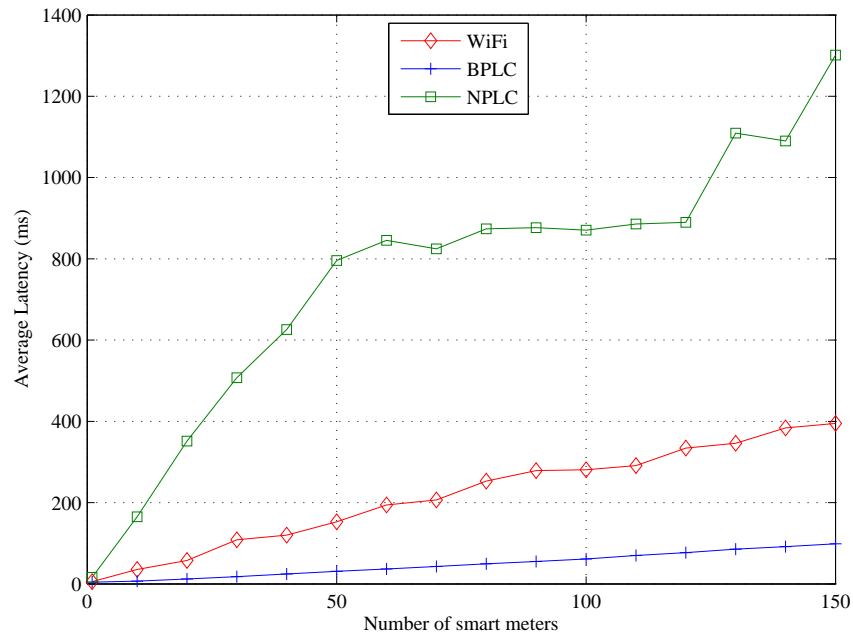


Figure 3.7: Smart metering round-trip latency versus number of smart meters

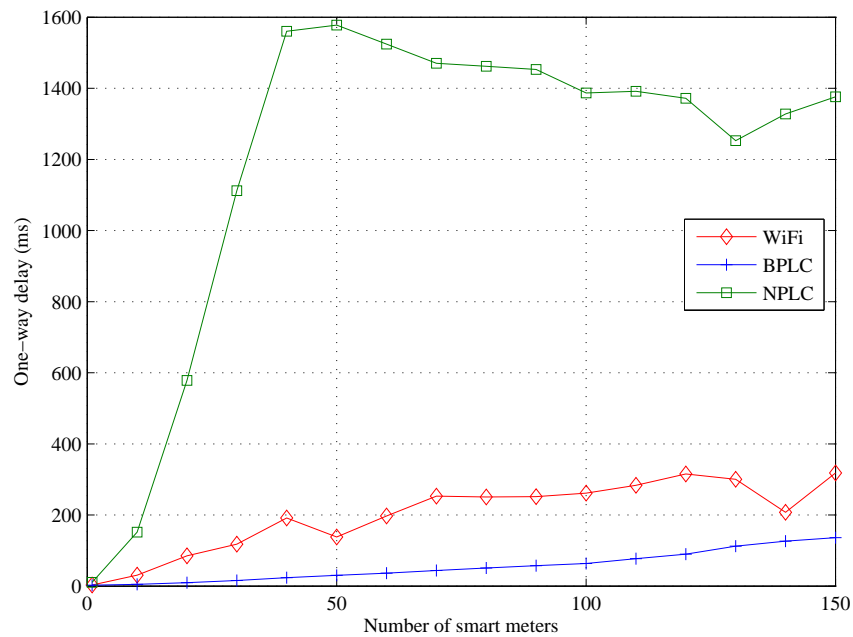


Figure 3.8: Peak price one-way delay versus number of smart meters

Within the 30 minutes window, SMDM is expected to return acknowledgment and only acknowledged uploads are counted as successful. Although NPLC exhibited an impressive performance in Figure 3.3, this is at the expense of high latency as observed in Figure 3.7. However, Figures 3.7 and 3.8,

indicate that even with the low rate modulation of BPLC in last mile and backhaul in a clustered network, it still provides a backhaul that meets the strict delay requirement of peak price signalling. The main observation thus far is that, BPLC has demonstrated capacity to convey metering traffic between the NAN and the provider's network.

3.3.1.2 Effect of Packet Size on Latency

It can be observed from Figures 3.3 and 3.6 that the three communication systems in the last mile achieved 100% packet delivery for cluster size 10-30. Given this level of reliability, the aim in this section is to determine whether there are other factors that could affect performance, and, if they exist, investigate to what extent they can offset system performance. We therefore select cluster sizes 10, 20 and 30 and study the effect of packet sizes on latency.

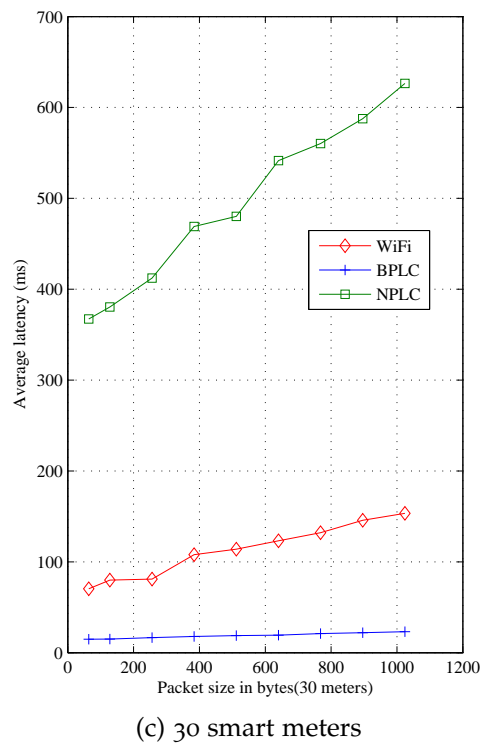
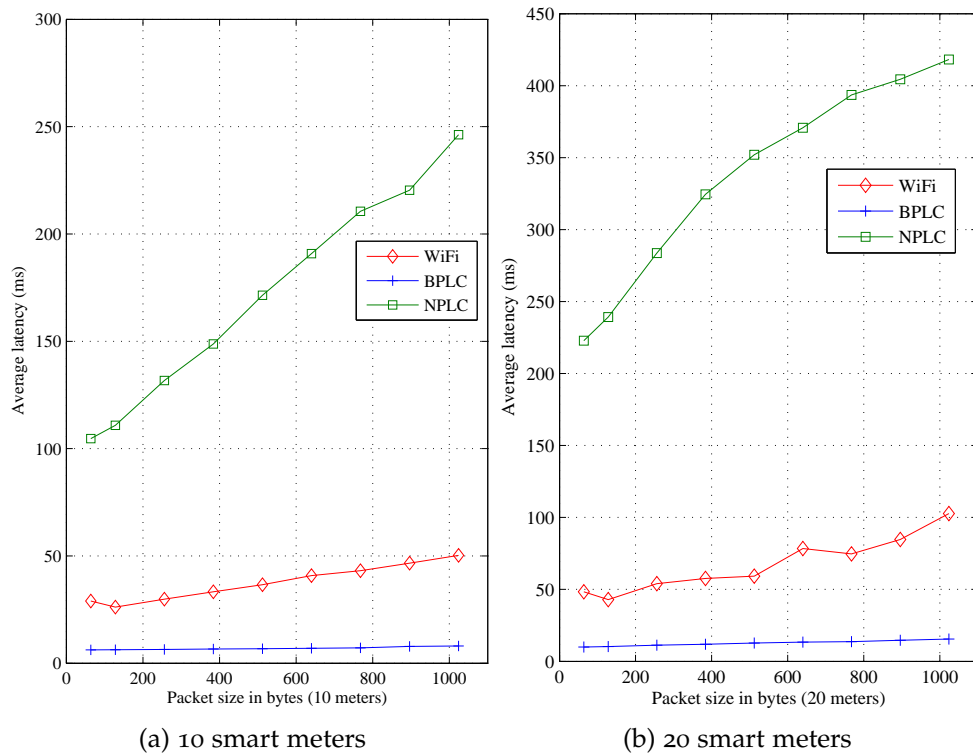


Figure 3.9: Variation of metering round-trip delay with application size

It is observed in Figure 3.9 that while large packet size transfers more data

per time given that overhead is fixed, it does not guarantee timely delivery of the packets. The impact of large packet size is worse in channels with low data rate as large packet occupy the channel for a longer duration than small ones. On the other hand, sending many small messages is less efficient as the overhead is duplicated in all packets; however, smaller packets are faster to deliver, resulting in lower latency, and are less prone to error. Figure 3.9 clearly shows that the performance gap between Wi-Fi and NPLC widens as the application packet size increases. It is therefore recommended that, in meeting QoS requirements of AMI traffic, efficiency should be matched with latency to determine application size. From the point of view of backhaul, these figures show that BPLC is capable of meeting these requirements.

3.3.1.3 Probability of Packet Delivery

In this section, while clustered and flat (without DC) networks are compared, the impacts of aggregation is discussed and the effects of DC position on probability of packet delivery (PPD) is also examined. PPD is defined here as the ratio of received to transmitted packets in a given flow. Since this quantity bears direct consequences on application, it is adopted as a measure of network reliability. Figure 3.10 illustrates the PPD performances of Wi-Fi, BPLC and NPLC in flat and clustered networks. As can be seen in the figure, for cluster sizes below 50 smart meters, Wi-Fi and BPLC are not affected by the DC. This is reasonably true given their capacities to push more data through the network compared with NPLC.

In clustered design, Wi-Fi exhibited an improvement (with respect to flat achitecture) in packet delivery by approximately 0.4% with 80 smart meters and 0.6% with 110 smart meters respectively. With BPLC, the performance gain from the DC is most evident at cluster sizes 100 to 150 smart meters. One plausible explanation is that as the number of smart meters increases, the contention for network resources also increases. Therefore, the chances of smart meters at the far end of the cluster to successfully deliver packet within the allotted time diminishes which translates to coverage limitation. The benefit of a DC in this case is to help enhance packet delivery and improve network coverage. In the case of NPLC, performance fluctuates with different cluster sizes. The maximum improvement of 1% is observed at cluster size 30 while the highest penalty of -2.5% is observed at 120 smart meters. Apart

from 130, for clusters between 60 and 150 smart meters, DC adversely affected the PPD. It is worthy to note that although DC, being a relay, contributes to network latency, its benefit is still visible because despite the additional latency, end-to-end delay falls within acceptable limits.

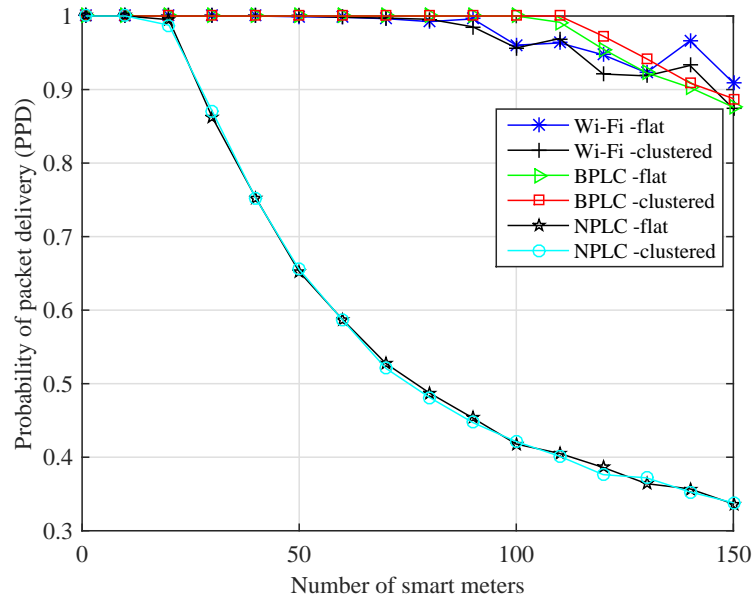


Figure 3.10: Probability of packet delivery of flat and clustered AMI

Figure 3.11 shows the effect of DC position on PPD performance when NPLC lastmile is used.

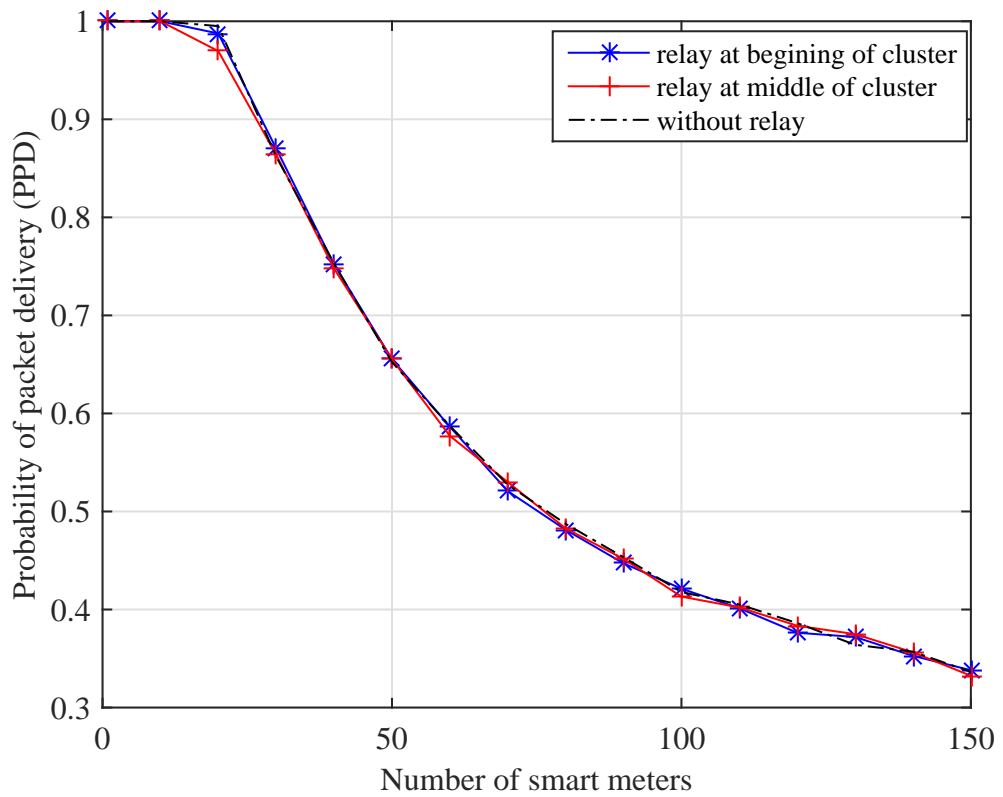
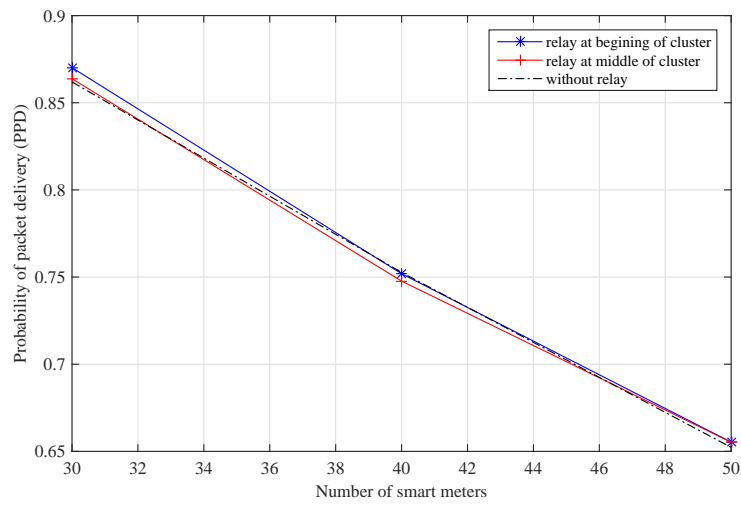
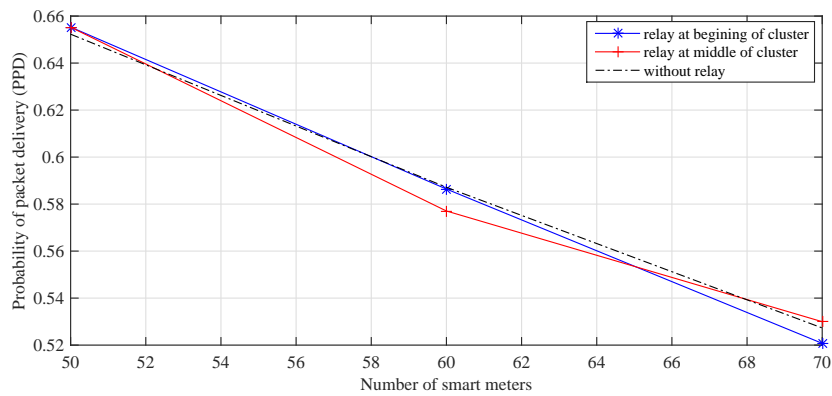


Figure 3.11: Variation of PPD performance with DC (relay) position

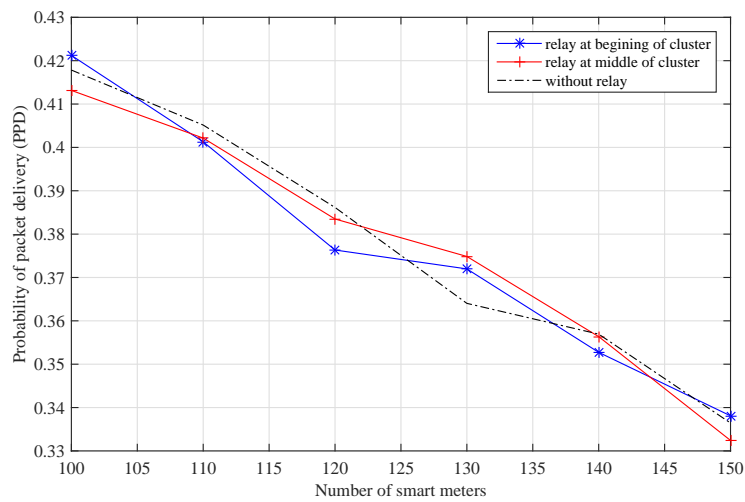
The expanded views of Figure 3.11 are provided in Figure 3.12



(a) Expanded view with 30-50 smart meters



(b) Expanded view with 50-70 smart meters



(c) Expanded view with 100-150 smart meters

Figure 3.12: DC position on PPD (with NPLC last mile)

As seen in this Figures 3.11, the effect of DC is negative for cluster sizes up to 20 smart meters, hence aggregation is not recommended for small cluster sizes, except where the smart meters are widely dispersed and direct communication with concentrator is not feasible. It can also be seen in Figure 3.12 that with the DC at the beginning of the cluster, PPD improves at 30, 50, 100 and 150 cluster sizes. The maximum improvement occurred at 30, where PPD increased by approximately 1%. With the DC at the middle of the cluster, PPD improved at 30, 50, 70 and 130, the maximum occurred at 130 where it rose by approximately 3%. These improvements in probabilities could potentially increase the number of successful reading uploads by smart meters and improve coverage.

3.3.2 Network Energy Efficiency

For large service areas found in many European cities, single-hop communication may not be adequate to satisfy the QoS requirements of smart metering or DR applications. Expectedly, the meters at the extreme ends of the field will be most affected by distance-related losses. Due to attenuation of signal power, a packet can be lost, corrupted, malformed or incorrectly received by the next hop switch, (DC or concentrator). In any of these cases, the performance of the application will be affected and the energy spent in transmitting the packet will be wasted as well. In order to optimally satisfy application QoS requirements, two options are feasible.

- Option 1: Introduce network relays. This reduces distance-related losses and since the switches are repeaters, regenerating the signals, link qualities such as PDR and throughput generally improve. However, this improvement comes at the expense of higher power consumption by the intermediary switches.
- Option 2: Improve packet delivery. As seen in Figures 3.4, 3.5 and 3.10, employing BPLC in the last mile can reduce the end-to-end packet losses. In the LV domain, electrical cables run from transformers in the secondary substation to neighbourhoods, branching off to individual homes. Since power line is a shared medium, if multiple users transmit simultaneously, signals from one home may interfere with another. As the number of concurrent transmissions increases in the neighbourhood,

the chances of interference also increases [113]. The larger bandwidth of BPLC (1 - 100 MHz implementation) [50] enables it to avoid some frequency bands without compromising the data rate [8, 50, 114, 115]. This resilience makes a huge difference between NPLC and BPLC in terms of effective, latency, throughput and PDR which are important communication qualities.

The clustered AMI proposed in this chapter combines the features of these options by exploiting the network topology to improve PPD without dedicated relays. Adopting the expressions in [116], for readings transmitted from a smart meter to the concentrator, the end-to-end packet loss probability can generally be written as

$$P_{Loss} = 1 - (1 - \eta^a) \left[1 - \prod_{j \in \mathcal{H}} (1 - \eta_j^r) \right] (1 - \eta^l)^d \quad (3.5)$$

where \mathcal{H} is the set of switches between the smart meters and the concentrator; $d = 1$ if meter and the concentrator are in the same cluster and 0 otherwise. η^a , η_j^r , η^l are packet-error rate (PER) for the intra-cluster, inter-cluster and last-hop. For each hop, the PER is given by

$$\eta = 1 - (1 - BER)^\delta \quad (3.6)$$

where BER is the bit-error-rate of the power line channel and δ is the packet size (in bits). Given a power line network characterised by total noise power P_N , in order to maintain an acceptable level of SNR at the receiver, the transmit power required by the signal can be expressed as

$$P_T = \text{SNR}(\text{dB}) + P_N + P_L \quad (3.7)$$

where P_L is the lost power due to attenuation. Hence, it is clear from (3.6) - (3.7) that in order to obtain the minimum transmit power that satisfies the SNR requirement (at the receiver side), the packet loss must be minimised. Therefore, using energy efficiency as a metric of performance, improvement in PPD translates to reduction in the transmit power requirements of end-to-end packet delivery over the PLC network.

3.4 Chapter Summary

This chapter investigated BPLC as a backhaul for AMI and discussed its prospects. Simulation results have shown that BPLC is a promising backhaul technique for AMI applications, with energy-saving potentials. The main outcome of this study is that, with clustered architecture packet losses can be reduced. One key benefit seen in the results is that using a local aggregator (DC), network coverage can potentially be improved by at least 3% relative to flat AMI (this follows from about 3% increase in PPD). The result also showed that for small cluster sizes of 1-20 smart meters, the use of DC can be a disadvantage. Therefore the scheme is not recommended for small cluster sizes except for geographically dispersed meters.

Chapter 4

Low-Power PLC for Energy Management Systems

The HAN is perhaps of most interest to consumers and is equally crucial to the success of the smart grid program. In order to leverage the mass market offered by energy management in homes, a new generation of low-power communication systems is actively needed. Among other qualities, such communication systems must be pervasive throughout the home. Although PLC technology has evolved in the last two decades, its adaptation for constrained networks is not fully charted and untapped potentials still exists. This chapter explores an experimental adaptation of IPv6 over LoWPAN (6LoWPAN) features in PLC networks for monitoring and control applications within the in-building micro-grid. This low-power PLC system is referred to as 6LoPLC whose performance is evaluated in a HEMS network. Thus, the essence of this chapter is to demonstrate 6LoPLC as alternative and complimentary low-power technology for environments with a strong diversity of appliances or multi-dwelling units where a single wireless solution may not meet the network requirements. The model was developed in NS-3 and in validating it, two basic HEMS applications namely light control and temperature sensing are investigated. The results¹ show that 6LoPLC is promising and can satisfy the QoS requirements of typical HEMS application traffic within acceptable limits, provided application data size does not exceed 64 bytes. The results further reveal that to optimally balance energy savings with transceiver cost, differential binary phase shift keying (DBPSK)

¹Most of the results discussed in this chapter are published in [80]

modulation scheme should be employed. This chapter is organised as follows. Section 4.1 begins with a general discussion of HEMS, followed by a description of the proposed 6LoPLC and brief analysis of the hardware used in the experimental part of the study. In section 4.2, modalities for evaluating 6LoPLC is presented. In particular, the experimental set-up, derivation of model parameters and NS-3 simulation environment are discussed. Performance of 6LoPLC system is analysed in section 4.3 based on measurements and simulation result while the main conclusions of this study are highlighted. in section 4.4.

4.1 Home Energy Management System

It was seen in Chapter 3 that the AMI sub-system provides infrastructural connection between the consumer domain and the power utility's network. The DR programs (outlined in Section 2.1.6), coupled with the rapid development of technology and profitable feed-in tariff are empowering customers for flexible demands [117] and to gain control over the way energy is produced and consumed [118,119]. In view of this, more DERs such as PV plants are increasingly being installed by home users to produce few kW to meet their energy requirements and sell excess to the market [119]. This duality of role is termed *prosuming*. As the deployment of DERs become common in homes, sophisticated monitoring and control are required to maximise the economic incentives arising from local generation and grid-balancing at peak periods. These can be realised through the integration of smart in-home appliances [120], DG systems and DS systems to form a HEMS. The HEMS functions as an integrated system to monitor the generation, storage and consumption of electricity in the home [121]. HEMS provides utilization status of appliances as well as activities of the DG and DS assets [121]. The role of the HEMS controller is to monitor and coordinate the operations of the loads and DERs in the most efficient ways [122,123].

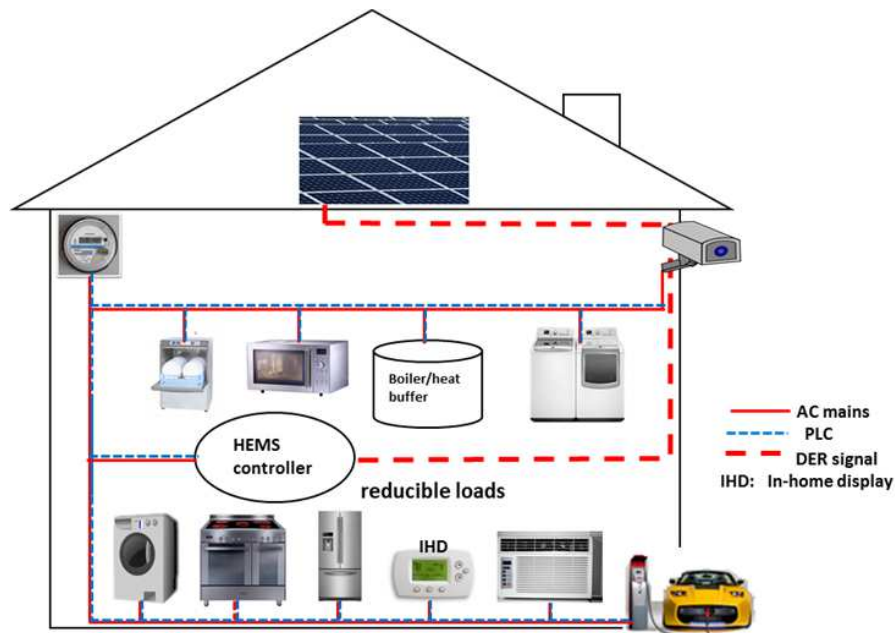


Figure 4.1: HEMS model showing various types of in-home loads.

Figure 4.1 illustrates a simple HEMS network showing the connection between smart in-home appliances and the controller. With such level of monitoring in the HAN, energy consumption data from all household devices can be collected and made available in near real-time to remote stations such as laptops and smart phones via different communication links. It was reported in [124, 125] that such awareness of energy usage by consumers can improve efficiency by as much as 12-15%. To maximize their benefits from the time-varying electricity price, residential users will continue to deploy HEMS to manage their heavy loads such as PEVs on one hand and monitor local generation on the other. Therefore, massive deployment of HEMS is imminent and this can potentially open new market opportunities such as demand for low-power PLC systems for low data-rate applications. Like other control networks, the design philosophy behind HEMS is that in-home smart appliances add more value when they are integrated and function as a network, than autonomous deployment of individual entities. In such case, the resulting network is as resilient as the underlying communication technology enabling it.

4.1.1 IPv6-enabled Low-Power PLC (6LoPLC)

In HEMS, ZigBee is one of the widely-deployed low-power communication technologies, with solutions such as SEP 1.x and SEP 2.0 available on the market. Of course, there are use-cases where ZigBee is arguably preferred above others (e.g., battery thermostats, gas metering and water metering), there are also HEMS applications where the PLC solution is more appropriate (e.g., sensing of power quality, load control, PEV management, DG/DS management, etc.). Rather than debate the merits or otherwise of low-power wireless system for HEMS applications, this thesis accepts the substantial work already done in that area and extends some of its capabilities into power line networks. This should inspire a new wave of complimentary or alternate communication systems for HEMS applications. For example, wireless communication in buildings with metallic walls, cellars and underground structures can be severely challenging and often results in blind spots (locations where the wireless signal is weak or absent). PLC is specifically suitable for such situations and generally appealing for HEMS, not only because it is pervasive in most homes, but it also provides the scalability and availability needed by HEMS applications.

4.1.2 Hanadu PLC Transceivers

The purpose of this section is to briefly describe the hardware used in the experimental phase of this study. The hardware is called Hanadu². The Hanadu PLC transceivers consist of low-power PLC chips which specify the PHY and MAC layers, coupled with 6LoWPAN and upper layer protocols at network, transport and application layers. The hardware and its emulation are based on department of defence (DoD) four-layer TCP/IP reference model, widely used in practical systems. The protocol mapping between TCP/IP suite and the implemented model, which includes 6LoPLC at the adaptation layer in accordance with RFC 2460, is illustrated in Figure 4.2.

²Low-power PLC evaluation hardware code-named “Hanadu” was developed by Xsilon Ltd- an industrial partner in a recently-concluded EPSRC-funded project with MMU

Application	CoAP
Transport	UDP, ICMPv6
Network	IPv6
	6LoPLC
MAC	IEEE 802.15.4
Physical	Hanadu PLC PHY

Figure 4.2: Protocol stack showing 6LoPLC.

Although, the evaluation systems employ 0-32 MHz, which is within the BPLC spectrum, in contrast with the conventional BPLC system (such as Homeplug), it was designed for low-rate in-home monitoring and control applications, such as smart lighting. Furthermore, the evaluation systems are based on OFDM, and the tone map is such that the 32-MHz spectrum is divided into 128 sub-carriers. Each sub-carrier occupies a bandwidth of 250 kHz, such that if further divided into five bands, approximately half the signal energy is contained in the middle band. Hence, for each carrier, the centre frequency is:

$$f_c = \frac{(f_l + f_h)}{2}, \quad (4.1)$$

where f_l is the lower frequency bound and f_h is the upper frequency bound.

To avoid interference with nearby radio transmissions and reduce inter symbol interference, only 86 channels are utilised, notching out broadcast and amateur radio frequencies (e.g., 28-29.875 MHz). As seen in Figure 4.2, evaluation hardware retains the 802.15.4 MAC sublayer and replaces the PHY with the 2-30 MHz power line PHY, thus transforming it into a PLC system. The test bed used for evaluating the 6LoPLC consists of three types of entities: lighting, communication system and application. While the lighting is made of an light-emitting diode (LED) fixture powered by 24 V DC, the Hanadu units provide the communication over power lines to convey control signals from the HEMS controller to the lamp and response in the opposite direction. In terms of protocol, the lighting and sensing applications are based on constrained application protocol (CoAP). CoAP was developed by IETF for resource-constrained nodes and networks (RFC 7252), such as the low data

rate sensor and lamp discussed in this work. Due to the high communication overhead associated with hypertext transfer protocol (HTTP), CoAP was developed to offer web services similar to HTTP, but with lower overhead by employing an asynchronous message exchange that relies on a data-oriented transport protocol [126]. Hence, the evaluation system and simulations are based on UDP, since CoAP natively supports it. In terms of use-cases, CoAP was intended for smart energy, building automation and control applications, which are in tune with this study as well.

4.2 6LoPLC System Evaluation

4.2.1 Methodology

This section describes the procedure carried out in evaluating 6LoPLC. The evaluation was carried in two parts; experimental measurements and modelling. Three units of evaluation hardware were available for the experiment, which limited the number of HEMS scenarios that could be studied in real network. To bridge the gap, a representative model is first developed in NS-3 to emulate the test bed. Following the necessary calibrations and validation of the model with experimental measurements, various HEMS configurations are then studied to cater for scenarios and configurations that cannot be investigated on the test bed.

4.2.2 Experimental Set-up and Measurement

The measurements in this section were carried in the power line network illustrated in Figure 2.8. The power lines converge at the consumer unit located in main lab where the network is segmented into four circuits. All experiments were carried out in the main lab during which connections to 2nd floor lab₁ and 5th floor lab₁ were isolated within the consumer unit. The simplified network layout is presented in Figure 4.3.

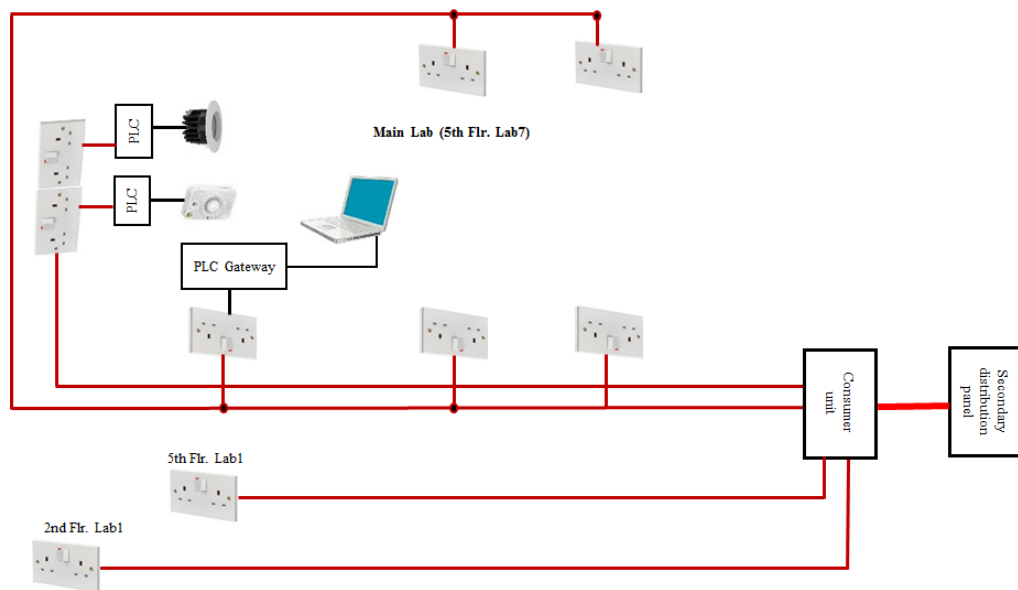
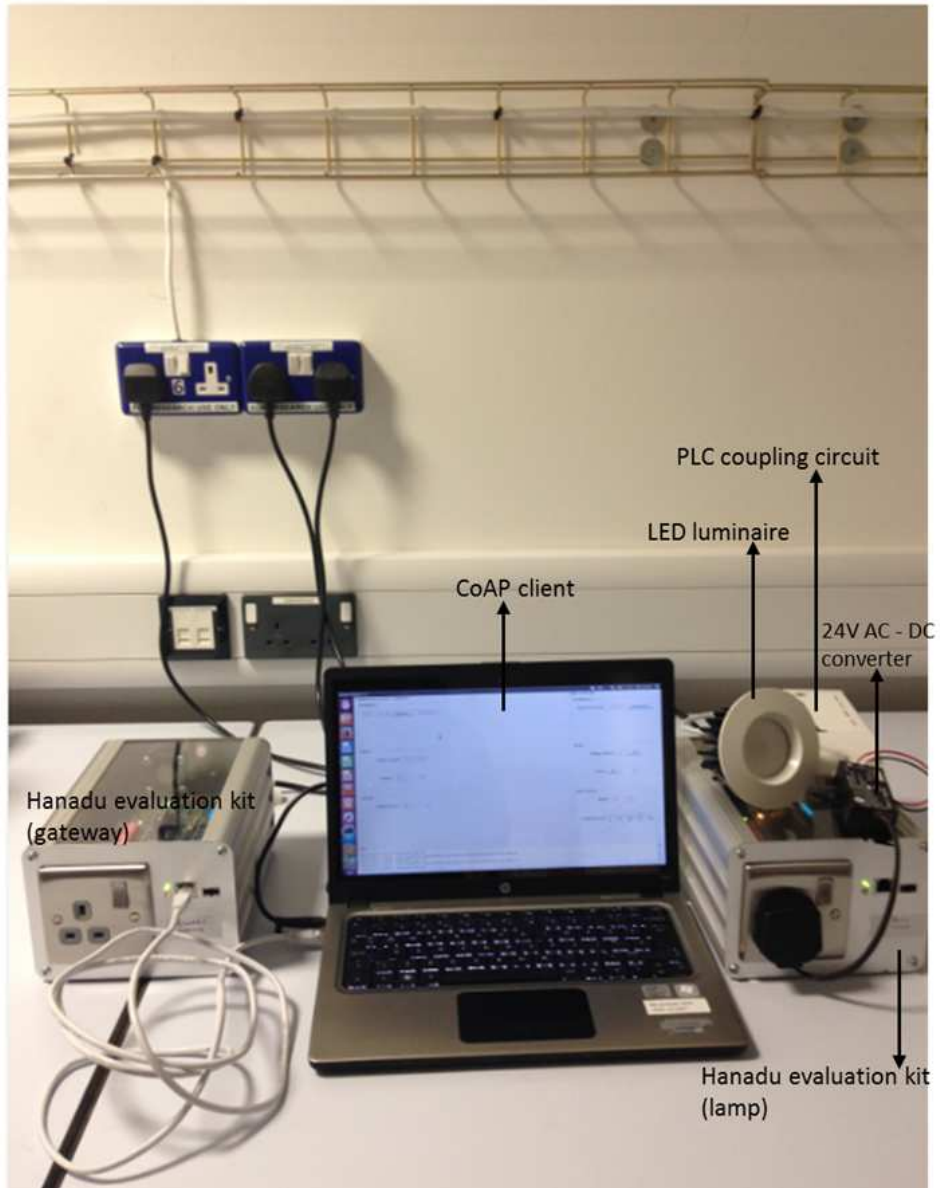
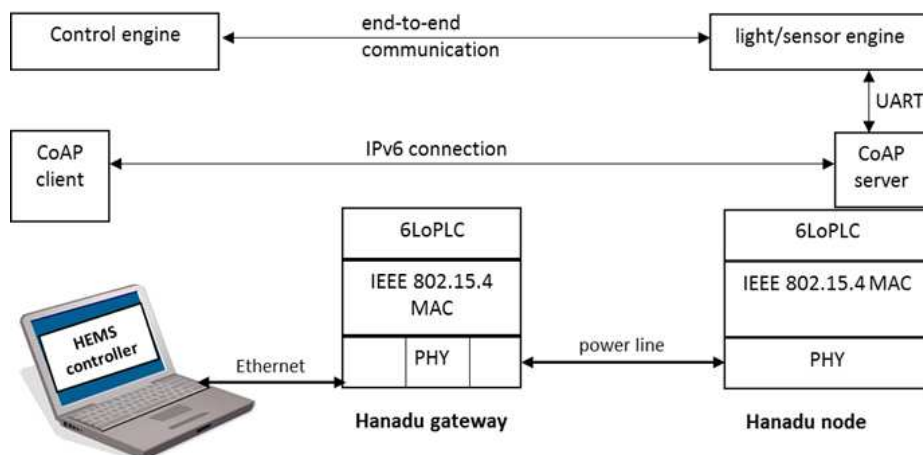


Figure 4.3: Experimental PLC network in the main lab



(a) The main functional components



(b) The communication among system components

Figure 4.4: Evaluation testbed for 6LoPLC

The measurement set-up used in this work is presented in Figure 4.4. Using the three units of evaluation PLC modems available, a HEMS network was setup such that the CoAP client is installed on the HEMS controller while the server is installed on the nodes (lamp and sensor). The CoAP client provides the mechanism for sending control commands and monitoring requests. For example, the CoAP client can request from the nodes, the energy consumed by the device connected to their attached sockets and can also send the control signal to alter the luminance of the LED lamp over the power line network. In the case of the temperature polling, when the client requests the ambient temperature from the sensor, the CoAP server (on the sensor) encodes the measured temperature into a CoAP message and returns it as response to the controller. Therefore, the role of the CoAP application is to provide an embedded web interface to interactively send control signals and receive measurements from the nodes. In both cases of the sensor and lamp, the CoAP server communicates with the respective engines through universal asynchronous receiver/transmitter (UART) commands, as shown in Figure 4.4b. The test bed is such that the monitoring (temperature, energy sensing) and control signalling are triggered manually. These are necessary to allow deep visibility into system behaviour. In real deployments, polling of sensor data will be automated based on a predefined schedule, while control will be on-demand.



Figure 4.5: Constrained Application Protocol (CoAP) interface showing the monitoring (sensor) and control (lamp) windows.

The interactions between the CoAP client and server is illustrated in Figure 4.5, showing some system-level information about communication activities between the HEMS controller and the lamp. For example, the log messages show that a control command was used to increase the luminance of the lamp from 63 to 74%, such low-level information are useful for system maintenance and support. Furthermore, samples of connectivity test results are presented in Figure 4.6 showing the communication between HEMS controller and the lamp using application data sizes 64 and 256 bytes. It should be noted that these values strictly represent the payload only as Internet control message protocol (ICMP) messages incur an overhead of 8 bytes as observed in the Figure 4.6.


```

ikpehai@ikpehai-laptop: ~
File Edit View Search Terminal Help
ikpehai@ikpehai-laptop:~$
ikpehai@ikpehai-laptop:~$
ikpehai@ikpehai-laptop:~$ ping6 4000:5::203:9a00:0:134 -s 64
PING 4000:5::203:9a00:0:134(4000:5::203:9a00:0:134) 64 data bytes
72 bytes from 4000:5::203:9a00:0:134: icmp_seq=1 ttl=63 time=16.2 ms
72 bytes from 4000:5::203:9a00:0:134: icmp_seq=2 ttl=63 time=16.5 ms
72 bytes from 4000:5::203:9a00:0:134: icmp_seq=3 ttl=63 time=16.1 ms
72 bytes from 4000:5::203:9a00:0:134: icmp_seq=4 ttl=63 time=15.9 ms
72 bytes from 4000:5::203:9a00:0:134: icmp_seq=5 ttl=63 time=16.3 ms
72 bytes from 4000:5::203:9a00:0:134: icmp_seq=6 ttl=63 time=16.6 ms
72 bytes from 4000:5::203:9a00:0:134: icmp_seq=7 ttl=63 time=16.1 ms
72 bytes from 4000:5::203:9a00:0:134: icmp_seq=8 ttl=63 time=16.6 ms
72 bytes from 4000:5::203:9a00:0:134: icmp_seq=9 ttl=63 time=16.3 ms
72 bytes from 4000:5::203:9a00:0:134: icmp_seq=10 ttl=63 time=16.4 ms
72 bytes from 4000:5::203:9a00:0:134: icmp_seq=11 ttl=63 time=16.4 ms
72 bytes from 4000:5::203:9a00:0:134: icmp_seq=12 ttl=63 time=16.8 ms
72 bytes from 4000:5::203:9a00:0:134: icmp_seq=13 ttl=63 time=16.5 ms
72 bytes from 4000:5::203:9a00:0:134: icmp_seq=14 ttl=63 time=16.6 ms
72 bytes from 4000:5::203:9a00:0:134: icmp_seq=15 ttl=63 time=16.5 ms
72 bytes from 4000:5::203:9a00:0:134: icmp_seq=16 ttl=63 time=16.1 ms
72 bytes from 4000:5::203:9a00:0:134: icmp_seq=17 ttl=63 time=16.5 ms

```

(a) Latency with payload size of 64 bytes

```

ikpehai@ikpehai-laptop: ~
File Edit View Search Terminal Help
ikpehai@ikpehai-laptop:~$
ikpehai@ikpehai-laptop:~$
ikpehai@ikpehai-laptop:~$ ping6 4000:5::203:9a00:0:134 -s 256
PING 4000:5::203:9a00:0:134(4000:5::203:9a00:0:134) 256 data bytes
264 bytes from 4000:5::203:9a00:0:134: icmp_seq=1 ttl=63 time=37.7 ms
264 bytes from 4000:5::203:9a00:0:134: icmp_seq=2 ttl=63 time=38.0 ms
264 bytes from 4000:5::203:9a00:0:134: icmp_seq=3 ttl=63 time=38.6 ms
264 bytes from 4000:5::203:9a00:0:134: icmp_seq=4 ttl=63 time=38.4 ms
264 bytes from 4000:5::203:9a00:0:134: icmp_seq=5 ttl=63 time=38.4 ms
264 bytes from 4000:5::203:9a00:0:134: icmp_seq=10 ttl=63 time=38.4 ms
264 bytes from 4000:5::203:9a00:0:134: icmp_seq=11 ttl=63 time=38.1 ms
264 bytes from 4000:5::203:9a00:0:134: icmp_seq=12 ttl=63 time=38.3 ms
264 bytes from 4000:5::203:9a00:0:134: icmp_seq=13 ttl=63 time=38.5 ms
264 bytes from 4000:5::203:9a00:0:134: icmp_seq=14 ttl=63 time=38.2 ms
264 bytes from 4000:5::203:9a00:0:134: icmp_seq=15 ttl=63 time=37.9 ms
264 bytes from 4000:5::203:9a00:0:134: icmp_seq=16 ttl=63 time=38.3 ms
264 bytes from 4000:5::203:9a00:0:134: icmp_seq=17 ttl=63 time=38.8 ms
264 bytes from 4000:5::203:9a00:0:134: icmp_seq=18 ttl=63 time=38.4 ms
264 bytes from 4000:5::203:9a00:0:134: icmp_seq=19 ttl=63 time=38.5 ms
264 bytes from 4000:5::203:9a00:0:134: icmp_seq=20 ttl=63 time=38.2 ms

```

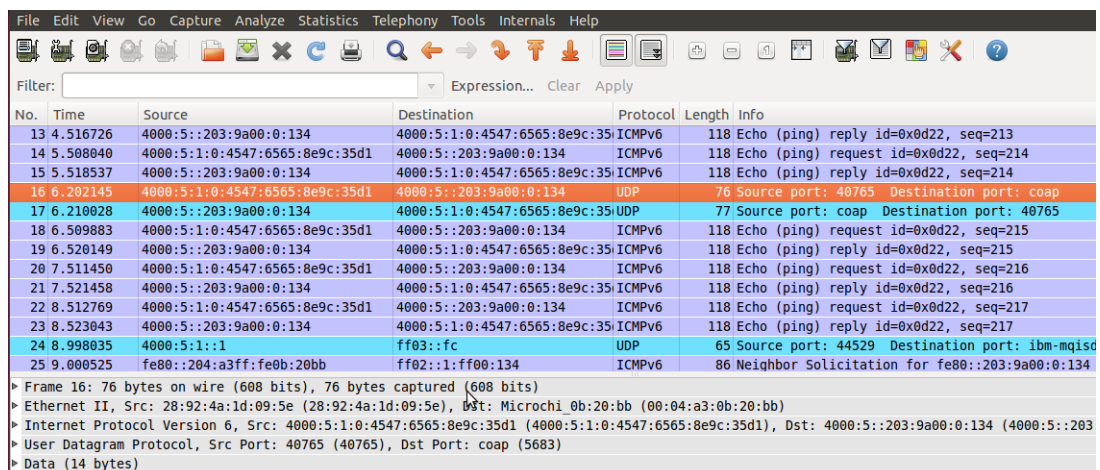
(b) Latency with payload size of 256 bytes

Figure 4.6: Samples of two-way delay

4.2.3 System Parameterisation and Traffic Analysis

To successfully develop a network model for the HEMS, it is necessary to understand not only the PLC transceiver system parameters but also the application traffic characteristics. The idea of this section is therefore to extract network traffic parameters from the test bed and apply them to develop the

network model in NS-3. One modem (connected to the HEMS controller) and two others (used as nodes) are employed in this section. We begin by setting up a PLC network between the controller and one of the nodes designated as the LED-lamp. In contrast with filament-based lights, the LED-lamp fixture used in this work is a full-fledged network node with valid network properties such as the IPv6 address; same applies to the sensor. For experimental purposes, the lamp is deployed as the light source whose intensity is controlled over the power line network. To view the bi-directional communication, Wireshark, an open source packet sniffer was installed on a Linux laptop and connected to the Ethernet port of the HEMS controller to monitor the end-to-end communication traffic. A sample of the traffic analysis is presented in Figure 4.7.



No.	Time	Source	Destination	Protocol	Length	Info
13	4.516726	4000:5::203:9a00:0:134	4000:5:1:0:4547:6565:8e9c:35d1	ICMPv6	118	Echo (ping) reply id=0x0d22, seq=213
14	5.508040	4000:5:1:0:4547:6565:8e9c:35d1	4000:5::203:9a00:0:134	ICMPv6	118	Echo (ping) request id=0x0d22, seq=214
15	5.518537	4000:5::203:9a00:0:134	4000:5:1:0:4547:6565:8e9c:35d1	ICMPv6	118	Echo (ping) reply id=0x0d22, seq=214
16	6.202145	4000:5:1:0:4547:6565:8e9c:35d1	4000:5::203:9a00:0:134	UDP	76	Source port: 40765 Destination port: coap
17	6.210028	4000:5::203:9a00:0:134	4000:5:1:0:4547:6565:8e9c:35d1	UDP	77	Source port: coap Destination port: 40765
18	6.509883	4000:5:1:0:4547:6565:8e9c:35d1	4000:5::203:9a00:0:134	ICMPv6	118	Echo (ping) request id=0x0d22, seq=215
19	6.520149	4000:5::203:9a00:0:134	4000:5:1:0:4547:6565:8e9c:35d1	ICMPv6	118	Echo (ping) reply id=0x0d22, seq=215
20	7.511450	4000:5:1:0:4547:6565:8e9c:35d1	4000:5::203:9a00:0:134	ICMPv6	118	Echo (ping) request id=0x0d22, seq=216
21	7.521458	4000:5::203:9a00:0:134	4000:5:1:0:4547:6565:8e9c:35d1	ICMPv6	118	Echo (ping) reply id=0x0d22, seq=216
22	8.512769	4000:5:1:0:4547:6565:8e9c:35d1	4000:5::203:9a00:0:134	ICMPv6	118	Echo (ping) request id=0x0d22, seq=217
23	8.523043	4000:5::203:9a00:0:134	4000:5:1:0:4547:6565:8e9c:35d1	ICMPv6	118	Echo (ping) reply id=0x0d22, seq=217
24	8.998035	4000:5:1::1	ff03::fc	UDP	65	Source port: 44529 Destination port: ibm-mqids
25	9.000525	fe80::204:a3ff:fe0b:20bb	ff02::1:ff00:134	ICMPv6	86	Neighbor Solicitation for fe80::203:9a00:0:134

▶ Frame 16: 76 bytes on wire (608 bits), 76 bytes captured (608 bits)
 ▶ Ethernet II, Src: 28:92:4a:1d:09:5e (28:92:4a:1d:09:5e), Dst: Microchi_0b:20:bb (00:04:a3:0b:20:bb)
 ▶ Internet Protocol Version 6, Src: 4000:5:1:0:4547:6565:8e9c:35d1, Dst: 4000:5::203:9a00:0:134 (4000:5::203:9a00:0:134)
 ▶ User Datagram Protocol, Src Port: 40765 (40765), Dst Port: coap (5683)
 ▶ Data (14 bytes)

Figure 4.7: HEMS traffic analysis with Wireshark

Figure 4.7 was obtained by sending a command from the HEMS controller to change the intensity of the light using the IPv6 addresses of the HEMS controller and the lamp as the message source and destination, respectively. The traffic analysis in Figure 4.7 reveals some important characteristics of the control messages and acknowledgement exchanged between the controller and the lamp. For example, it reveals the size of control messages, the transport layer protocol, the network layer protocol, the application layer protocol and the UDP port number used during the communication. This set of information combined with the PLC specifications and other system parameters are used in the NS-3 model discussed in the next section. The key system parameters are summarised in Table 4.1.

Table 4.1: System information comprising of communication and application parameters

Parameter	Value
Available spectrum	0 - 32 MHz
Used bandwidth	2 - 28 MHz
Impedance	50 Ω (fixed)
Number of OFDM carriers	128 (86 active)
Carrier spacing	250 kHz
Symbol length	4 μs
Modulation	DBPSK
Bits per carrier	1
Background noise PSD	-96.52 dBm/Hz
Adaptation layer	6LoPLC
Network layer	IPv6
Transport/application model	UDP/server-client
Distance between sockets	2.5 m
Transmission line length between nodes	5.5 m
MTU	127 bytes (power line)

Application parameters include control message (controller - lamp) 30 bytes, response (lamp - controller) 8 bytes and monitoring message (controller - sensor) 28 bytes as well as response (sensor - controller) 15 bytes. It should be noted that these application sizes are payloads only.

4.2.4 NS-3 Model for HEMS Network

Three units of evaluation hardware were used on the test bed hence, limited HEMS application scenarios could be studied on the real network. To bridge the gap, this section describes the network model developed to represent the HEMS in NS-3. A simulation approach similar to [127] is employed, but with some modifications. Rather than MATLAB and OMNeT++ utilised in [127], MATLAB is combined with NS-3 in this work. As the mainstream NS-3 is devoid of the power line channel, this work adopts the power line channel provided in [108] which is based on TL theory. Although the module supports BPLC and NPLC, only the BPLC spectrum is employed in this chapter. For simplicity, fixed line impedance is applied for the duration of monitoring and control events. With NS-3, upper layer protocols (IP, transport, application) can run on top of the PHY/MAC provided in the PLC module to investigate complete PLC networks. However, since the communication networks under investigation are intended for low-rate application, an adaptation layer is included in the system model. As with the evaluation kits, the adaptation layer is agnostic of the underlying PHY and MAC layers. It is designed to support any standard lower layer protocols. This model employs IPv6 at the network layer. IP is generally attractive in service-oriented networks such as HEMS because: (i) it aids the integration of existing appliances, (ii) it renders the overlaying network non-disruptive during architecture change, (iii) it is agnostic of the low layers protocols; this helps to seamlessly integrate a variety of link layer technologies, and finally, it eliminates the use of the application gateway to translate across protocols, which promotes convergence and reduces the cost of implementation.

Multicasting will be beneficial in some HEMS applications (such as temperature sensing) such that a CoAP server monitors its attached sensor and sends out observations to all connected CoAP clients over IPv6 multicast address. However, since guidelines for group communication for CoAP (RFC 7390) is still at experimental phase and has not attained full RFC status, all communications in the simulation and test bed are based on unicast. According to IETF RFC 2460 (page 23-24), the IPv6 specification requires that every link provides an MTU of 1280 bytes or more. The 6LoWPAN was developed for constrained wireless networks to support an MTU size of 127 bytes at the MAC layer; hence, a complete IPv6 packet of 1280 bytes cannot fit into

a single LoWPAN frame. In order to meet the IPv6 minimum MTU requirement and facilitate two-way communication with conventional IPv6-capable networks, IETF developed RFC 4944 [128] for transmission of IPv6 packets over IEEE 802.15.4 networks. The standard recommends an adaptation layer below the network layer for fragmentation and reassembly of frames. The realisation that IEEE 802.15.4 networks (LoWPANs) share certain PHY/MAC characteristics with PLC renders them attractive to be adapted for low-power, low-rate communication over power lines. In line with that, the NS-3 model applies 6LoPLC (6LoWPAN in PLC) at the adaptation layer as shown in Figure 4.2 while OFDM with DBPSK and CSMA/CA are applied at PHY and MAC respectively.

As this work is exploratory in nature, first, we emulate the HEMS in NS-3 and investigate the network performance for the given values of background noise. However, since diverse types of appliances are typically found in homes, the effects of impulsive noise on HEMS system is also of interest in this work as impulsive noise imposes performance constraints on PLC systems. Therefore, the SNR generated in NS-3 is fed into MATLAB to evaluate the BER performance as a function of SNR. As discussed in Chapter 2, the key characteristics of impulsive noise are impulse amplitude, inter-arrival time and duration of impulse. To capture these realities, two random number generators (rng) in NS-3 are employed to generate a random value within 1-10, each. Thus, in each instantiation, the first generator creates a value within 1-10 s for the impulsive noise interval, and the second generator creates a value within 1-10 ms for pulse duration. Impulsive noise power of 9.91 dBm is employed as this was the peak value observed in the laboratory. Using these values, an instance of impulsive noise characterised by inter-arrival time and durations of 1-10 s and 1-10 ms, respectively, is then created to interfere with the data signal. To ensure that the results of the same scenario are consistent and reproducible, a fixed seed value is used in the rng in each simulation. The results of the simulations are presented and discussed in the next section.

4.3 Results and Performance Analysis

This section presents and discusses the performance of the system under consideration in various scenarios. The scenarios include monitoring of ambient

temperature using sensors and light control over power line. Using the parameters in Table 4.1, as well as adopting 6LoPLC, extensive simulations were conducted to assess the performance of the basic HEMS applications (monitoring of temperature and lamp control) over the power line. The idea here is to use the model developed, to assess various HEMS scenarios and use-cases that cannot be easily investigated with the three units of hardware available.

4.3.1 Communications Delay

In order to evaluate the system performance, it is necessary to first validate the developed network model upon which subsequent investigations will be based. As with other communication networks, here delay is used as a basic indicator of the network performance. The two types of delay considered here are illustrated in Figure 4.8.

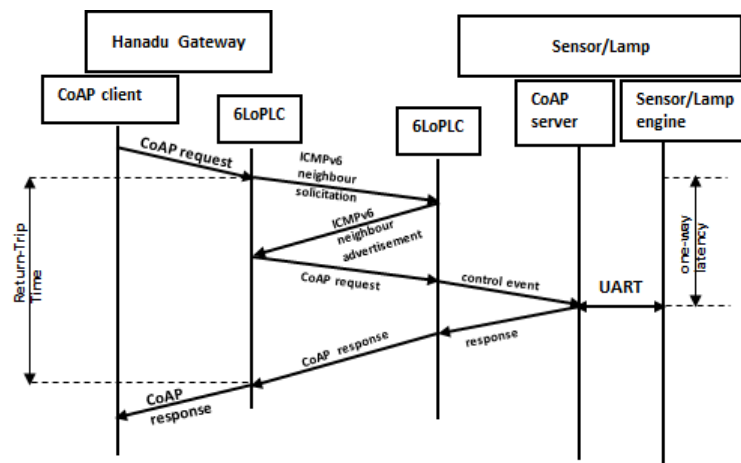


Figure 4.8: A schematic showing the end-to-end delay.

This schematic illustrates the end-to-end delay between the HEMS controller and the node (sensor or lamp). One-way latency denotes the time taken to send a signal from the controller to a node or vice versa while the return trip time (RTT) refers to the time taken to deliver the signal and receive the acknowledgement or response from the node. As seen from Figure 4.8, the network layer connection is established at the start of each session following which monitoring/control messages are exchanged. Since the controller, sensor and lamp are already encoded with CoAP messages of fixed length, ping of various payload sizes are sent from the controller to the lamp, and the

RTT in each case is measured. To ensure that the model adequately represents the investigated HEMS network, simulation results are validated with those measurements. A comparison of RTT from simulation and measurement is presented in Figure 4.9.

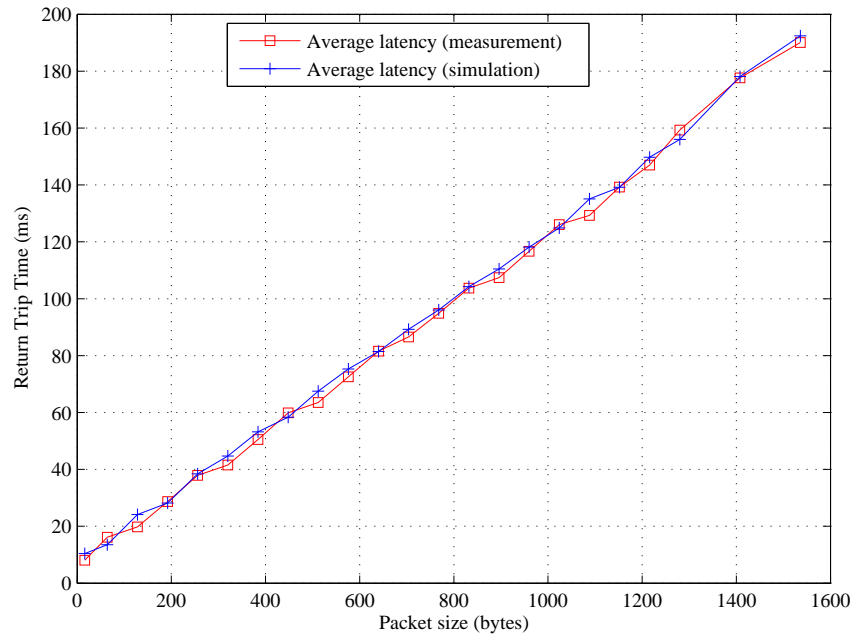


Figure 4.9: Model validation by comparing RTT from simulation with measurement.

Figure 4.9 shows that the NS-3 model is in good agreement with the measurements from the testbed. With a valid model now in place, diverse and more complex scenarios are studied. The significance of such an exercise is that understanding system performance in diverse scenarios and configurations can potentially provide new insights into how to meet communication requirements of current and future HEMS applications, as well as improve the quality of experience (QoE) of the users. For instance, in Figure 4.9 the steady rise in latency as the packet size increases is an indication that even with a single appliance, latency can be degraded if the data size is large. As monitoring and control operations typically involve several nodes, such as sensors, the effect of network load on the performance of the 6LoPLC system is also studied.

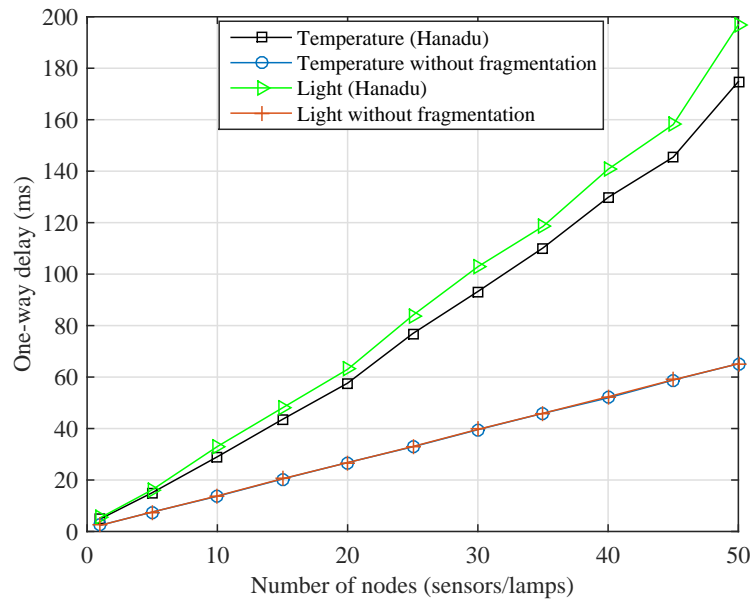


Figure 4.10: One-way delay for the sensor and lamp

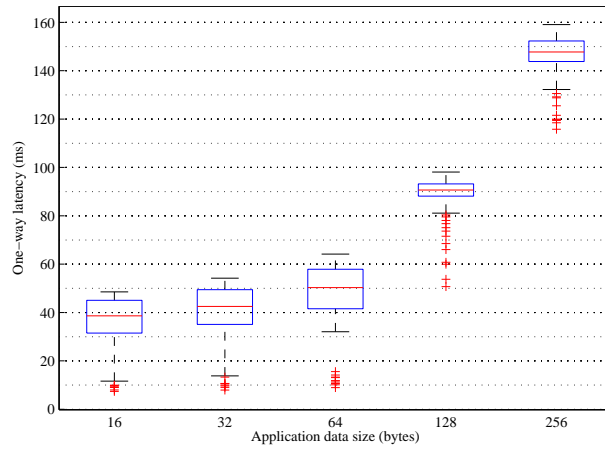
Figure 4.10 shows the variation of delay with HEMS network size over 6LoPLC. The figure illustrates two cases: receipt of data (temperature) from the sensor and transmission of the control message to the lamp to increase its luminance. In each case, performance without fragmentation and with 6LoPLC are considered. The main difference between these scenarios is that in the case of 6LoPLC, the MTU size of the communication medium is 127 bytes (in conformance with the adaptation layer), whereas without fragmentation, the MTU size is at least 1280 bytes. These MTU values represent the largest protocol data unit (PDU) that can be sent over the medium. In fact, without fragmentation, the minimum value of MTU is 1280 bytes, which corresponds to a full IPv6 packet.

While 1280 bytes is acceptable for in-home broadband services such as home multi-media sharing, it may be a disadvantage in energy management applications where data size is typically a few tens of bytes. It is therefore expected that future designs of PLC system for HEMS will include support for low data rate. This is where the 6LoPLC system becomes beneficial. Its low MTU of 127 bytes means the transceivers will incur lower processing power per transmission. In this simulation, the payload of sensor data is 15 bytes, while that of lamp control is 30 bytes (as encoded in the CoAP message).

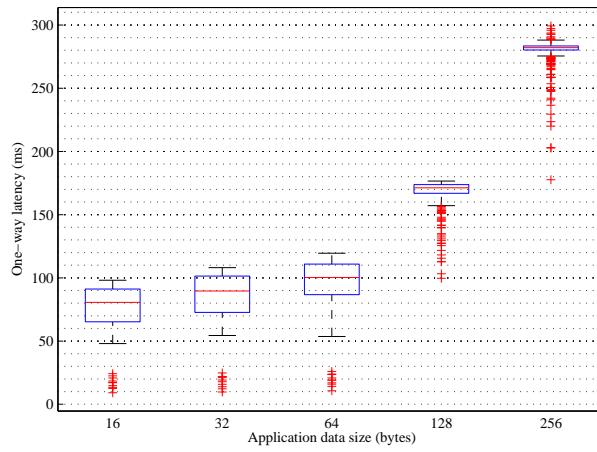
The figure shows that in both monitoring and lamp control, the one-way delay increases as more home appliances are connected to the network. This is expected, as additional appliances signifies more network load, which invariably increases the end-to-end delay.

Although the adaptation layer is introduced to facilitate the low-rate communication of home appliances in HEMS, as seen in Figure 4.10, there is clearly a cost for that as packets are subjected to fragmentation. One-way delay in Figure 4.10 is the time taken to send a message from the HEMS controller to the lamp/sensor in one direction. Various network sizes ranging from 1-50 smart appliances are investigated. As seen in the figure, although 6LoPLC allows us to adapt PLC for low-rate applications, such as HEMS, that comes at a price in terms of additional delay, which could be up to 131.7512 ms in the case of lamp control signalling (controller - lamp) and 109.6414 ms for monitoring (sensor - controller), however, these values are within typical ranges [129] and do not adversely affect the application performance.

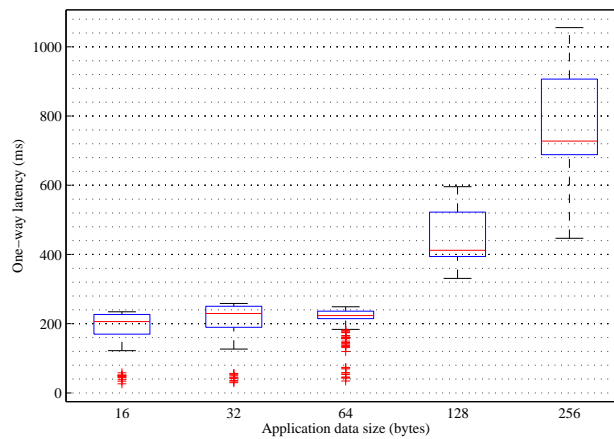
As seen in Figure 4.3, the CoAP client is resident on a standard network node (a laptop) with full IPv6 capability. The latency performance described above is therefore logical, given that fragments received from the HEMS controller have to wait in the buffer until all bits belonging to the same flow are received before reassembly and further processes are carried out. The significance of this result is that for planning and design purposes, apart from application data size shown in Figure 4.9, large number of nodes per controller can remarkably increase delay. Therefore, the network size of HEMS must be carefully chosen to ensure the latency is within acceptable limits.



(a) 10 smart appliances



(b) 20 smart appliances



(c) 50 smart appliances

Figure 4.11: Statistical distribution of one-way latency for various HEMS

Figure 4.11 presents the box plots of latency distribution with 10, 20 and 50 appliances. It can be seen that as the number of appliances increases from 10 to 50 and data size increases to 256 bytes, the network becomes slower. For example, in Figure 4.11b, with 20 appliances in the home, using data size of 64 bytes, although latency of 53 ms is possible, majority (75%) of the latency in the data sample are 87 ms or more. This is most prominent in Figure 4.11c.

4.3.2 Network Capacity

This section investigates the maximum network capacity in terms of raw throughput. The throughput measures the amount of data (sensor data, control message, luminance instruction and all communication overheads) successfully delivered over the network per unit time. Figure 4.12 illustrates the variation of system throughput with data size. This simulation is based on one controller and one node.

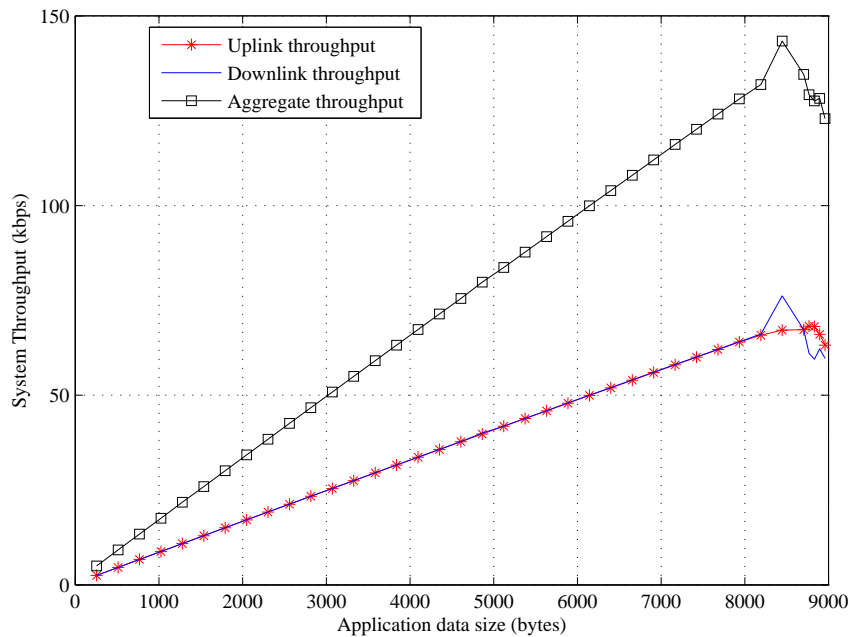


Figure 4.12: System throughput as a function of application data size.

By increasing the network load from 256-9216 bytes (steps of 256 bytes), the throughput increases until it attains its peak value and begins to drop. That upper threshold signifies the maximum achievable throughput. Although the evaluation kits are envisioned to provide a maximum data rate

of 250 kbps (assumed to be symmetric), Figure 4.12 shows that at the application layer, the hardware used in the test bed can deliver a maximum of 68.198 kbps and 76.2275 kbps in uplink and downlink, respectively. As an illustration, in the 76 bytes contained in the sniffed packet (Figure 4.7), data payload accounts for only 14 bytes (18.42%), and the rest is communication overhead. Since the overhead (which represents 81.52% of the message) is fixed and the payload is typically small, the current throughput is sufficient for HEMS monitoring and control applications.

4.3.3 Network Reliability

HEMS is generally a low-rate system, but a minimum reliability of 99% [48] is required to ensure that monitoring information from the sensor and control message are delivered as needed. We investigate network reliability in terms of PDR with various packet sizes and different network configurations. PDR here is defined as the ratio of the received packets to the transmitted packets. A packet is deemed to have been received when all of its bits have been delivered to the destination service engine. This stateful approach ensures that the upper layer processes only complete packets. The result is presented in Figure 4.13.

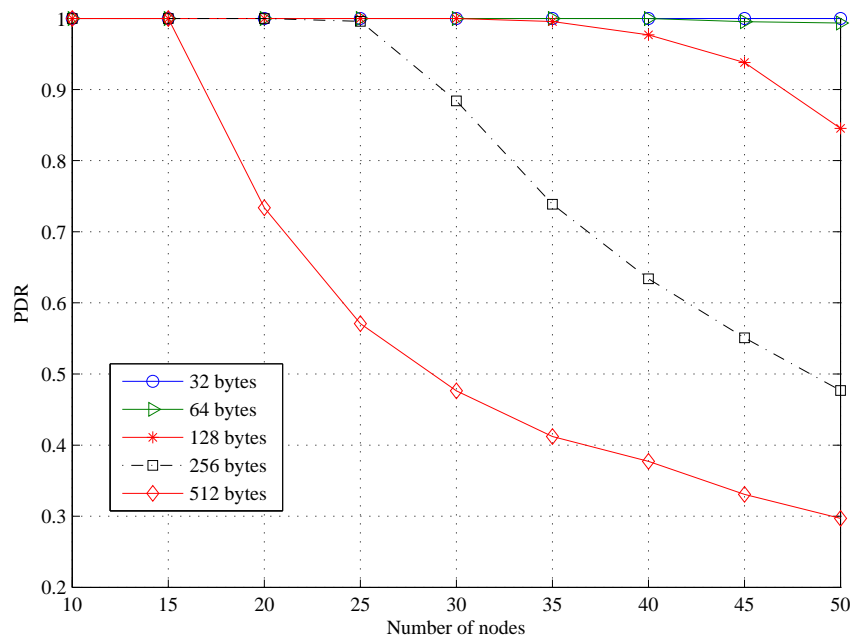
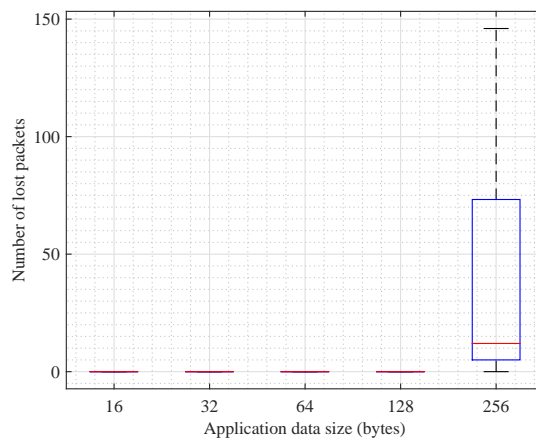
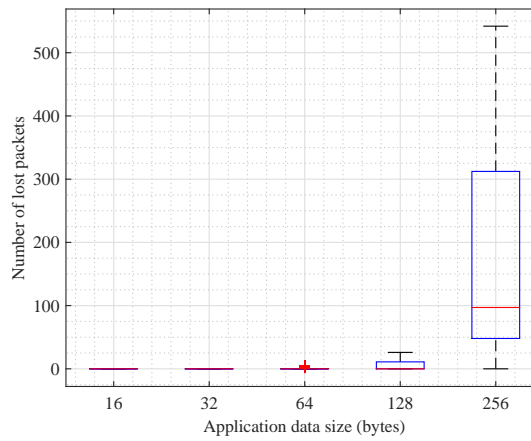


Figure 4.13: Packet delivery ratio vs number of nodes.

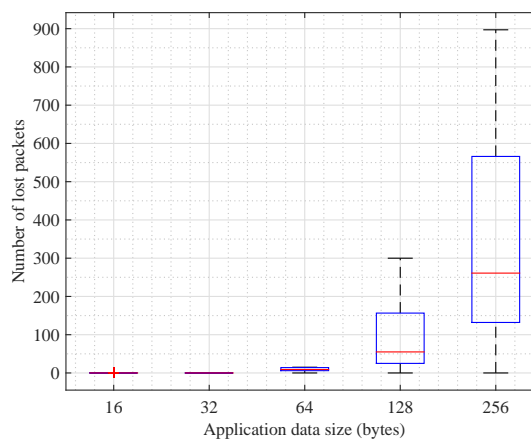
As seen in Figure 4.13, all of the network sizes favour small application data. From the design point of view and based on the system configuration employed in this work, it is also observed that in a HEMS that comprises 50 smart appliances, in order to guarantee at least 99% packet delivery, the size of the payload in the message exchanged between the nodes and controller must be 64 bytes or less. This is because as packet size increases and more appliances are connected to the HEMS network, the contention for network resources also increases, and more packets are fragmented, all of which result in lower PDR. Hence, larger data sizes tend to result in higher throughput (Figure 4.12), but this often comes at the expense of lower reliability, as seen in Figure 4.13.



(a) 30 smart appliances



(b) 40 smart appliances



(c) 50 smart appliances

Figure 4.14: Distribution of lost packets for various HEMS

Figure 4.14 illustrates the distribution of packet loss counts in HEMS with 30, 40 and 50 appliances. The number of lost packets increases with the network size in each case. For each data size, the gap between the median and the first quartile widens as the data size increases to 256 bytes.

4.3.4 Effects of Impulsive Noise

It was observed in Section 4.3.3 that in a network of 50 nodes, application size must not exceed 64 bytes to guarantee at least 99% packet delivery. Using the same network configuration here, we investigate the effect of impulsive noise on the HEMS application performance using an application size ranging from 16-128 bytes. By varying the number of appliances on the HEMS network, this section highlights the impacts of background and impulsive noise on the one-way delay. The delay here is the time taken to deliver a request from the controller to the node. By simulating different packet sizes, we cover both monitoring and control types of traffic. The result is presented in Figure 4.15.

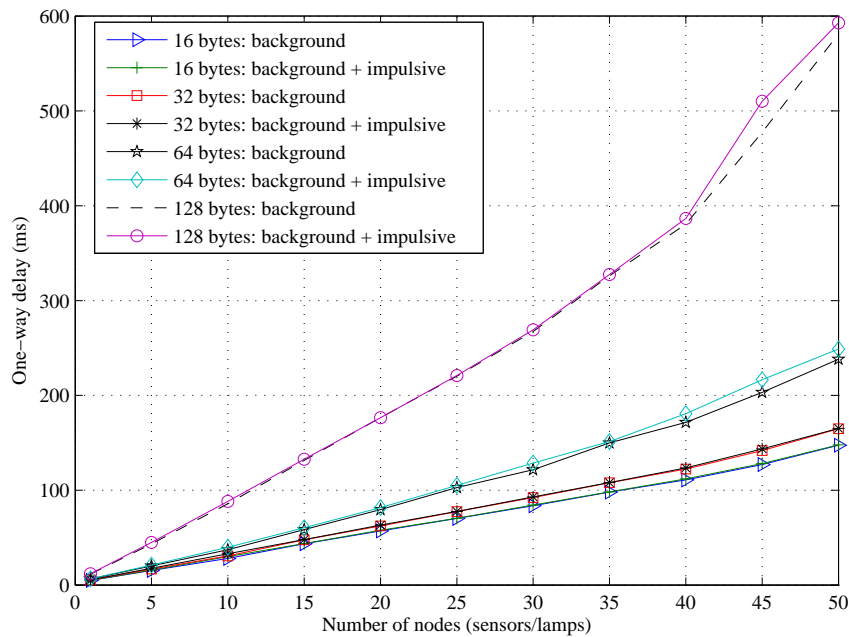


Figure 4.15: Effect of impulsive noise on one-way delay.

Although it is generally known that impulsive noise degrades PLC system performance, two key observations can be derived from Figure 4.15: (i) impulsive noise degrades the latency performance of the HEMS, regardless of

the application size; (ii) larger application data are more susceptible to degradation, for example in the case of the 128-byte and 16-byte data sizes, the degradation in latency is as high as 32.759 ms and 1.8977 ms, respectively, in terms of additional delay caused by impulsive noise. These occur because as impulsive noise degrades the power line channel in terms of signal-to-noise ratio, more transmit power is needed to guarantee consistent error-free transmission. In the absence of higher transmit power, the price to pay is higher latency or outage in extreme case.

4.3.5 Power Line Channel Performance

This section discusses the BER performance of the power line channel employed in the current evaluation hardware. Two scenarios are considered: (i) the BER of different modulation schemes; and (ii) the effects of impulsive noise on BER. Figure 4.16 compares BER performance for different modulation schemes with only coloured background noise.

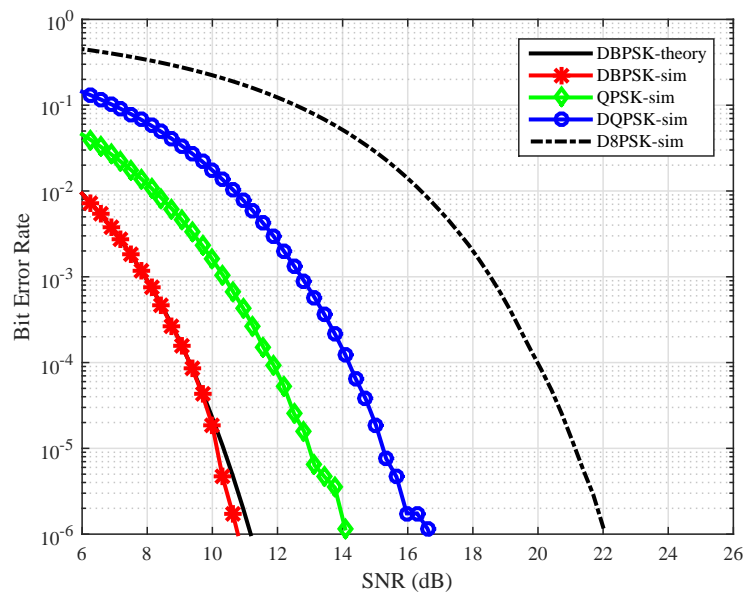


Figure 4.16: System BER performance as a function of SNR.

From the communications requirements outlined in [48], the HEMS application requires 99.0%-99.99% reliability, which translates to a BER of 10^{-3} (median). This is the typical BER needed to guarantee the QoS of HEMS application traffic. Generally, differential Phase Shift Keying schemes allow

non-coherent detection [130–133]. Hence, phase-tracking circuits are not required at the receivers, which consequently reduces the design and implementation complexities, as well as the cost. The current 6LoPLC system is based on DBPSK, and as seen in Figure 4.16, with coloured background noise alone, the current hardware requires an SNR of 7.8150 dB to achieve a BER of 10^{-3} . DBPSK is attractive because it supports non-coherent detection which does not require carrier phase-tracking circuit at the receiver. This reduces design complexity which can potentially reduce implementation cost. It can also be seen that, to guarantee 99.9% reliability, SNRs of 10.4164 dB, 12.8197 dB and 18.5068 dB are required by quadrature PSK (QPSK), Differential QPSK (DQPSK) and Differential 8-PSK (D8PSK) respectively. Therefore, compared with QPSK-based systems, such as HomePlug Green PHY, this result shows that a 2.6014 dB power saving can be achieved by employing DBPSK instead of higher order PSK schemes. Although DQPSK and D8PSK can offer higher data rates, employing them will potentially undermine the energy efficiency of the system. Since HEMS applications typically require low data rates, which can be satisfied by DBPSK, such a trade-off is not necessary. Next, the effects of impulsive noise on BER are illustrated for various impulsive noise probabilities in Figure 4.17.

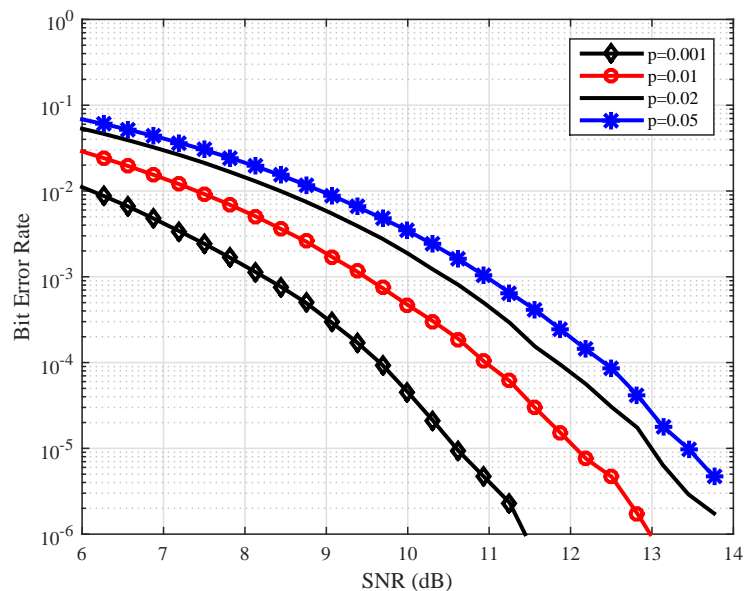


Figure 4.17: BER performance with various impulsive noise probabilities (p) using DBPSK.

Figure 4.17 shows the BER when the coloured background and impulsive noise are present, where p represents the probability of the appearance of impulsive noise. The figure illustrates BER performance with impulsive noise probabilities of 0.001, 0.01, 0.02 and 0.05. These values signify that impulsive noise occurs 0.1%, 1%, 2% and 5% of the time. As seen in the figure, to achieve the same BER of 10^{-3} with $p = 0.001$, the SNR requirement increases to 8.1266 dB for the current system, meaning that an additional 0.3116 dB of transmit power is needed in the current hardware kits to combat the effect of impulsive noise. Another inference from Figure 4.17 is that for higher probabilities of impulsive noise, higher power levels are required at the transmitter. For example, with a probability of 0.05, an SNR of 10.9381 dB is required to achieve a BER of 10^{-3} , translating to an additional 2.8115 dB, compared with the probability of 0.001.

It should be noted that these results are specific to the hardware and model employed in this study and may not fully apply to all HEMS scenarios. For example, line impedance may vary and impulsive noise characteristics may differ from those employed in this work, expectedly, these will affect the results. Again, as this work is exploratory, the measurements were conducted in a lab specifically setup for this research in which the inter-socket distance is 2.5m. As power line is prone to distance-related attenuation, it is also acknowledged that 2.5 m may not uniformly apply to all houses.

4.4 Chapter Summary

An empirical assessment of 6LoPLC for HEMS has been presented in this chapter. A model was developed in NS-3 and validated with measurement results from the test bed using the evaluation kits. This chapter demonstrated that 6LoPLC can adequately support HEMS monitoring and control applications. Based on the parameters employed in this work, in order to guarantee 99% minimum system reliability, it was shown that the application data must not exceed 64 bytes. These results could provide some useful insights for system designers and application developers. The results also revealed that in a HEMS containing 50 appliances, latencies of 238.117 ms and 248.959 ms are achievable for monitoring and control applications, respectively, provided the data size is 64 bytes or less. Finally, it was shown that, with the CoAP payload

of 128 bytes, impulsive noise can further degrade the latency by an additional 32.759 ms.

It was generally observed that larger application data sizes are more affected by impulsive noise and 6LoPLC fragmentation/reassembly processes. Beyond HEMS, the model presented in this chapter is also feasible for low-rate smart grid applications and other cyber-physical systems where high reliability and low cost are of higher priority than high throughput. The significance of the results in this chapter is that although the evaluation was carried out with three units of hardware, knowledge of larger and diverse networks obtained from simulation results, can help improve system tolerance.

Chapter 5

Energy-Efficient Vector-OFDM In PLC Systems

It was shown in chapter 4 that energy efficiency in PLC systems can be improved at the adaptation layer by applying some of the low-power features of constrained wireless networks. The aim of this chapter is to extend the investigation of energy-efficient transmission to physical layer.¹ Current PLC standards for smart grid applications such as [134] PRIME, G₃-PLC, IEEE 1901.2 and Homeplug Green PHY are based on OFDM due to its ability to combat inter-symbol interference (ISI) [135–137]. This unique property makes OFDM a technique of choice in frequency-selective channels including power line. Other features of OFDM include high spectral efficiency and ease of implementation with IFFT and FFT [138]. However, the main drawback of OFDM is its high PAPR [139, 140] which reduces the energy efficiency of PLC transmitters. High PAPR is a result of high fluctuation in OFDM symbol peaks and requires highly-linear PA (HPA). From design point of view, the HPAs must have large linear range that can cope with the irregular high OFDM symbol peaks. However, such PAs are impractical because they are expensive, bulky and challenging to design. Hence, non-linear PAs are commonly found in practical systems. Furthermore, EMC regulations limit peak value of PA in PLC transmitters, hence large PAPR causes signal distortion which results in increased complexity [141, 142]. To reduce PAPR in OFDM systems, different techniques have been proposed such as amplitude

¹These results in this chapter are included in the paper recently published with IEEE Access

clipping, tone reservation, partial transmit sequence [143] and selective mapping [144], [140]. However, such techniques may cause signal distortion and require side information which can be computationally complex and energy inefficient [145]. To overcome this, the PLC system in discussed in this work employs V-OFDM.

It will be seen at the end of this chapter that due to its low PAPR properties, V-OFDM is less sensitive to impulsive noise and by exploiting this property, power requirements of the PA can be reduced relative to conventional OFDM. The energy efficiency of the PLC system is further improved by exploiting the higher SNR of DPTE technique at the receiver.

This Chapter is organised as follows. Section 5.1 examines the effects of communication network on smart grid applications. In section 5.2, V-OFDM is presented as an energy-efficient alternative to OFDM in power line channel while section 5.3 describes the V-OFDM model employed in this work. Section 5.4 discusses the PAPR and transmit power in V-OFDM while section 5.5 examines output SNR of V-OFDM at the receiver of PLC system using the conventional blanking technique. In section 5.6, DPTE is investigated as an efficient noise cancellation method and the SNR gain of DPTE over conventional blanking is presented in section 5.7.

5.1 Effects of Communication Network on Smart Grid Applications

Before we delve into the details of V-OFDM and DPTE, it is helpful to first understand how the variability of communication network affects smart grid applications. The aim of this section is therefore, to illustrate some of those effects. The underlying communication system must seamlessly support automation, sensing and control through a bi-directional exchange of information- this is the promise of smart grid. As discussed in chapter 2, channel impairments such as frequency selectivity, varying impedance, limited signal power, multi-path propagation, attenuation and non-Gaussian noise [70] generally degrade PLC system performance in terms of achievable data rate, latency and SNR at the receiver. The PRIME standard defines the PHY and

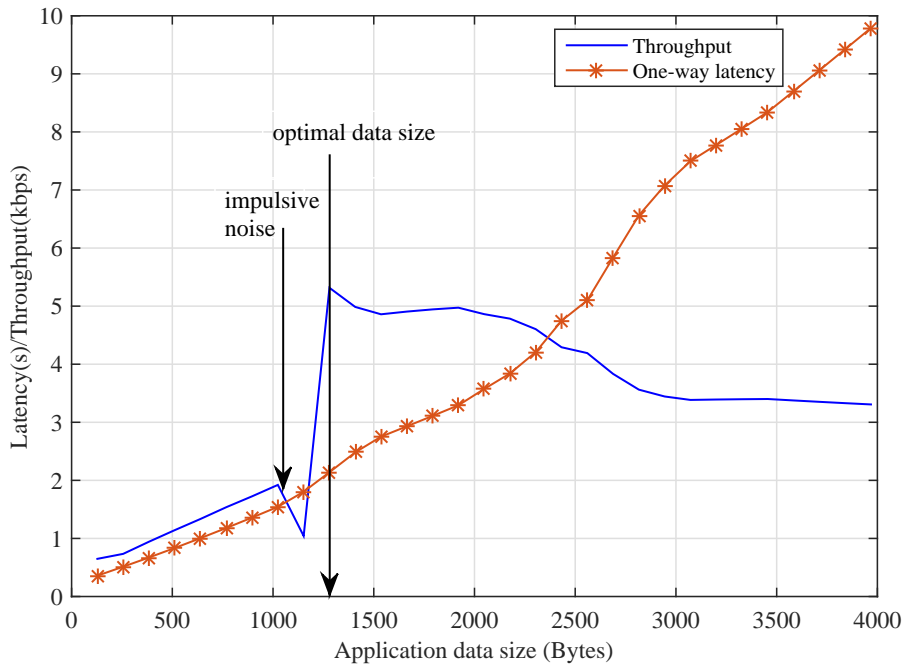


Figure 5.1: Variation of communication delay with throughput and data size using uncoded OFDM with DBPSK

MAC layers specifications for NPLC. The PHY features include OFDM (combined with long cyclic prefix of $192\mu s$) to provide delay spread used to combat frequency selectivity while the MAC includes automatic repeat request (ARQ), TDMA over carrier CSMA/CA for contention-free transmission, using DPSK modulation schemes. PRIME supports DBPSK, DQPSK and D8PSK.

Existing literature in this area mostly describes system performance at the PHY in terms of BER results of the underlying power line channel [146]. In order to maximise the potentials of PLC, it is necessary to assess the smart grid as an integrated system by also considering the performance at upper layers as well. The PLC network discussed in this section is based on PRIME v1.4 standard and includes not only realities such as effects of impulsive noise but also accounts for key network performance metrics such as end-to-end latency and throughput in smart grid networks. It should be noted that the use of PLC in smart grid is not restricted to NPLC, in practice there are smart meters embedded with BPLC chips and other BPLC-enabled smart grid applications.

Figure 5.1 illustrates variation of network performance with application

data sizes between a smart meter and a concentrator in the LV domain. The figure shows that there exists an optimal data size at which the PLC network maximises delivery of packets from smart meters to the concentrator.

However, the first notch observed in the figure can be attributed to transient network impairment due to impulsive noise. This is a classic example of the effect of impulsive noise on data signal which can be explained as follows. The interference arising from the impulsive noise events creates domino effects in which SINR reduces, followed by PHY data rate reduction. The reduced PHY data rate forces packets to remain in transit for longer period during which they could be corrupted, damaged or lost. In fact, this effect is worse in sensitive applications such as smart metering that depend on reliable transport protocols such as TCP. For such applications, packet retransmission implies that, successful packets will remain in the buffer until all packets belonging to the same fragment or flow are received before they are passed to the application layer. This improves reliability, but it does so at the expense of increased latency, higher computational overhead and lower goodput (useful throughput at application layer). From the result in Figure 5.1, although the network recovered after the impulsive noise activity, such sporadic events can severely degrade smart grid application performance. Therefore, to provide acceptable QoS to smart grid applications, effective techniques must be developed to mitigate the harmful effects of impulsive noise on data signals. In order to address the issue, this chapter exploits the low PAPR property of V-OFDM in the detection and cancellation of noise at the receiver.

5.2 V-OFDM in PLC Systems

V-OFDM was first introduced by Xia in [147] to reduce the cyclic prefix length in OFDM systems. Thereafter, various aspects of it have been studied in wireless systems [148], [148–152]. Among other outcomes, these studies found and agreed that in frequency-selective channels, V-OFDM generally improves system performance [148] relative to OFDM and that the gain increases with number of vector blocks (VBs). Specifically, studies such as [142, 153–156] show that V-OFDM exhibits lower PAPR than conventional OFDM systems. However, till date, only [145] and [157] have so far investigated V-OFDM in power lines.

Furthermore, impulsive noise has been identified as a major performance inhibitor in PLC [80], [85]. To mitigate the harmful effects of impulsive noise, a number of techniques have been proposed. The simplest and most common approach is to precede the OFDM demodulator with a memory-less, non-linear preprocessors such as a blanker or clipper [158, 159]. In line with that, the investigation of V-OFDM in PLC systems reported in [145] is based on conventional blanking and clipping techniques.

5.3 V-OFDM Model

V-OFDM is a generalisation of conventional OFDM approach. In principle, it combines a number of consecutive information symbols into a vector, this is equivalent to blocking operation in conventional OFDM. The V-OFDM system model considered in this work is illustrated in Figure 5.2 in which the modulated symbols are processed block by block.

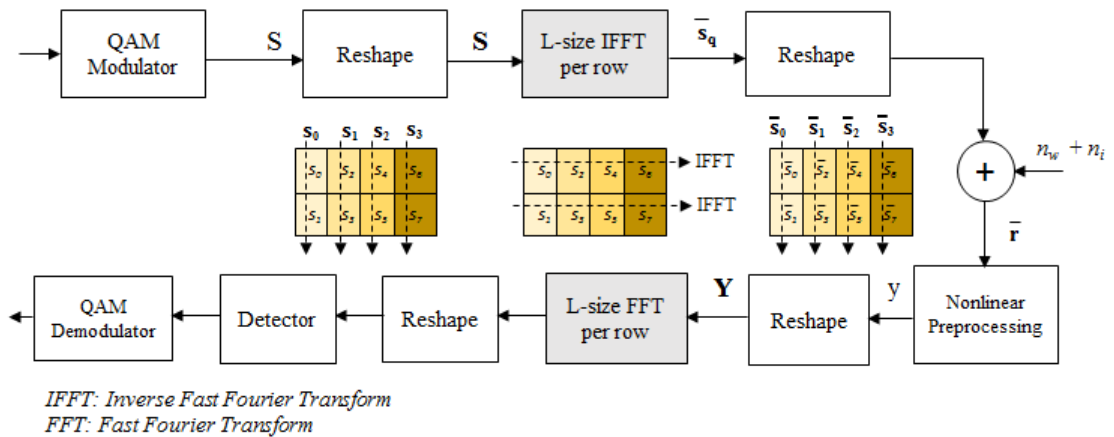


Figure 5.2: V-OFDM block diagram showing nonlinear preprocessors at the receiver

This figure shows the transmitter and receiver of the V-OFDM system. At the transmitter, the information bits are first mapped using the quadrature amplitude modulation (QAM) to produce base-band QAM symbols denoted as S . Then a sequence $\{s_n\}_{n=0}^{N-1}$ of N modulated symbols is column-wise blocked to L vectors each of length M , i.e. $N = ML$. These vectors will be

referred to as vector blocks (VBs). Accordingly, the l^{th} VB can be represented as

$$\mathbf{s}_l = [s_{lM}, s_{lM+1}, \dots, s_{lM+M-1}]^T \quad l = 0, 1, \dots, L-1 \quad (5.1)$$

Now, this data vector is reshaped into a matrix \mathbf{S} of M rows and L columns such that $N = LM$ and

$$\mathbf{S} = \begin{pmatrix} s_0 & s_M & s_{2M} & \dots & s_{(L-1)M} \\ s_1 & s_{M+1} & s_{2M+1} & \dots & s_{(L-1)M+1} \\ \vdots & \vdots & \vdots & \ddots & \vdots \\ s_{M-1} & s_{2M-1} & s_{3M-1} & \dots & s_{LM-1} \end{pmatrix} \quad (5.2)$$

V-OFDM then performs L size IFFT over the L VBs row-wise as illustrated in Figure 5.2 for $N = 8$ (i.e $M = 2$ and $L = 4$). The V-OFDM time domain signal after the IFFT can be expressed as

$$\bar{\mathbf{s}}_q = \frac{1}{\sqrt{L}} \sum_{l=0}^{L-1} \mathbf{s}_l \exp\left(\frac{j2\pi ql}{L}\right), \quad q = 0, 1, \dots, L-1 \quad (5.3)$$

which can also be expressed in a vector form as

$$\bar{\mathbf{s}}_q = [\bar{s}_{qM}, \bar{s}_{qM+1}, \dots, \bar{s}_{qM+M-1}]^T \quad q = 0, 1, \dots, L-1. \quad (5.4)$$

Similar to conventional OFDM, the vectors $\{\bar{\mathbf{s}}_q\}_{q=0}^{L-1}$ in (5.4) are reshaped to a length N vector

$$[\bar{\mathbf{s}}_0^T, \bar{\mathbf{s}}_1^T, \dots, \bar{\mathbf{s}}_{L-1}^T] = [\bar{s}_0, \bar{s}_1, \dots, \bar{s}_{N-1}], \quad (5.5)$$

accordingly the PAPR of this signal is

$$\text{PAPR} = \frac{\max(|\bar{s}_k|^2)}{\mathbb{E}[|\bar{s}_k|^2]}, \quad k = 0, 1, \dots, N-1 \quad (5.6)$$

where \max is the maximum argument, $|\cdot|$ is the absolute value and $\mathbb{E}[\cdot]$ denotes the expectation operator. The V-OFDM signal is then transmitted over the PLC channel where it is corrupted by the background and impulsive noise. The received signal can generally be written as

$$\bar{r}_k = A(f, d) \bar{s}_k + n_{w,k} + n_{i,k}, \quad k = 0, 1, \dots, N-1 \quad (5.7)$$

where \bar{r}_k is the received signal, $A(f, d)$ is the frequency- and distance-dependent attenuation caused by the cable imperfections, f is the operating frequency and d is the source-destination distance. In the time-domain, the received V-OFDM symbol vector and the received VB can be respectively expressed as

$$\bar{\mathbf{r}} = [\bar{r}_0, \bar{r}_1, \dots, \bar{r}_{N-1}]^T \quad (5.8)$$

$$\bar{\mathbf{r}}_q = [\bar{r}_{qM}, \bar{r}_{qM+1}, \dots, \bar{r}_{qM+M-1}]^T \quad (5.9)$$

where n_w and n_i are the background and impulsive noise components, respectively. It should be noted that \bar{s}_k , n_w and n_i are assumed to be mutually independent and the noise is uncorellated with the data signal, which implies that $\mathbb{E}[n_w \bar{s}_k^*] = \mathbb{E}[n_i \bar{s}_k^*] = 0$. This work applies the Bernoulli-Gaussian model for generating impulsive noise as described in section 2.3.4.1 such that the input SNR and SINR are respectively expressed as $\text{SNR} = 10 \log_{10} \left(\frac{\sigma_s^2}{\sigma_w^2} \right)$ and $\text{SINR} = 10 \log_{10} \left(\frac{\sigma_s^2}{\sigma_i^2} \right)$, where σ_s^2 is the transmitted signal variance.

At the receiver, in order to suppress impulsive noise, the non-linear processor (blinker or clipper) is situated before OFDM demodulator. For each received symbol, the side information is QAM-demodulated, from which the extractor retrieves the peak value corresponding to the V-OFDM symbol and adjusts the threshold of the blanker/clipper threshold accordingly. The received signal \bar{r}_k is then passed through the non-linear preprocessor where it is nulled or clipped when it exceeds a certain threshold defined according to the associated peak value. In principle, blanking and clipping can generally be described as

- Blanking

$$y_k = \begin{cases} \bar{r}_k, & |\bar{r}_k| \leq T_b \\ 0, & |\bar{r}_k| > T_b \end{cases} \quad k = 0, 1, \dots, N-1 \quad (5.10)$$

- Clipping

$$y_k = \begin{cases} \bar{r}_k, & |\bar{r}_k| \leq T_c \\ T_c \exp(j \arg(\bar{r}_k)), & |\bar{r}_k| > T_c \end{cases} \quad (5.11)$$

where y_k is the output of the nonlinear pre-processor and T_b and T_c are the blanking and clipping thresholds respectively. It is worth noting that careful selection of the threshold value is important to maximize the system performance. Hence, non-linearity (5.10) and (5.11) reduce the effect of large received signal values which are considered to result from impulsive noise. Next, we column-wise block $\{y_0, y_1, \dots, y_{N-1}\}$ to an $M \times L$ matrix as follows

$$\mathbf{Y} = \begin{pmatrix} y_0 & y_M & y_{2M} & \cdots & y_{(L-1)M} \\ y_1 & y_{M+1} & y_{2M+1} & \cdots & y_{(L-1)M+1} \\ \vdots & \vdots & \vdots & \ddots & \vdots \\ y_{M-1} & y_{2M-1} & y_{3M-1} & \cdots & y_{LM-1} \end{pmatrix} \quad (5.12)$$

and then perform the fast Fourier transform (FFT) over every row to produce the frequency domain signal. The matrix is then reshaped to produce a $1 \times N$ -size vector before performing the base-band QAM demodulation and decision.

5.4 PAPR and Transmit Power in V-OFDM

The total power consumed, P_T , by a PLC transceiver is a combination of static and dynamic power. This can be expressed as [19]

$$P_T = P_0 + P(l) \quad (5.13)$$

where l is the transmitted traffic load in bits/s or packets/s. P_0 is the power consumed (in Watts) in idle state and is fixed for a given device while $P(l)$ is an increasing function of load (dynamic power). The inevitable choice of OFDM in current PLC systems is at the expense of high PAPR. In this case, PAPR is the ratio of the maximum instantaneous power of the signal to its average power. High PAPR requires highly-linear PA (HPA) at the transmitter. In the absence of HPA, high PAPR can cause the PA to be overloaded after which it transits to nonlinear operation (distortion). This phenomenon results

in low power efficiency and unwanted electromagnetic emissions. Hence, timely techniques are needed to reduce PAPR in PLC systems.

In order to discuss the PAPR property of V-OFDM, it is necessary to first establish the relationship between PAPR values and the number of VBs in V-OFDM compared with typical OFDM. In logarithmic scale, (5.6) can be rewritten as

$$\text{PAPR}(dB) = 10 \log \left(\frac{\max(|\bar{s}_k|^2)}{\mathbb{E}[|\bar{s}_k|^2]} \right) \quad (5.14)$$

Now let us consider the class-A PAs which are the most linear. They consume a constant amount of power, P_{DC} regardless of the input power [160]. The PA's energy efficiency is defined as the portion of P_{DC} delivered to the load. Under perfect linear condition, the energy efficiency of the class-A PA can be expressed as [160, 161]

$$\eta_{EE} = \frac{P_{out,ave}}{P_{DC}} \approx \frac{0.5}{\text{PAPR}} \quad (5.15)$$

where $P_{out,ave}$ is the average output power of the PA. For an OFDM system, the design could warrant that no more than a certain number of the symbols exceed the average power in order to avoid saturation. We define α as the probability that PAPR of the V-OFDM symbol block exceeds a certain value PAPR_0 . Figure 5.3 depicts the relationship between PAPR and number of VBs (M) for different values of α , where $M = 1$ is equivalent to conventional OFDM.

Figure 5.3 clearly reveals that for all values of α , PAPR of the V-OFDM symbol reduces as the number of VBs increases. It follows that regardless of the α applied, provided $M > 1$, the PAPR of V-OFDM is always lower than that of OFDM. This lower PAPR property arises from the fact that V-OFDM uses a relatively smaller IFFT size to generate its signals compared with conventional OFDM. Figure 5.3 further shows that the PAPR reduction is more significant in low values of α . For example, the PAPR reduction achieved when $\alpha = 0.001$ at $M = 64$ is about 4.9 dB compared with the conventional OFDM system whereas when $\alpha = 0.5$ at the same value of M , only about 1.7 dB reduction is achieved. According to (5.15) these PAPR reductions will improve energy efficiency of the PA. Finally, it can be seen that for large M ($M \rightarrow 64$), the PAPR converges to 6dB, for all the α considered. In other

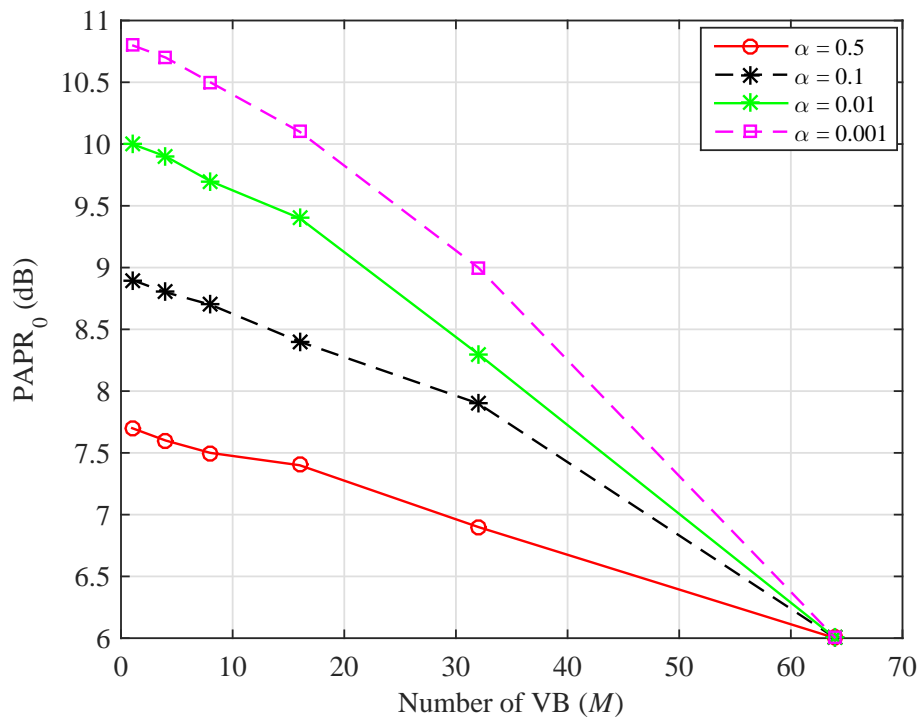


Figure 5.3: PAPR performance of V-OFDM system as a function of the number of VBs for different values of α , ($M = 1$ is equivalent to conventional OFDM), $n = 10^5$, $N = 256$, 16QAM

words, at large value of M , PAPR performance is equal for all values of α . Later in this Chapter, this low PAPR property of V-OFDM is combined with advanced signal processing at the receiver to further improve energy efficiency of PLC transceivers.

5.5 Output SNR of V-OFDM With Conventional Blanking and Clipping

This section presents the transmit power savings achievable when V-OFDM is implemented with conventional noise cancellation techniques in PLC transceivers. This is done by computing the SNR at the output of the preprocessor using various thresholds values of T_b and T_c . In that regard, we investigate SNR performance of different VBs in V-OFDM and compare the results with OFDM. To do this, let us consider the SNR at the output of the nonlinear preprocessor which can be expressed as [84, 86, 87, 158, 162]

$$SNR_1 = \frac{\mathbb{E} [|K_0 \bar{s}_k|^2]}{\mathbb{E} [|y_k - K_0 \bar{s}_k|^2]} = \left(\frac{\mathbb{E} [|y_k|^2]}{2K_0^2} - 1 \right)^{-1} \quad (5.16)$$

where K_0 is a real constant chosen such that $K_0 = (1/2) \mathbb{E} [|y_k \bar{s}_k^*|^2]$. Equation (5.16) has been extensively used in the literature however, since $\mathbb{E} [|y_k|^2]$ represents the total signal power (data signal plus noise) at the output of the nonlinear preprocessor, it can be rewritten as

$$SNR_1 = \frac{2K_0^2}{E_{out} - 2K^2}, \quad (5.17)$$

E and K depend on the type of nonlinear preprocessor used and can be expressed as

- Blanking,

$$K_0^{\{blanking\}} = 1 - \sum_{i=0}^{L-1} \left(1 + \frac{T_b^2}{2(1 + \sigma_i^2)} \right) p_i \exp \left(-\frac{T_b^2}{2(1 + \sigma_i^2)} \right) \quad (5.18)$$

$$E_{out}^{\{blanking\}} = 2 + 2 \sum_{i=0}^{L-1} p_i \left(\sigma_i^2 - \left[\frac{T_b}{2} + (1 + \sigma_i^2) \right] \exp \left(-\frac{T_b^2}{2(1 + \sigma_i^2)} \right) \right) \quad (5.19)$$

- Clipping

$$K_0^{\{clipping\}} = 1 - \sum_{i=0}^{L-1} p_i \left[\exp\left(-\frac{T_c^2}{2(1+\sigma_i^2)}\right) - \sqrt{\frac{\pi}{2}} \frac{T_c}{\sqrt{1+\sigma_i^2}} Q\left(\frac{T_c}{\sqrt{1+\sigma_i^2}}\right) \right] \quad (5.20)$$

$$E_{out}^{\{clipping\}} = 2 + \sum_{i=0}^{L-1} p_i \left(2\sigma_i^2 - (1 + \sigma_i^2) \exp\left(-\frac{T_c^2}{2(1+\sigma_i^2)}\right) \right) \quad (5.21)$$

where K_0 is a scaling factor and E_{out} is the total signal power at the output of the nonlinear preprocessor [87, 158].

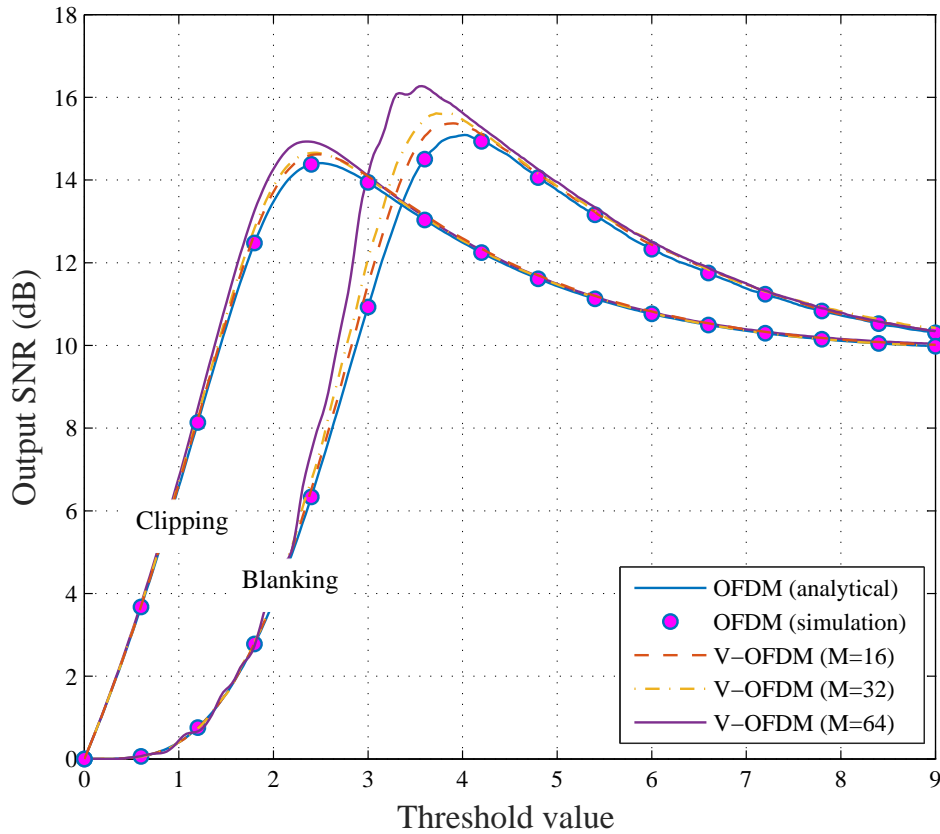


Figure 5.4: Output SNR performance of the V-OFDM system versus the threshold with blanking and clipping using input SNR = 25 dB, SINR = -10 dB and $p = 0.01$, 16QAM

Figure 5.4 illustrates the achievable SNR at the output of the conventional blanker and clipper. It is observed that simulation results closely match the analytical ones obtained from (5.17) which validates the model used in this

work. Within the intermediate region, this figure shows that V-OFDM ($M = 64$) achieves a maximum of about 1.9 dB SNR improvement over conventional OFDM with blanking and about 0.5 dB in the case of clipping. The figure also reveals that for all $M > 1$, V-OFDM always outperforms OFDM. However, in both blanking and clipping, when the threshold value (T_b or T_c) is too low, the SNR degrades rapidly as part of data signal power is lost during noise cancellation. Conversely, when the threshold value is too high, some of the impulsive noise samples push through the system undetected, thereby degrading the SNR at the receiver. It is further observed at these extreme thresholds that OFDM achieves the same performance as V-OFDM. However, between these extremes, there exists a value of T_b and T_c which maximise the output SNR.

5.6 Energy Efficiency in V-OFDM with DPTE

As mentioned in previous section, there are various techniques for suppressing noise. Common methods include, the conventional blanking, clipping and hybrid. This section presents the DPTE as a more efficient noise cancellation technique.

5.6.1 Dynamic Peak-Based Threshold Estimation Technique

From this point onward, subsequent discussions and SNR comparison are relative to conventional blanking. In conventional blanking, received signals are nulled when their power exceed the blanking threshold T_b . The challenge with this approach is that detailed noise characteristics such as SINR and probability of occurrence p must be known apriori at the receiver in order to accurately determine the optimal value of T_b [84]. In determining the values of the SINR and p , transient variations in the noise pattern may be undetected. Therefore, the conventional blanking method is prone to errors arising from sub-optimal threshold values and short term variations in noise characteristics both of which degrade performance. To address this issue in V-OFDM, this work employs DPTE technique. DPTE relies on the premise that if V-OFDM symbol peaks are measured at the transmitter and correctly received by the blanker, output SNR can be significantly improved without regard to the short

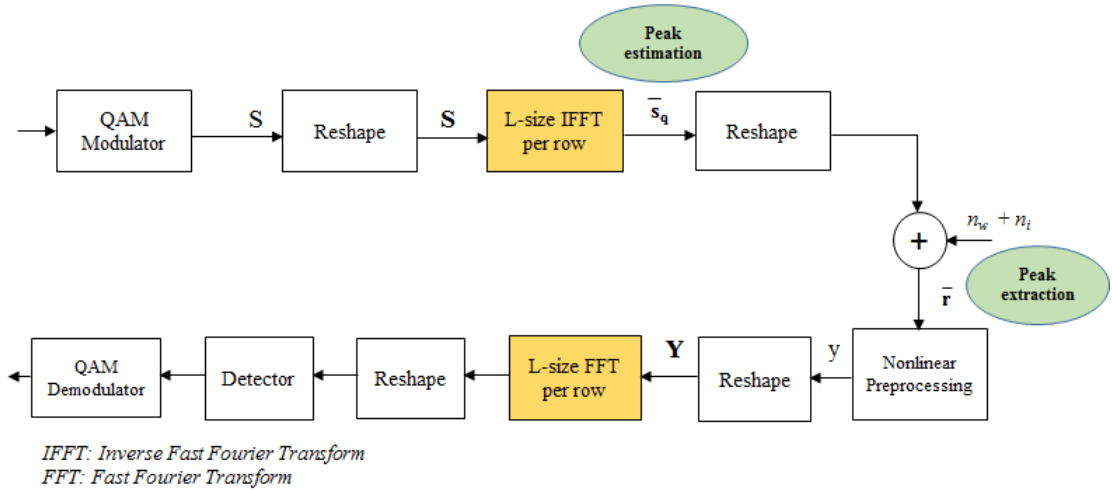


Figure 5.5: V-OFDM with DPTE system showing the peak extractor at the receiver

term variation in noise [85]. The the idea of combining V-OFDM with DPTE in this Chapter is that together, they can significantly improve energy efficiency of the PLC systems. The V-OFDM block diagram with DPTE is presented in Figure 5.5.

In this section, using n samples and N modulated symbols which can be reshaped into $N = M \times L$, information bits are generated, mapped and blocked into VBs as described in section 5.3. The corresponding V-OFDM symbol $\{s^{(k)}\}$ is then generated and its peak value $Peak(k)$ is measured. Thereafter, $\{s^{(k)}\}$ is transmitted through the PLC channel where it is contaminated with noise vector $\{n^{(k)}\}$ (a composition of background and impulsive noise) to produce received signal $\{r^{(k)}\}$. $\{s^{(k)}\}$, $\{n^{(k)}\}$ and $\{r^{(k)}\}$ are vectors such that $k = 0, 1, 2, \dots, n$.

In practical systems, $Peak(k)$ can be sent as control message to the receiver through dedicated channel or contention-free timeslots such as TDMA slots defined in IEEE 1901.2, PRIME and other NPLC standards for smart grid. At the receiver, the peak extractor retrieves the $Peak(k)$ value associated with the k^{th} symbol and dynamically adjusts the blanking threshold accordingly. The k^{th} symbol is then blanked according to the value of $Peak(k)$.

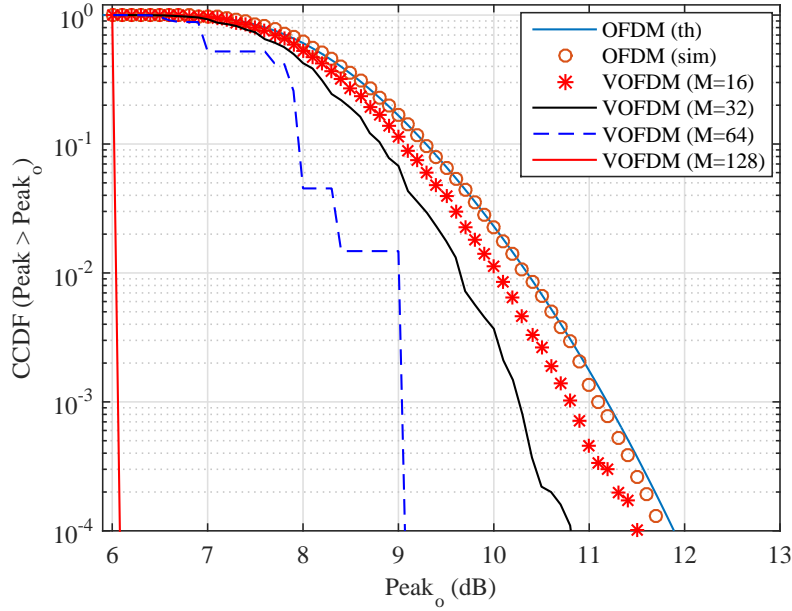
5.6.2 Signal Peak Estimation

Here we investigate the effects of number of VBs on V-OFDM symbol peaks. However, it is practically challenging in multicarrier systems to accurately determine the peak of every V-OFDM symbol. This is because the symbol peak values are random, by calculating the average rate at which they exceed a threshold value, the complimentary cumulative distribution function (CCDF) can be computed for different peak values. Therefore, this work adopts the CCDF expression (5.22), which is widely used in the literature. Here, the CCDF is defined as the probability that the peak of V-OFDM symbols exceeds a certain value $Peak_0$ and can be expressed as

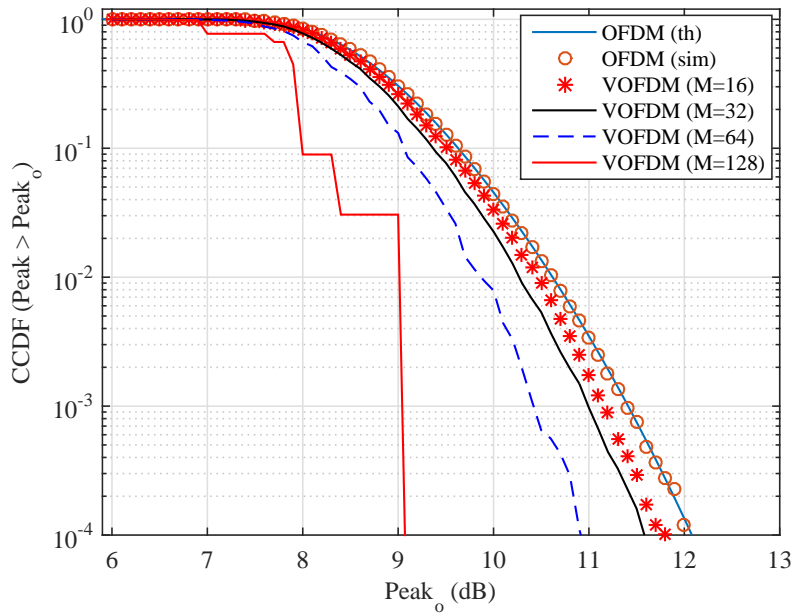
$$\text{CCDF} = 1 - \Pr \{ \text{Peak} \leq \text{Peak}_0 \} = \Pr \{ \text{Peak} > \text{Peak}_0 \}. \quad (5.22)$$

Although (5.22) is not precise for every symbol, it was shown in [85] that such approximation adequately represents average system performance. Based on (5.22), extensive simulations were conducted to determine the CCDF at different peak values for various numbers of VBs. Figure 5.6 depicts the variation of V-OFDM symbol peaks with number of VBs, where $M = 1$ is equivalent to conventional OFDM.

Two cases: $N = 512$ and $N = 1024$ with various VBs are considered. Figure 5.6 shows clearly that provided there are more than one VB, ($M > 1$), V-OFDM achieves lower peak values than the typical OFDM and that the symbol peaks reduce as the number of VBs increases. It is seen that for a given peak value $Peak_0$, CCDF decreases as the number of VBs in the V-OFDM system increases. This brings new flexibilities into design of PLC systems. Furthermore, unlike the COB, shifting peak estimation to the transmitter-side relieves the receiver of some computational overhead which can further reduce the effect of transmitter-receiver unbalanced complexity in systems design. Also, for each number of VBs, the performance gap closes as the subcarriers increase from 512 to 1024. The figure generally indicates that for a fixed N , as the number of VB increases, V-OFDM symbol peaks becomes less likely to be higher than $Peak_0$. For example, in Figure 5.6b, it is observed that in V-OFDM, the symbol peak values are more likely to be higher than 9 dB as the number of VBs decreases from 128. It can generally also be inferred that although symbol peak value of V-OFDM decreases with number of VBs but



(a) CCDF of symbol peak values when $N = 512$



(b) CCDF of symbol peak values when $N = 1024$

Figure 5.6: CCDF as a function of V-OFDM symbol peak values for various N and VB ($M = \{16, 32, 64, 128\}$) using 10^5 symbols. Analytical and simulated CCDF of the conventional OFDM are also included.

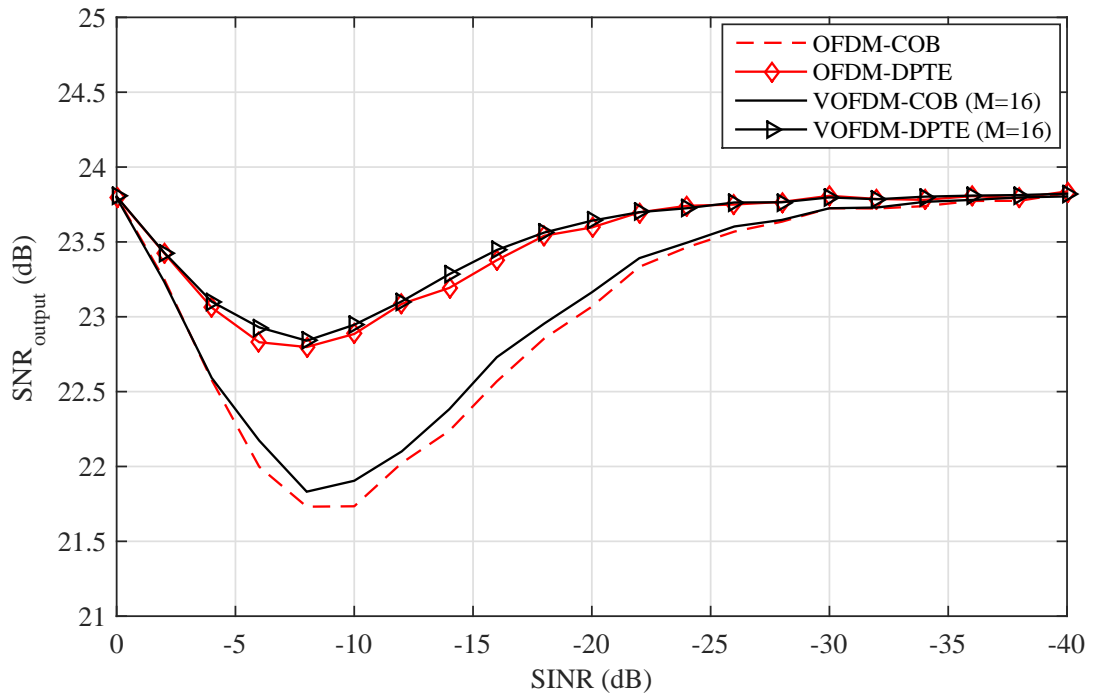


Figure 5.7: SNR performance of DPTE and COB in V-OFDM system with input SNR = 25dB, $p = 0.001$, $n = 5 \times 10^4$ and $N = 256$

that comes at the expense of computational complexity.

Finally, it is observed in Figure 5.6a for example, that by applying V-OFDM ($M = 128$) to QAM modulated signal with $N = 512$, symbol peak power reduces by about 5.8 dB relative to conventional OFDM. The practical implication is that, for example in PLC-based smart grid, if 20 dBm is required to transmit QAM symbols with OFDM, the transmitter's PA needs a maximum of 31.8 dBm to ensure linear operation whereas with V-OFDM, maximum of 26.1 dBm is needed. When aggregated over several thousands or millions of PLC nodes, this could yield significant power savings.

5.6.3 Output SNR of V-OFDM with DPTE

Here we first compare the SNR performance of DPTE and conventional blanking techniques.

Figure 5.7 compares output SNR performance between DPTE and conventional blanking in OFDM and V-OFDM. It is clear that DPTE outperforms

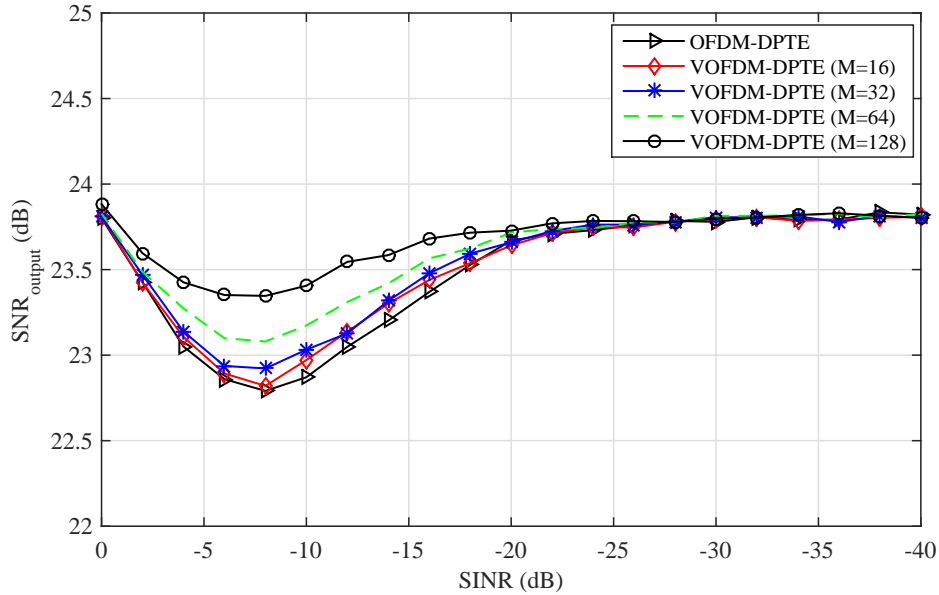
COB. This result demonstrates that if a certain QAM modulated symbol sequence of length N signal is blanked using DPTE techniques, even with OFDM and 16 VBs, output SNR can be improved by 1.1 dB in each case, relative to COB. The figure further shows that at extreme values (very low and very high) of SINRs, output SNR is not affected by number of VBs in V-OFDM, as it becomes identical for both systems. This is logical because at one extreme, when SINR is very high, the system tends to behave as if impulsive noise does not exist, yielding maximum SNR. Given that amplitude of affected symbols is typically higher than the average amplitude of symbols, at the other extreme, when SINR is very low, impulsive noise samples can be more easily detected and cancelled which also results in maximum SNR.

Figure 5.8 presents the variation of output SNR with SINR in V-OFDM for different numbers of VBs. It is obvious from the results that for each value of N , output SNR performance generally improves with the number of VBs. This result underscores the earlier observation in Figure 5.7. However, regardless the number of VBs used in V-OFDM, as N increase from 256 to 1024, the performance of V-OFDM approaches that of conventional OFDM. For example, in Figure 5.8a at $M=128$, DPTE can increase output SNR by about 0.6 dB (relative to OFDM) compared with Figure 5.8b in which the gain reduces to about 0.25 dB at the same value of M .

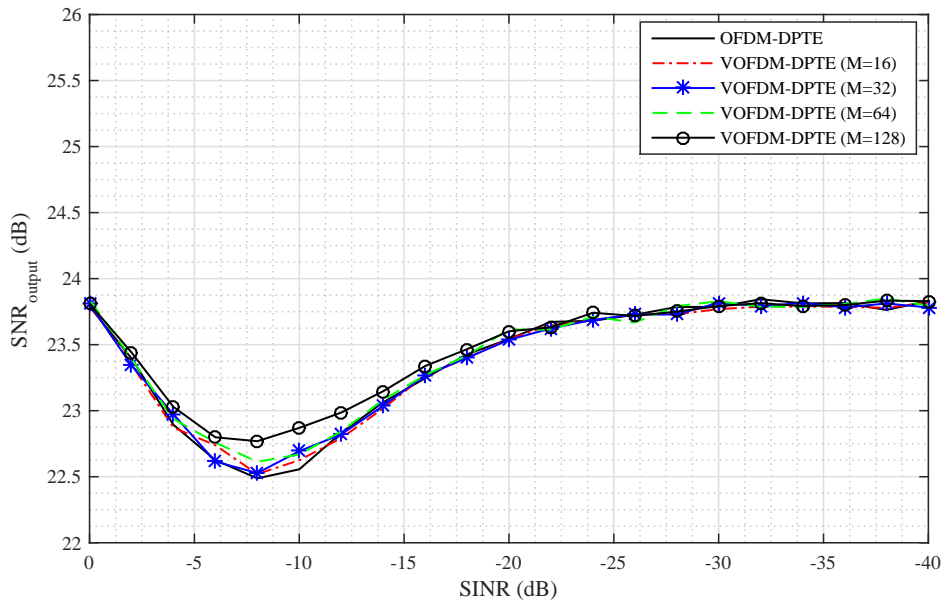
5.6.4 Comparative SNR Performance for Various Impulsive Noise Cases

In a smart grid where several thousands or millions of heterogeneous devices with different operational characteristics are interconnected, the probability of impulsive noise can be significantly high. Here we investigate the SNR performance of DPTE and COB under different impulsive noise conditions.

Figure 5.9 compares the output SNR of DPTE with COB in V-OFDM system under various channel conditions based on impulsive noise events. It is observed that for all VBs, DPTE consistently outperforms conventional blanking method. For example, it can also be seen that the output SNR improves with the number of VBs such that peak SNR is achieved when $M=128$, yielding a maximum SNR improvement of about 2.1 dB over conventional blanking. Finally, the figure reveals that at extreme SINRs, output

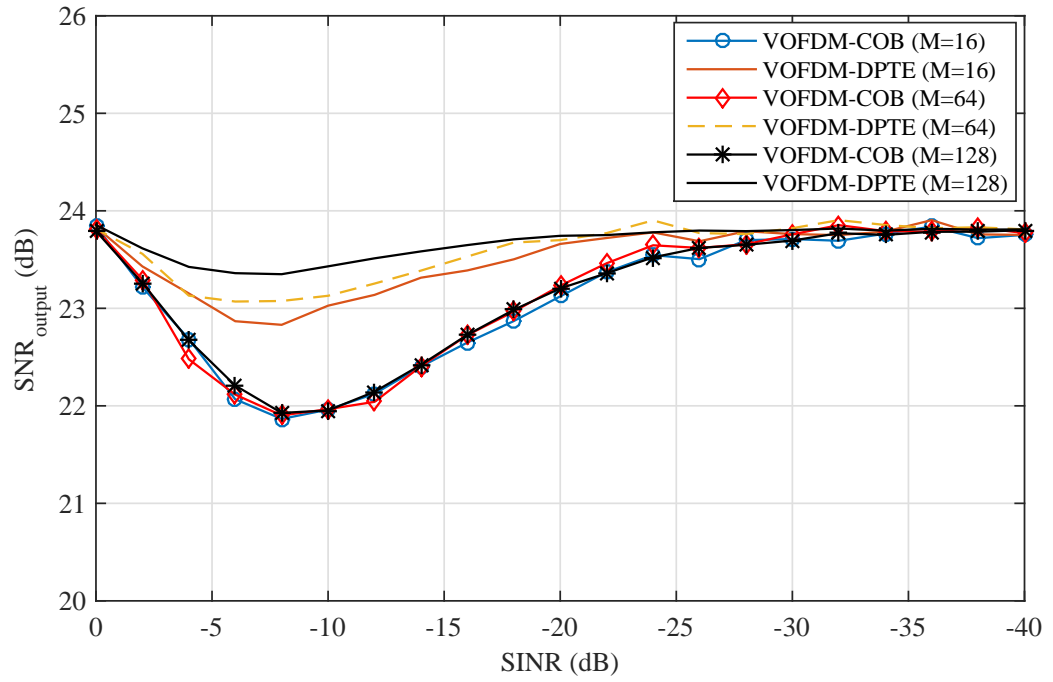


(a) when $N = 256$

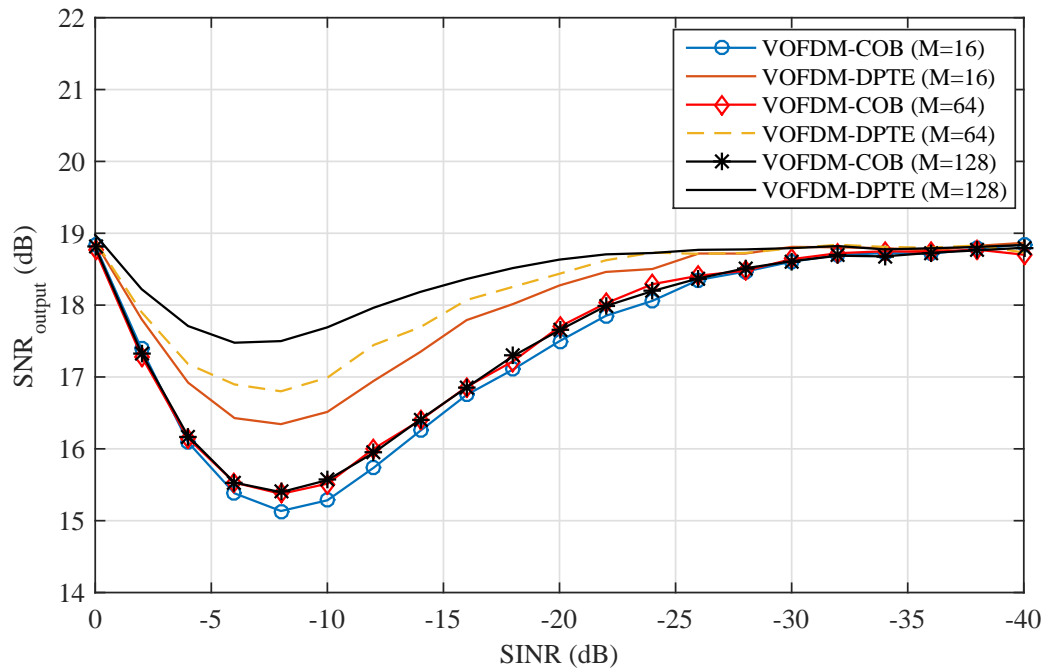


(b) when $N = 1024$

Figure 5.8: Blanker output SNR as a function of SINR using DPTE with parameters $N = 256$, $n = 10^4$ symbols in 16QAM, $p = 0.001$ input SNR = 25dB.



(a) when $p = 0.001$



(b) when $p = 0.01$

Figure 5.9: Comparative SNR performance of DPTE and COB in various impulsive noise conditions using $p = \{0.001, 0.01\}$ SNR=25, $N = 256$, 16QAM, $n = 10^4$

SNR is independent of number of VBs. The practical consequence of these results is that unlike OFDM ($M = 1$), the existence of $M = \{16, 32, 64, 128, \dots\}$ in V-OFDM provides significant flexibility in system design as complexity can now be matched with performance without losing the fundamental benefits of OFDM as a multi-carrier system.

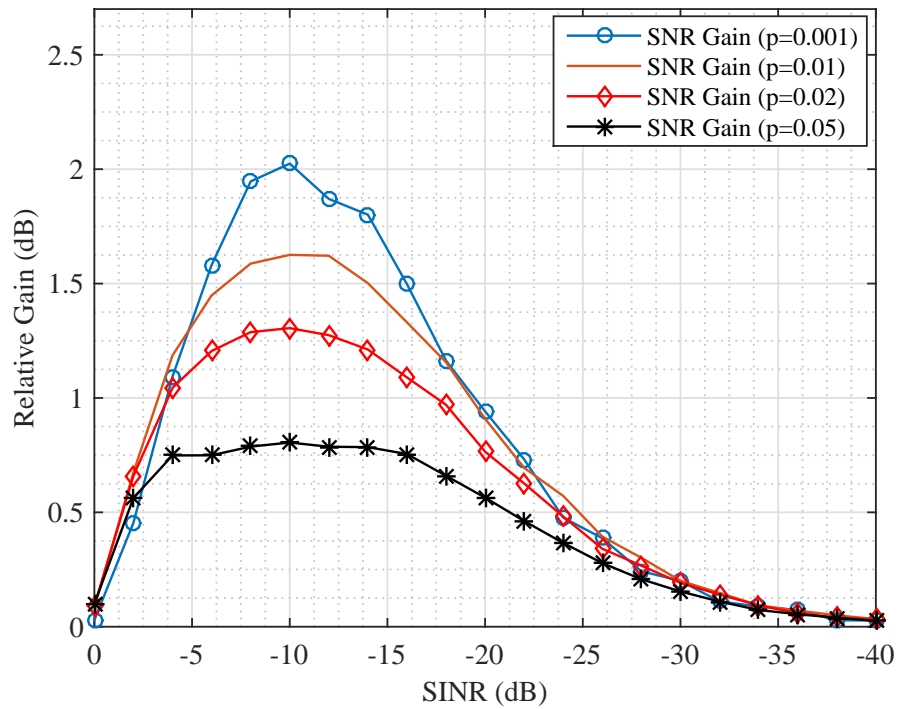
5.6.5 DPTE Gain Relative to Conventional Blanking

This section presents the SNR gain of DPTE technique relative to COB for different probabilities of impulsive noise. The relative gain $G_{Relative}$ is therefore defined as

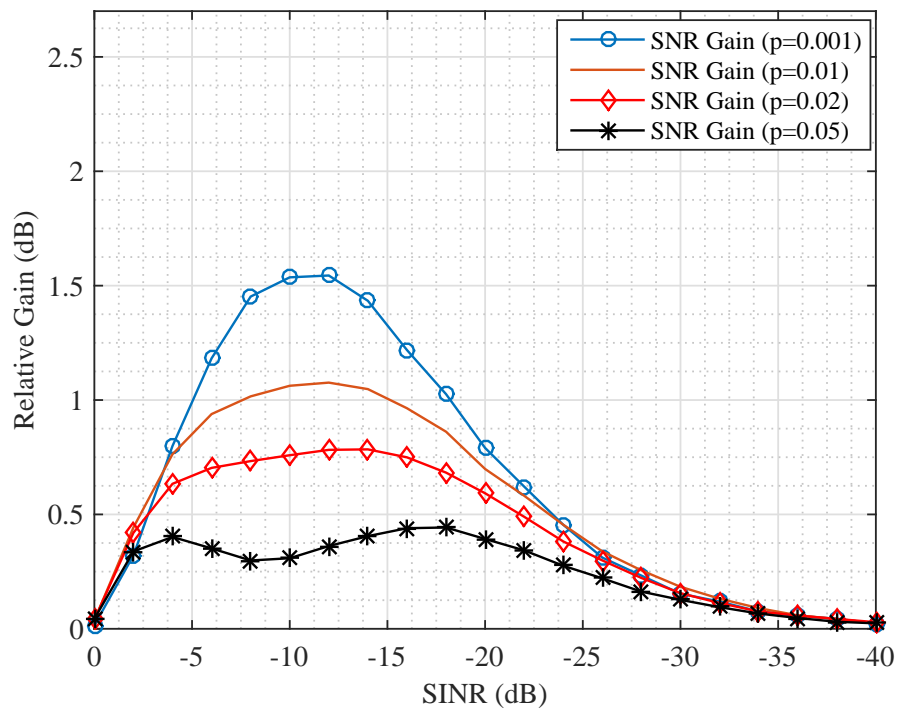
$$G_{Relative} = 10 \log_{10} \left(\frac{SNR_{DPTE}}{SNR_{COB}} \right). \quad (5.23)$$

The relative gain in blanker output SNR is illustrated in Figure 5.10.

It is clear from these results that, given the same channel conditions, DPTE always achieves higher SNR at the output of the blanker relative to conventional blanking. It is also observed that, the relative SNR gain increases as p decreases. For example, it is observed in the figure that at $p = 0.001$ a relative gain of 2 dB is achieved, but when p increases to 0.05, the maximum gain reduces to about 0.74 dB. In both cases of $N = 256$ and $N = 512$, it is obvious that, for all values of p , there is a certain value of SINR at which $G_{Relative}$ is highest, in this figure, that value is -10 dB. Finally, the mere fact that $G_{Relative} > 0$ in all cases clearly indicates that DPTE always performs better than conventional blanking, even when the peak estimates are corrupted by impulsive noise. This can be explained by the fact that DPTE dynamically tunes the blanking threshold, in the event that the side information is corrupted by impulsive noise, only a very small fraction of the peak values are affected whereas short-term variations in impulsive noise behavior may consistently be undetected in conventional blanking. Hence, given the same transmit power on both systems, DPTE is more energy efficient.



(a) $N = 256, n = 5000, M = 16$



(b) $N = 512, n = 5000, M = 16$

Figure 5.10: Relative SNR gain of V-OFDM with DPTE over COB for different impulsive noise probabilities for $N = 256$ and $M = 64$ at input SNR = 30 dB, $p = 0.05, n = 10^4, 16QAM$

5.7 Chapter Summary

This Chapter investigated the energy efficiency of V-OFDM relative to conventional OFDM in PLC systems. The results reveal that the proposed V-OFDM can provide significant transmit power savings compared to the conventional OFDM system under same transmit power and PLC channel conditions. Therefore, V-OFDM is more suitable for the non-Gaussian PLC channel than conventional OFDM especially if energy efficiency is considered as a performance metric. The lower PAPR property of V-OFDM not only allows the deployment of cheaper low power PAs at the transmitting PLC modems, but also, with some basic processing at the receiving PLC modem, it can make such systems more energy efficient.

To improve energy efficiency, this Chapter has shown that existence of VBs in V-OFDM offers variable IFFT size which introduces new design choices to match complexity with energy efficiency. Furthermore, to suppress noise at the receiver, DPTE was also investigated and it consistently outperformed conventional blanking technique in terms of output SNR. By exploiting the low PAPR and high SNR properties of V-OFDM and DPTE respectively, this Chapter showed that transmit power can be reduced by about 5.8 dB while the output SNR of the blanker is increased by 2.1 dB relative to conventional OFDM. Together, these can simplify design, reduce cost and improve energy efficiency of future PLC transceivers beyond state-of-the-art. Although the V-OFDM performance gains come at the expense of computational complexity, however, ultra-fast, inexpensive chips are readily available to ease implementation. Hence, this is a reasonable sacrifice.

Chapter 6

Conclusions and Future Work

6.1 Conclusions

With the successful trials and some commercial deployments of smart grid applications in some parts of the globe, the transition to an intelligent grid is already a *fait accompli*. The next step in this evolution is to improve the smart grid operation in the most secure, sustainable and economic manner. One of the areas that need improvements is energy consumption of the enabling communication systems. Among the contending communication technologies, PLC stands out not only because power lines are readily available but also they simplify the communication network management. To this end, in Chapter 1, while the current trend in the energy sector was briefly discussed, the motivation to investigate energy-efficient PLC for smart grid application was also presented.

In the distribution domain, the power lines originate from the LV substation and branch off into individual homes, each point of termination and joint represents a point of impedance mismatch which adds to the inherent challenges such as various forms of noise originating from the heterogeneous loads connected on the network and unpredictability of the power line channel. These factors combine to degrade PLC systems performance. To understand these challenges, Chapter 2 is dedicated to fundamental analysis of power lines, including channel characterisation and signal propagation challenges. It provides detailed numerical analysis of channel modelling techniques widely used. Furthermore, the chapter discussed the various forms

of noise and their characteristics as well as the widely used modelling techniques. In addition, a comprehensive review of smart grid applications, their traffic characteristics, QoS requirements in terms data rate, latency and reliability are provided. A comparative analysis of wired and wireless technologies is also given and lastly, energy efficiency was discussed as one area of PLC that has not received enough research attention despite its importance.

In Chapter 3, a clustered architecture was proposed for AMI to take advantage of the network topology to improve the communication network performance in terms of coverage and reliability. The chapter began by investigating BPLC as a backhaul solution for clustered AMI using smart metering and DR applications. The main modification in the network topology is the use of one of the smart meters as local aggregator (DC) which collates and dispatches the reading from other meters in the NAN, thus the DC behaved like a relay. The result showed that position of the DC can affect network performance gain in terms of packet delivery probability. The maximum improvement was achieved when the DC was positioned at the middle of the NAN, during which probability of successful packet delivery rose by about 3% relative to flat AMI which translates to saving of the energy that would have been expended to retransmit lost packets. The results in this chapter clearly showed that the proposed scheme may be a disadvantage in small clusters. Hence, the clustered AMI approach is not recommended for small cluster sizes except for geographically dispersed meters.

Chapter 4 of this project proposed a low-power PLC for HEMS application. The chapter provided an empirical assessment of 6LoPLC for basic applications such as temperature sensing and light control within the HAN. The main idea in this chapter was adaptation of 6LoWPAN in power lines. The study involved an NS-3 model which was validated with experimental results. The validated model was consequently used to study diverse complicated HEMS scenarios. The results demonstrated that the proposed scheme can save up to 2.6014 dB in transmit power compared with conventional PLC systems. Furthermore, it was shown that relative to conventional system, although 6LoPLC introduced additional latency which could be up to 131.7512 for control and 108.8314ms for monitoring applications in worst case, these values are within acceptable limits and do not adversely affect application performance. It was also revealed that in order to guarantee a minimum of

99% system reliability, the application must be 64 bytes or less. Lastly, this chapter showed that the presence impulsive noise in the power line channel can cause additional delay of about 32.759 ms in some some cases.

Chapter 5 proposed V-OFDM combined with DPTE to improve energy efficiency of PLC transceivers. This approach exploited the low PAPR property of V-OFDM to enhance impulsive noise detection and cancellation at the receiver which results in higher SNR at the output of the blanking device. Unlike the conventional blanking system, the proposed approach does not rely on measurement of noise at the receiver, hence it is insensitive to short-term changes in noise characteristics. Results show that due to its low PAPR properties, VOFDM is less sensitive to impulsive noise and provides a reduction of 5.8 dB in transmit power requirement relative to conventional OFDM. Furthermore, unlike the existing impulsive noise cancellation methods, the DPTE technique also improves the SNR at the receiver by about 2.1 dB which further reduces the power requirement of the PLC transceiver. The conclusions of this thesis can be summarised as follows.

- Energy efficiency of PLC systems can be approached in a variety of ways, including network configuration, hardware design and signal processing.
- Smart grid can take advantage of existing LV distribution network to improve packet delivery over the PLC network for AMI applications such smart metering and demand response.
- Low data rate transmission techniques such as DBPSK and 6LoPLC can result in energy savings for monitoring and control applications such as energy management in homes.
- In PLC networks, impulsive noise is a major performance inhibitor of applications, hence smart techniques are needed to mitigate it.
- From design perspective, significant energy savings can be achieved by exploiting the low PAPR of V-OFDM system for symbol processing at the transmitter and impulsive noise cancellation (DPTE) at the receiver.
- The better performance of V-OFDM system comes at the expense of additional computational complexity however, system implementation

can take advantage of the inexpensive, ultra-fast chips that are readily available.

6.2 Future Work

This thesis consists of three pieces of work conducted at physical, adaptation and network layers. At the PHY layer, V-OFDM has been proposed to reduce transmit power requirement of PLC transceivers. In order to take forward the work reported in this thesis, some areas are suggested for further study. Given the use of VBs in V-OFDM, one of the future research areas include implementation of V-OFDM in field-programmable gate array (FPGA) to evaluate the trade-off between design complexity and energy efficiency. Although V-OFDM introduces new flexibilities in system design by exploiting the inherent VBs, it is necessary to compare the computational complexity between conventional OFDM and V-OFDM systems. In particular, this aspect will evaluate additional computational resources required by V-OFDM relative to OFDM and conduct a cost-benefit analysis in order to justify use-cases for the different number of VBs.

At the adaptation layer, since NPLC inherently provides longer transmission range than the BPLC demonstrated in this thesis, it will also be interesting in the future to recalibrate the model developed in this thesis and use it to investigate low-rate, low-power NPLC in multi-tenant buildings such as large commercial buildings, office complexes, university campuses or small/mid-size industrial facilities. By applying 6LoPLC over NPLC for monitoring/control applications, the study can provide new insight into cost-effective building managements techniques with extended scope covering the monitoring and control of heating, ventilation and air-conditioning (HVAC) systems.

The work in Chapter 3 of this thesis was based on fixed impedance. However, as the NAN is inhabited by consumers with different dispositions in the manner they connect to the grid, it is also recommended that AMI clustering be further investigated taking into account variable line impedance and different channel conditions in terms of impulsive noise events. Lastly, this thesis investigated the energy-saving potentials of V-OFDM generally and it was shown that V-OFDM is less sensitive to impulsive noise than conventional

OFDM. In the future, it is desirable to investigate how the various smart grid applications can benefit from the noise-immunity in terms of improved good-put and network reliability.

Bibliography

- [1] Y. Kabalci, "A survey on smart metering and smart grid communication," *Renewable and Sustainable Energy Reviews*, vol. 57, pp. 302–318, 2016.
- [2] R. H. Khan and J. Y. Khan, "A comprehensive review of the application characteristics and traffic requirements of a smart grid communications network," *Computer Networks*, vol. 57, no. 3, pp. 825–845, 2013.
- [3] K. Dostert, "Propagation channel characterization and modeling outdoor power supply grids as communication channels," *Keynote Presentation, ISPLC 2005*.
- [4] T. Esmailian, F. Kschischang, and P. Gulak, "An in-building power line channel simulator," in *Proc. IEEE Int. Symp. on Power Line Commun. and Its Appl. (ISPLC)*, pp. 27–29, 2002.
- [5] T. Esmailian, F. R. Kschischang, and P. Glenn Gulak, "In-building power lines as high-speed communication channels: channel characterization and a test channel ensemble," *Int. Journal of Commun. Systems*, vol. 16, no. 5, pp. 381–400, 2003.
- [6] A. Ikpehai, B. Adebisi, and R. Kharel, "Smart street lighting over narrowband plc in a smart city: The triangulum case study," in *Proc. IEEE 21st Int. Workshop on Comp. Aided Modelling and Design of Commun. Links and Networks (CAMAD)*, pp. 242–247, 2016.
- [7] H. Farhangi, "The path of the smart grid," *IEEE Power and Energy Mag.*, vol. 8, no. 1, 2010.
- [8] S. Galli, A. Scaglione, and Z. Wang, "For the grid and through the grid:

- The role of power line communications in the smart grid," *Proc. of the IEEE*, vol. 99, no. 6, pp. 998–1027, 2011.
- [9] B. Adebisi, S. Ali, and B. Honary, "Space-frequency and space-time-frequency M₃FSK for indoor multiwire communications," *IEEE Trans. on Power Del.*, vol. 24, no. 4, pp. 2361–2367, 2009.
- [10] P. Amirshahi and M. Kavehrad, "High-frequency characteristics of overhead multiconductor power lines for broadband communications," *IEEE Journal on Sel. Areas in Commun.*, vol. 24, no. 7, pp. 1292–1303, 2006.
- [11] T. A. Papadopoulos, C. G. Kaloudas, A. I. Chrysochos, and G. K. Papagiannis, "Application of narrowband power-line communication in medium-voltage smart distribution grids," *IEEE Trans. on Power Del.*, vol. 28, no. 2, pp. 981–988, 2013.
- [12] H. Meng, S. Chen, Y. Guan, C. Law, P. So, E. Gunawan, and T. Lie, "Modeling of transfer characteristics for the broadband power line communication channel," *IEEE Trans. on Power Del.*, vol. 19, no. 3, pp. 1057–1064, 2004.
- [13] J.-Y. Baudais, A. M. Tonello, and A. Hamini, "Energy efficient resource allocation for quantity of information delivery in parallel channels," *Trans. Emerging Telecommun. Technol.*, 2014.
- [14] L. Lampe, R. Schober, and S. Yiu, "Distributed space-time coding for multihop transmission in power line communication networks," *IEEE Journal Sel. Areas Commun.*, vol. 24, no. 7, pp. 1389–1400, 2006.
- [15] S. D'Alessandro, A. M. Tonello, and F. Versolatto, "Power savings with opportunistic decode and forward over in-home PLC networks," in *Proc. IEEE Int. Symp. on Power Line Commun. and Its Appl. (ISPLC)*, pp. 176–181, 2011.
- [16] K. M. Rabie, B. Adebisi, H. Gacanin, N. Galymzhan, and I. Augustine, "On the Energy Efficiency of Multi-hop Relaying Power Line Communication Systems," *Journal of Commun. and Networks*, 2017 (accepted).

- [17] K. M. Rabie, B. Adebisi, and A. Salem, "Improving energy efficiency in dual-hop cooperative PLC relaying systems," in *Proc. IEEE Int. Symp. on Power Line Commun. and its Appl. (ISPLC)*, pp. 196–200, 2016.
- [18] K. M. Rabie, B. Adebisi, A. M. Tonello, and G. Nauryzbayev, "For more energy-efficient dual-hop DF relaying power-line communication systems," *IEEE Systems Journal*, 2017.
- [19] W. Bakkali, M. Tlich, P. Pagani, and T. Chonavel, "A measurement-based model of energy consumption for PLC modems," in *Proc. IEEE Int. Symp. on Power Line Commun. and its Appl. (ISPLC)*, pp. 42–46, 2014.
- [20] W. Bakkali, P. Pagani, T. Chonavel, and A. M. Tonello, "Energy efficiency performance of decode and forward MIMO relay PLC systems," in *Proc. IEEE Int. Symp. on Power Line Commun. and its Appl. (ISPLC)*, pp. 201–205, 2016.
- [21] W. Bakkali, P. Pagani, and T. Chonavel, "Experimental analysis and modeling of energy consumption behaviour for MIMO PLC modems," in *Proc. IEEE Global Commun. Conf. (GLOBECOM)*, pp. 1–5, 2015.
- [22] ———, "Energy efficiency performance of relay-assisted power-line communication networks," in *Proc. IEEE Consumer Commun. and Networking Conf.*, pp. 525–530, 2015.
- [23] M. E. El-Hawary, "The smart grid state-of-the-art and future trends," *Electric Power Components and Sys.*, vol. 42, no. 3-4, pp. 239–250, 2014.
- [24] Y. Yan, Y. Qian, H. Sharif, and D. Tipper, "A survey on smart grid communication infrastructures: Motivations, requirements and challenges," *IEEE commun. Surv. & Tut.*, vol. 15, no. 1, pp. 5–20, 2013.
- [25] M. Erol-Kantarci and H. T. Mouftah, "Energy-efficient information and communication infrastructures in the smart grid: A survey on interactions and open issues," *IEEE Commun. Surv. & Tut.*, vol. 17, no. 1, pp. 179–197, 2015.
- [26] M. L. Tuballa and M. L. Abundo, "A review of the development of smart grid technologies," *Renewable and Sustainable Energy Reviews*, vol. 59, pp. 710–725, 2016.

- [27] V. C. Gungor, D. Sahin, T. Kocak, S. Ergut, C. Buccella, C. Cecati, and G. P. Hancke, "A survey on smart grid potential applications and communication requirements," *IEEE Trans. on Ind. Informat.*, vol. 9, no. 1, pp. 28–42, 2013.
- [28] D. Kaleshi and T. Song, "Smart grids and communications systems," *HubNet Position Paper Series*, 2014.
- [29] D. G. Photovoltaics and Storage, "IEEE guide for smart grid interoperability of energy technology and information technology operation with the electric power system (EPS), end-use applications, and loads," *IEEE Std.*
- [30] G. López, P. Moura, J. I. Moreno, and J. M. Camacho, "Multi-faceted assessment of a wireless communications infrastructure for the green neighborhoods of the smart grid," *Energies*, vol. 7, no. 5, pp. 3453–3483, 2014.
- [31] A. Ikpehai, B. Adebisi, and K. M. Rabie, "Broadband PLC for clustered advanced metering infrastructure (AMI) architecture," *Energies*, vol. 9, no. 7, pp. 569–569, 2016.
- [32] G. R. Newsham and B. G. Bowker, "The effect of utility time-varying pricing and load control strategies on residential summer peak electricity use: a review," *Energy policy*, vol. 38, no. 7, pp. 3289–3296, 2010.
- [33] S. Shao, M. Pipattanasomporn, and S. Rahman, "Grid integration of electric vehicles and demand response with customer choice," *IEEE Trans. on Smart Grid*, vol. 3, no. 1, pp. 543–550, 2012.
- [34] J. Taylor, A. Maitra, M. Alexander, D. Brooks, and M. Duvall, "Evaluation of the impact of plug-in electric vehicle loading on distribution system operations," in *Proc. IEEE Power & Energy Society General Meeting*, pp. 1–6, 2009.
- [35] K. J. Dyke, N. Schofield, and M. Barnes, "The impact of transport electrification on electrical networks," *IEEE Trans. on Ind. Electronics*, vol. 57, no. 12, pp. 3917–3926, 2010.

- [36] P. Richardson, D. Flynn, and A. Keane, "Impact assessment of varying penetrations of electric vehicles on low voltage distribution systems," in *Proc. IEEE Power and Energy Society General Meeting*, pp. 1–6, 2010.
- [37] S. Shao, M. Pipattanasomporn, and S. Rahman, "Challenges of PHEV penetration to the residential distribution network," in *Proc. IEEE Power & Energy Society General Meeting*, pp. 1–8, 2009.
- [38] K. Clement-Nyns, E. Haesen, and J. Driesen, "The impact of charging plug-in hybrid electric vehicles on a residential distribution grid," *IEEE Trans. on Power Sys.*, vol. 25, no. 1, pp. 371–380, 2010.
- [39] E. Sortomme, M. M. Hindi, S. J. MacPherson, and S. Venkata, "Coordinated charging of plug-in hybrid electric vehicles to minimize distribution system losses," *IEEE Trans. on smart grid*, vol. 2, no. 1, pp. 198–205, 2011.
- [40] W. Kempton and J. Tomić, "Vehicle-to-grid power implementation: From stabilizing the grid to supporting large-scale renewable energy," *Journal of power sources*, vol. 144, no. 1, pp. 280–294, 2005.
- [41] J. García-Villalobos, I. Zamora, J. San Martín, F. Asensio, and V. Aperribay, "Plug-in electric vehicles in electric distribution networks: A review of smart charging approaches," *Renewable and Sustainable Energy Reviews*, vol. 38, pp. 717–731, 2014.
- [42] B. Kroposki, R. Lasseter, T. Ise, S. Morozumi, S. Papatlianassiou, and N. Hatziaargyriou, "Making microgrids work," *IEEE power and energy mag.*, vol. 6, no. 3, 2008.
- [43] B. Kroposki, T. Basso, and R. DeBlasio, "Microgrid standards and technologies," in *IEEE Power and Energy Society General Meeting-Conversion and Delivery of Electrical Energy in the 21st Century*, 2008, pp. 1–4.
- [44] A. Naumann, P. Komarnicki, M. Powalko, Z. Styczynski, J. Blumschein, and M. Kereit, "Experience with PMUs in industrial distribution networks," in *IEEE Power and Energy Society General Meeting*, 2010, pp. 1–6.

- [45] M. Wache and D. Murray, "Application of synchrophasor measurements for distribution networks," in *Proc. IEEE Power and Energy Society General Meeting*, pp. 1–4, 2011.
- [46] ETSI, "Draft TR 102 935, version: 0.1.3 M2M;applicability of M2M architecture to smart grid networks;impact of smart grids on M2M platform, 2012," in <http://www.etsi.org> (accessed on 25 March 2017), 2012.
- [47] L. Shen, H. Wang, X. Duan, and X. Li, "Application of wireless sensor networks in the prediction of wind power generation," in *Proc. 4th IEEE Int. Conf. on Wireless Communi., Networking and Mobile Comput.*, pp. 1–4, 2008.
- [48] A. Ikpehai and B. Adebisi, "6LoPLC for smart grid applications," in *Proc IEEE Int. Symp. on Power Line Communications and its Appl. (ISPLC)*, 2015, pp. 211–215.
- [49] M. Kuzlu, M. Pipattanasomporn, and S. Rahman, "Communication network requirements for major smart grid applications in HAN, NAN and WAN," *Computer Networks*, vol. 67, pp. 74–88, 2014.
- [50] C. Cano, A. Pittolo, D. Malone, L. Lampe, A. M. Tonello, and A. G. Dabak, "State of the art in power line communications: From the applications to the medium," *IEEE Journal on Sel. Areas in Commun.*, vol. 34, no. 7, pp. 1935–1952, 2016.
- [51] A. Sendin, T. Arzuaga, I. Urrutia, I. Berganza, A. Fernandez, L. Marron, A. Llano, and A. Arzuaga, "Adaptation of powerline communications-based smart metering deployments to the requirements of smart grids," *Energies*, vol. 8, no. 12, pp. 13 481–13 507, 2015.
- [52] B. Adebisi, A. Khalid, Y. Tsado, and B. Honary, "Narrowband PLC channel modelling for smart grid applications," in *Proc. 9th IEEE Int. Symp. on Commun. Systems, Networks & Digital Signal Processing (CSNDSP)*, pp. 67–72, 2014.
- [53] W. Luan, D. Sharp, and S. Lancashire, "Smart grid communication network capacity planning for power utilities," in *Proc. IEEE Trans. and Distrib. Conf. and Exposit.*, pp. 1–4, 2010.

- [54] D. Della Giustina and S. Rinaldi, "Hybrid communication network for the smart grid: validation of a field test experience," *IEEE Trans. on Power Del.*, vol. 30, no. 6, pp. 2492–2500, 2015.
- [55] J. Varela, L. J. Puglisi, T. Wiedemann, U. Ysberg, D. Stein, Z. Pokorna, C. Arnoult, R. Garaud-Verdier, and L. Consiglio, "Show me!: Large-scale smart grid demonstrations for European distribution networks," *IEEE Power and Energy Mag.*, vol. 13, no. 1, pp. 84–91, 2015.
- [56] K. M. Rabie and E. Alsusa, "On improving communication robustness in PLC systems for more reliable smart grid applications," *IEEE Trans. on Smart Grid*, vol. 6, no. 6, pp. 2746–2756, 2015.
- [57] D. Dzung, I. Berganza, and A. Sendin, "Evolution of powerline communications for smart distribution: from ripple control to OFDM," in *Proc. IEEE Int. Symp. on Power Line Commun. and Its Appl. (ISPLC)*, pp. 474–478, 2011.
- [58] L. T. Berger, A. Schwager, and J. J. Escudero-Garzás, "Power line communications for smart grid applications," *Journal of Elect. and Comp. Eng.*, vol. 2013, pp. 3–3, 2013.
- [59] M. Biagi and L. Lampe, "Location assisted routing techniques for power line communication in smart grids," in *Proc First IEEE Int. Conf. on Smart Grid Commun. (SmartGridComm)*, 2010, pp. 274–278.
- [60] S. Mudriievskiy, "Power line communications: State of the art in research, development and application," *AEU-Int. Journal of Electronics and Commun.*, vol. 68, no. 7, pp. 575–577, 2014.
- [61] M. Zimmermann and K. Dostert, "A multi-path signal propagation model for the power line channel in the high frequency range," in *Proc. IEEE Int. Symp. Power Line Commun. and Its App. (ISPLC)*, pp. 48–51, Apr. 1999.
- [62] —, "A multipath model for the powerline channel," *IEEE Trans. on commun.*, vol. 50, no. 4, pp. 553–559, 2002.

- [63] B. Adebisi, A. Treytl, A. Haidine, A. Portnoy, R. U. Shan, D. Lund, H. Pille, and B. Honary, "IP-centric high rate narrowband PLC for smart grid applications," *IEEE Commun. Mag.*, vol. 49, no. 12, 2011.
- [64] L. Tang, P. So, E. Gunawan, Y. Guan, S. Chen, and T. Lie, "Characterization and modeling of in-building power lines for high-speed data transmission," *IEEE Trans. on Power Del.*, vol. 18, no. 1, pp. 69–77, 2003.
- [65] H. Philipps, "Modeling of powerline communication channels," in *Proc. IEEE Int. Symp. Power Line Commun. and Its App. (ISPLC)*, pp. 14–15, Apr. 1999.
- [66] D. Anastasiadou and T. Antonakopoulos, "Multipath characterization of indoor power-line networks," *IEEE Trans. on Power Del.*, vol. 20, no. 1, pp. 90–99, 2005.
- [67] H. T. Hui, "Transmission lines - basic theories," *NUS/ECE Lecture Notes*, 2011.
- [68] S. Galli and T. Banwell, "A novel approach to the modeling of the indoor power line channel part ii: Transfer function and its properties," *IEEE Trans. on Power Del.*, vol. 20, no. 3, pp. 1869–1878, 2005.
- [69] T. Banwell and S. Galli, "A novel approach to the modeling of the indoor power line channel part i: circuit analysis and companion model," *IEEE Trans. on power Del.*, vol. 20, no. 2, pp. 655–663, 2005.
- [70] M. Rozman, A. Ikpehai, B. Adebisi, and K. M. Rabie, "Channel characterisation of cooperative relaying power line communication systems," in *Proc. 10th IEEE Int. Symp. on Commun. Systems, Networks and Digital Signal Processing (CSNDSP)*, pp. 1–5, 2016.
- [71] G. Ndo, F. Labeau, and M. Kassouf, "A markov-middleton model for bursty impulsive noise: Modeling and receiver design," *IEEE Trans. on Power Del.*, vol. 28, no. 4, pp. 2317–2325, 2013.
- [72] M. Zimmermann and K. Dostert, "Analysis and modeling of impulsive noise in broad-band powerline communications," *IEEE Trans. Electromagn. Compat.*, vol. 44, no. 1, pp. 249–258, Feb. 2002.

- [73] J. Lin, M. Nassar, and B. L. Evans, "Impulsive noise mitigation in powerline communications using sparse bayesian learning," *IEEE Journal on Sel. Areas in Commun. (JSAC)*, vol. 31, no. 7, pp. 1172–1183, 2013.
- [74] O. G. Hooijen, "A channel model for the residential power circuit used as a digital communications medium," *IEEE Trans. on electromag. compatib.*, vol. 40, no. 4, pp. 331–336, 1998.
- [75] H. Meng, Y. L. Guan, and S. Chen, "Modeling and analysis of noise effects on broadband power-line communications," *IEEE Trans. on Power Del.*, vol. 20, no. 2, pp. 630–637, 2005.
- [76] B. Adebisi and B. Honary, "Comparisons of indoor PLC emissions measurement results and regulation standards," in *Proc. IEEE Int. Symp. on Power Line Commun. and Its Appl.*, pp. 319–324, 2006.
- [77] B. Adebisi, J. Stott, and B. Honary, "Experimental study of the interference caused by PLC transmission on HF bands," 2006.
- [78] M. Gotz, M. Rapp, and K. Dostert, "Power line channel characteristics and their effect on communication system design," *IEEE Commun. Mag.*, vol. 42, no. 4, pp. 78–86, 2004.
- [79] M. Zimmermann and K. Dostert, "An analysis of the broadband noise scenario in powerline networks," in *Proc. IEEE Int. Symp. on Powerline Commun. and its Appl. (ISPLC2000)*, pp. 5–7, 2000.
- [80] A. Ikpehai, B. Adebisi, K. M. Rabie, R. Haggar, and M. Baker, "Experimental study of 6LoPLC for home energy management systems," *Energies*, vol. 9, no. 12, pp. 1046–1046, 2016.
- [81] K. M. Rabie and E. Alsusa, "Impulsive noise blanking using quantized PAPR estimates in powerline communications," in *Proc. IEEE 78th Vehic. Technol. Conf. (VTC Fall)*, pp. 1–5, 2013.
- [82] D. Middleton, "Canonical and quasi-canonical probability models of class A interference," *IEEE Trans. on Electromag. Compatib.*, no. 2, pp. 76–106, 1983.

- [83] F. Gianaroli, F. Pancaldi, and G. M. Vitetta, "The impact of statistical noise modeling on the error-rate performance of OFDM power-line communications," *IEEE Trans. on Power Del.*, vol. 29, no. 6, pp. 2622–2630, 2014.
- [84] K. M. Rabie and E. Alsusa, "Preprocessing-based impulsive noise reduction for power-line communications," *IEEE Trans. on Power Del.*, vol. 29, no. 4, pp. 1648–1658, 2014.
- [85] E. Alsusa and K. M. Rabie, "Dynamic peak-based threshold estimation method for mitigating impulsive noise in power-line communication systems," *IEEE Trans. Power Del.*, vol. 28, no. 4, pp. 2201–2208, 2013.
- [86] K. M. Rabie and E. Alsusa, "Quantized peak-based impulsive noise blanking in power-line communications," *IEEE Trans. on Power Del.*, vol. 29, no. 4, pp. 1630–1638, 2014.
- [87] S. V. Zhidkov, "Analysis and comparison of several simple impulsive noise mitigation schemes for OFDM receivers," *IEEE Trans. Commun.*, vol. 56, no. 1, pp. 5–9, Jan. 2008.
- [88] M. Ghosh, "Analysis of the effect of impulse noise on multicarrier and single carrier QAM systems," *IEEE Trans. Commun.*, vol. 44, no. 2, pp. 145–147, Feb. 1996.
- [89] S. Battermann and H. Garbe, "Influence of modern broadband inhouse PLC transmission on short-wave reception," in *Proc. IEEE Int. Symp. on Electromag. Compatib. (EMC)*, pp. 283–288, 2015.
- [90] S. Barmada, A. Musolino, and M. Raugi, "Innovative model for time-varying power line communication channel response evaluation," *IEEE Journal on Sel. Areas in Commun.(JSAC)*, vol. 24, no. 7, pp. 1317–1326, 2006.
- [91] H. Sun, A. Nallanathan, and J. Jiang, "Improving the energy efficiency of power line communications by spectrum sensing," in *Proc. Int. Conf. on Advances in Comp., Commun. and Informat.*, pp. 758–762, 2012.

- [92] E. Ayanoglu, "Editorial launching IEEE transactions on green communications and networking," *IEEE Trans. on Green Commun. and Networking*, vol. 1, no. 1, pp. 1–2, 2017.
- [93] J. Joung, C. K. Ho, K. Adachi, and S. Sun, "A survey on power-amplifier-centric techniques for spectrum-and energy-efficient wireless communications," *IEEE Commun. Surv. & Tut.*, vol. 17, no. 1, pp. 315–333, 2015.
- [94] L. Guan and A. Zhu, "Green communications: Digital predistortion for wideband RF power amplifiers," *IEEE Microwave Mag.*, vol. 15, no. 7, pp. 84–99, 2014.
- [95] A. Ikpehai and B. Adebisi, "Home energy management system over low-power narrowband PLC," *IEEE 10th International Symposium on Communication Systems, Networks and Digital Signal Processing (CSNDSP)*, pp. 1–6, 2016.
- [96] A. Kailas, V. Cecchi, and A. Mukherjee, "A survey of communications and networking technologies for energy management in buildings and home automation," *Journal of Comp. Networks and Commun.*, vol. 2012, 2012.
- [97] M. Starsinic, "System architecture challenges in the home M2M network," in *Proc. IEEE Long Island Sys. Appl. and Technol. Conf. (LISAT), 2010*, pp. 1–7, 2010.
- [98]
- [99] M. R. Palattella, M. Dohler, A. Grieco, G. Rizzo, J. Torsner, T. Engel, and L. Ladid, "Internet of things in the 5G era: Enablers, architecture, and business models," *IEEE Journal on Sel. Areas in Commun.*, vol. 34, no. 3, pp. 510–527, 2016.
- [100] G. Wunder, P. Jung, M. Kasparick, T. Wild, F. Schaich, Y. Chen, S. Ten Brink, I. Gaspar, N. Michailow, A. Festag *et al.*, "5GNOW: non-orthogonal, asynchronous waveforms for future mobile applications," *IEEE Commun. Mag.*, vol. 52, no. 2, pp. 97–105, 2014.
- [101] V. C. Gungor, D. Sahin, T. Kocak, S. Ergut, C. Buccella, C. Cecati, and G. P. Hancke, "Smart grid technologies: Communication technologies

- and standards," *IEEE Trans. on Ind. informat.*, vol. 7, no. 4, pp. 529–539, 2011.
- [102] T. M. Lawrence, M.-C. Boudreau, L. Helsen, G. Henze, J. Mohammadpour, D. Noonan, D. Patteeuw, S. Pless, and R. T. Watson, "Ten questions concerning integrating smart buildings into the smart grid," *Building and Environment*, vol. 108, pp. 273–283, 2016.
- [103] N. M. G. Strategy, "Advanced metering infrastructure," *US Dep. of Energy Office of Electricity and Energy Reliability*, 2008.
- [104] S. Haben, C. Singleton, and P. Grindrod, "Analysis and clustering of residential customers energy behavioral demand using smart meter data," *IEEE Trans. on Smart Grid*, vol. 7, no. 1, pp. 136–144, 2016.
- [105] R. Al-Otaibi, N. Jin, T. Wilcox, and P. Flach, "Feature construction and calibration for clustering daily load curves from smart-meter data," *IEEE Trans. on Ind. Informat.*, vol. 12, no. 2, pp. 645–654, 2016.
- [106] W. Wang, N. Yu, B. Foggo, J. Davis, and J. Li, "Phase identification in electric power distribution systems by clustering of smart meter data," in *Proc. 15th IEEE Int. Conf. on Machine Learning and Appl. (ICMLA)*, pp. 259–265, 2016.
- [107] O. Ma, N. Alkadi, P. Cappers, P. Denholm, J. Dudley, S. Goli, M. Hummon, S. Kiliccote, J. MacDonald, N. Matson *et al.*, "Demand response for ancillary services," *IEEE Trans. on Smart Grid*, vol. 4, no. 4, pp. 1988–1995, 2013.
- [108] F. Aalamifar, A. Schlógl, D. Harris, and L. Lampe, "Modelling power line communication using network simulator-3," in *Proc. IEEE Global Commun. Conf. (GLOBECOM)*, pp. 2969–2974, 2013.
- [109] S. Dominiak, L. Andersson, M. Maurer, A. Sendin, and I. Berganza, "Challenges of broadband PLC for medium voltage smart grid applications," in *Proc. 6th WorkShop on Power Line Commun.*, pp. 20–21, 2012.
- [110] S. Goldfisher and S. Tanabe, "IEEE 1901 access system: An overview of its uniqueness and motivation," *IEEE Commun. Mag.*, vol. 48, no. 10, 2010.

- [111] V. Guillet and G. Lamarque, "Unified background noise model for power line communication," in *Proc. IEEE Int. Symp. on Power Line Commun. and Its Applications (ISPLC)*, pp. 131–136, 2010.
- [112] E. Liu, Y. Gao, G. Samdani, O. Mukhtar, and T. Korhonen, "Broadband powerline channel and capacity analysis," in *Proc. IEEE Int. Symp. on Power Line Commun. and Its Applications*, pp. 7–11, 2005.
- [113] S. Galli and O. Logvinov, "Recent developments in the standardization of power line communications within the IEEE," *IEEE Commun. Mag.*, vol. 46, no. 7, 2008.
- [114] M. Tlich, R. Razafferson, G. Avril, and A. Zeddami, "Outline about the EMC properties and throughputs of the PLC systems up to 100 MHz," in *Proc. IEEE Int. Symp. on Power Line Commun. and Its Appl.*, pp. 259–262, 2008.
- [115] T. N. Vo, K. Amis, T. Chonavel, and P. Siohan, "Achievable throughput optimization in OFDM systems in the presence of interference and its application to power line networks," *IEEE Trans. on Commun.*, vol. 62, no. 5, pp. 1704–1715, 2014.
- [116] L. Zheng, S. Parkinson, D. Wang, L. Cai, and C. Crawford, "Energy efficient communication networks design for demand response in smart grid," in *Proc. IEEE Int. Conf. on Wireless Commun. and Signal Processing (WCSP)*, pp. 1–6, 2011.
- [117] D. J. Olsen, M. R. Sarker, and M. A. Ortega-Vazquez, "Optimal penetration of home energy management systems in distribution networks considering transformer aging," *IEEE Trans. on Smart Grid*, 2017.
- [118] A. Moreno-Munoz, F. Bellido-Outeirino, P. Siano, and M. Gomez-Nieto, "Mobile social media for smart grids customer engagement: Emerging trends and challenges," *Renewable and Sustainable Energy Reviews*, vol. 53, pp. 1611–1616, 2016.
- [119] G. Brusco, A. Burgio, D. Menniti, A. Pinnarelli, and N. Sorrentino, "Energy management system for an energy district with demand response availability," *IEEE Trans. on Smart Grid*, vol. 5, no. 5, pp. 2385–2393, 2014.

- [120] G. Lobaccaro, S. Carlucci, and E. Löfström, "A review of systems and technologies for smart homes and smart grids," *Energies*, vol. 9, no. 5, pp. 348–348, 2016.
- [121] B. Zhou, W. Li, K. W. Chan, Y. Cao, Y. Kuang, X. Liu, and X. Wang, "Smart home energy management systems: Concept, configurations, and scheduling strategies," *Renewable and Sustainable Energy Reviews*, vol. 61, pp. 30–40, 2016.
- [122] S. D'Alessandro, A. M. Tonello, A. Monacchi, and W. Elmenreich, "Home energy management systems: Design guidelines for the communication infrastructure," in *Proc. IEEE Int. Energy Conf. (ENERGY-CON), Dubrovnik, Croatia*, pp. 805–812, 2014.
- [123] N. Andreadou, M. O. Guardiola, and G. Fulli, "Telecommunication technologies for smart grid projects with focus on smart metering applications," *Energies*, vol. 9, no. 5, pp. 375–375, 2016.
- [124] A. Haidine, B. Adebisi, A. Treytl, H. Pille, B. Honary, and A. Portnoy, "High-speed narrowband PLC in smart grid landscape—state-of-the-art," in *Proc. IEEE Int. Symp. on Power Line Commun. and Its Appl. (ISPLC)*, pp. 468–473, 2011.
- [125] B. L. Thomas and D. J. Cook, "Activity-aware energy-efficient automation of smart buildings," *Energies*, vol. 9, no. 8, pp. 624–624, 2016.
- [126] Shelby, et al, "IETF RFC 7252, the constrained application protocol (CoAP)," in <https://tools.ietf.org/html/rfc7252> (accessed on 10 April 2017). IETF, 1998.
- [127] J. Matanza, S. Kiliccote, S. Alexandres, and C. Rodríguez-Morcillo, "Simulation of low-voltage narrow-band power line communication networks to propagate openadr signals," *IEEE Journal of Commun. and Networks*, vol. 17, no. 6, pp. 656–664, 2015.
- [128] IETF, "IETF RFC 4944, transmission of ipv6 packets over IEEE 802.15.4 networks," in <https://tools.ietf.org/html/rfc4944> (accessed on 12 January 2017). IETF, 2014.

- [129] C. Gezer and C. Buratti, "A zigbee smart energy implementation for energy efficient buildings," in *Proc. IEEE 73rd Veh. Technol. Conf. (VTC Spring)*, pp. 1–5, 2011.
- [130] D. Makrakis and K. Feher, "Optimal noncoherent detection of PSK signals," *IET Electronics Letters*, vol. 26, no. 6, pp. 398–400, 1990.
- [131] I. D. Marsland and P. T. Mathiopoulos, "On the performance of iterative noncoherent detection of coded M-PSK signals," *IEEE Trans. Commun.*, vol. 48, no. 4, pp. 588–596, 2000.
- [132] M. Zhou, M. R. Yuce, and W. Liu, "A non-coherent DPSK data receiver with interference cancellation for dual-band transcutaneous telemetries," *IEEE Journal of Solid-State Circuits*, vol. 43, no. 9, pp. 2003–2012, 2008.
- [133] H. Leib, "Data-aided noncoherent demodulation of DPSK," *IEEE trans. commun.*, vol. 43, no. 234, pp. 722–725, 1995.
- [134] S. Mudriievskiyi, I. Tsokalo, A. Haidine, B. Adebisi, and R. Lehnert, "Performance evaluation of mac backoff algorithm in narrowband plc," in *IEEE Int. Conf. on Smart Grid Commun (SmartGridComm)*, 2011, pp. 108–113.
- [135] S. D'Alessandro, A. M. Tonello, and L. Lampe, "On power allocation in adaptive cyclic prefix OFDM," in *IEEE Int. Symp. on Power Line Commun. and Its Appl. (ISPLC)*, 2010, pp. 183–188.
- [136] B. Adebisi, S. Ali, and B. Honary, "Multi-emitting/multi-receiving points mmfsk for power-line communications," in *IEEE Int. Symp. on Power Line Commun. and Its Applications*, 2009, pp. 239–243.
- [137] —, "A hopping code for mmfsk in a power-line channel." *JCM*, vol. 4, no. 6, pp. 429–436.
- [138] X.-L. Huang, G. Wang, and F. Hu, "Minimal Euclidean distance-inspired optimal and suboptimal modulation schemes for vector OFDM system," *Int. Journal of Commun. Sys.*, vol. 24, no. 5, pp. 553–567, 2011.

- [139] K. Rabie, E. Alsusa, A. Familua, and L. Cheng, "Constant envelope OFDM transmission over impulsive noise power-line communication channels," in *Proc. IEEE Int. Symp. Power Lines Commun. and Its Appl. (ISPLC)*, pp. 13–18, Mar. 2015.
- [140] J. S. Lee, H. M. Oh, J. T. Kim, and J. Y. Kim, "Performance of scaled SLM for PAPR reduction of OFDM signal in PLC channels," in *Proc. IEEE Int. Symp. Power Lines Commun. and Its Appl. (ISPLC)*, pp. 166–170, March 2009.
- [141] X. Zhu, W. Pan, H. Li, and Y. Tang, "Simplified approach to optimized iterative clipping and filtering for PAPR reduction of OFDM signals," *IEEE Trans. Commun.*, vol. 61, no. 5, pp. 1891–1901, May. 2013.
- [142] Y. Li, I. Ngehani, X.-G. Xia, and A. Høst-Madsen, "On performance of vector OFDM with linear receivers," *IEEE Trans. Signal Process.*, vol. 60, no. 10, pp. 5268–5280, Nov. 2012.
- [143] T. T. Nguyen and L. Lampe, "On partial transmit sequences for PAR reduction in OFDM systems," *IEEE Trans. Wireless Commun.*, vol. 7, no. 2, pp. 746–755, Feb. 2008.
- [144] K. M. Rabie and E. Alsusa, "Efficient SLM based impulsive noise reduction in powerline OFDM communication systems," in *Proc. IEEE Global Commun. Conf. (GLOBECOM)*, pp. 2915–2920, Dec. 2013.
- [145] B. Adebisi, K. M. Rabie, A. Ikpehai, A. Wells, and S. Cinna, "Vector OFDM transmission over non-Gaussian power line communication channels," *IEEE Systems*, 2017.
- [146] J. Matanza, S. Kiliccote, S. Alexandres, and C. Rodríguez-Morcillo, "Simulation of low-voltage narrow-band power line communication networks to propagate openADR signals," *IEEE Journal of Commun. and Networks*, vol. 17, no. 6, pp. 656–664, 2015.
- [147] X.-G. Xia, "Precoded and vector OFDM robust to channel spectral nulls and with reduced cyclic prefix length in single transmit antenna systems," *IEEE Trans. on commun.*, vol. 49, no. 8, pp. 1363–1374, 2001.

- [148] P. Cheng, M. Tao, Y. Xiao, and W. Zhang, "V-OFDM: On performance limits over multi-path rayleigh fading channels," *IEEE Trans. Commun.*, vol. 59, no. 7, pp. 1878–1892, 2011.
- [149] H. Zhang, X.-G. Xia, L. J. Cimini, and P. C. Ching, "Synchronization techniques and guard-band-configuration scheme for single-antenna vector-OFDM systems," *IEEE Trans. Wireless Commun.*, vol. 4, no. 5, pp. 2454–2464, 2005.
- [150] H. Zhang, X.-G. Xia, Q. Zhang, and W. Zhu, "Precoded OFDM with adaptive vector channel allocation for scalable video transmission over frequency-selective fading channels," *IEEE Trans. mobile comput.*, vol. 99, no. 2, pp. 132–142, 2002.
- [151] H. Zhang and X.-G. Xia, "Iterative decoding and demodulation for single-antenna vector OFDM systems," *IEEE Trans. on Veh. Technol.*, vol. 55, no. 4, pp. 1447–1454, 2006.
- [152] J. Han and G. Leus, "Space-time and space-frequency block coded Vector OFDM modulation," *IEEE Commun. Letters*, vol. 21, no. 1, pp. 204–207, 2017.
- [153] I. Ngebani, Y. Li, X.-G. Xia, H. S. Ahmed, and M. Zhao, "Analysis of phase noise in vector OFDM systems," in *Proc. IEEE Global Commun. Conf. (GLOBECOM)*, pp. 3602–3607, Dec. 2013.
- [154] W. Zhou, L. Fan, and H. Chen, "Vector orthogonal frequency division multiplexing system over fast fading channels," *IET Commun.*, vol. 8, no. 13, pp. 2322–2335, Sept. 2014.
- [155] P. Cheng, M. Tao, Y. Xiao, and W. Zhang, "V-OFDM: On performance limits over multi-path rayleigh fading channels," *IEEE Trans. Commun.*, vol. 59, no. 7, pp. 1878–1892, Jul. 2011.
- [156] I. Ngebani, Y. Li, X.-G. Xia, and M. Zhao, "EM-based phase noise estimation in vector OFDM systems using linear MMSE receivers," *IEEE Trans. Veh. Technol.*, vol. 65, no. 1, pp. 110–122, Jan. 2016.

- [157] C. Soltanpur, K. Rabie, B. Adebisi, and A. Wells, "Masreliez-equalized VOFDM in non-Gaussian channels: power line communication systems," *IEEE Systems*, Jan. 2017.
- [158] S. V. Zhidkov, "Performance analysis and optimization of OFDM receiver with blanking nonlinearity in impulsive noise environment," *IEEE Trans. on Veh. Technol.*, vol. 55, no. 1, pp. 234–242, 2006.
- [159] —, "On the analysis of OFDM receiver with blanking nonlinearity in impulsive noise channels," in *Proc. Int. Symp. Intell. Signal Process. Commun. Syst.*, pp. 492–496, Nov. 2004.
- [160] R. J. Baxley and G. T. Zhou, "Power savings analysis of peak-to-average power ratio in OFDM," *IEEE Trans. on Consumer Electronics*, vol. 50, no. 3, pp. 792–798, 2004.
- [161] S. Cripps, *RF Power Amplifiers for Wireless Communications*. Norwood, MA: Artech House, 1999.
- [162] K. M. Rabie and E. Alsusa, "Improving blanking/clipping based impulsive noise mitigation over powerline channels," pp. 3413–3417, 2013.

Production Notes

This thesis was typeset using LyX version 2.1.4 (24 July 2015). LyX is an open source document processor supported on Unix and Windows platforms, the Windows version was employed in this thesis. Within the LyX environment, Bibtex was used for organising the bibliography. The block diagrams including the system models were drawn using Microsoft Excel 2013. Furthermore, all physical layer simulations were carried out in MATLAB (R2014a) while upper layers such as adaption, network, transport and application layers were investigated in NS-3 (version 21). Finally, the afore-mentioned tools/software were installed and used on a Dell latitude E4310 with core i5 CPU and 4G memory running 64-bit Windows 7 Ultimate (SP 1).